Doppler-only Target Tracking for a Multistatic Radar Exploiting FM Band Illuminators of Opportunity

Francois De Villiers Maasdorp
MEng(Electronic) UP

Thesis Presented for the Degree of

DOCTOR OF PHILOSOPHY

in the Department of Electrical Engineering

UNIVERSITY OF CAPE TOWN

December 2015

“Knowledge is Power.”

-Francis Bacon

Declaration

I declare that this thesis is my own, unaided work. It is being submitted for the degree of Doctor of Philosophy in Engineering in the University of Cape Town. It has not been submitted before for any degree or examination in any other university.

Signature of Author .....

Cape Town
December 6, 2015

Abstract

Commensal Radar (CR), defined as a subclass of Passive Radar (PR), is a receive only radar that exploits non-cooperative illuminators of opportunity for target detection, location and subsequent tracking.

The objective of this thesis is to evaluate the feasibility of using a Frequency Modulation (FM) Broadcast band CR system as a cost effective solution for Air Traffic Control (ATC). An inherent complication by exploiting FM is the low range resolution due to the low bandwidth of FM radio signals. However, due to typical long integration times associated with CR, the frequency domain resolution is typically very good. As a result, measurements of the target's Doppler shift are highly accurate and could potentially make FM illuminators a viable source for ATC purposes. Accordingly, this thesis aims to obtain a comprehensive understanding of using high resolution Doppler measurements to accurately track the position of a target. This objective have been addressed by performing a comprehensive mathematical analysis for a Doppler only tracking CR system. The analysis is verified with a tracking simulation, in which the Recursive Gauss Newton Filter (RGNF) is used and lastly, a field experiment was conducted to produce tracking results based on real measurement data.

Results demonstrated that Doppler only target tracking from real measurement data is possible, even when the initial target state vector is initialised from real measurement data. A good degree of correlation is achieved between the theoretical, simulated and measured results, hence verifying the theoretical findings of this thesis. Ensuring that the observation matrix is properly conditioned in Doppler only tracking applications is important, as failure to do so results in

tracking instability. Factors that influence the conditioning of the observation matrix are; the number of receivers used (assuming the basic observation criteria is met) and the placement of the receivers, keeping in mind the possibility of Doppler correlation in the measurements. The possibility of improving an ill-conditioned observation matrix is also demonstrated. In general, tracking filters, for example the RGNF, typically employ time history information and therefore, a direct comparison to the Cramer Rao Lower Bound (CRLB) is unrealistic and accordingly a new theoretical lower bound, called the Cumulative CRLB was derived that does account for time history measurements. Although the best results for this thesis are achieved by using long integration periods (4 s), the effect of Doppler walk was not compensated for and is an aspect that requires further investigation to potentially further improve on the results obtained in this thesis. As a final conclusion for this thesis; the Doppler only target tracking delivered some encouraging results, however a qualification test in the form of an extensive trial period is next required to motivate Doppler only tracking for ATC purposes.

Acknowledgements

Above all, I would like to thank ***My Heavenly Father*** for blessing me with many talents and determination in order to pursue the goals in my life. Therefore, I dedicate this study to my God Almighty.

Further, I would like to thank the following individuals for their assistance and support during this research, that I am deeply grateful for:

My Wonderful Parents: For being an example in life to strive for. Without their continuous support and guidance over the years, I would never have attained the successes in life as it stands today.

My Wife and Children: For the sacrifice in not having a husband and father around during the final stages of this study, but stood by me. For that, I am truly grateful for.

My supervisor Prof Michael Inggs: For his insight and guidance throughout the duration of this study and making me part of one of his many research initiatives.

University of Cape Town Personal: Notably, Dr Craig Tong for all the valuable discussions and ideas that we shared amongst each other over the duration of this research, as well as Dr Roaldje Nadjiasngar for his valuable suggestions to the Cramer Rao work of this study. Also, Mr Justin Coetser and Dr Andrew van der Byl for their assistance during the final field deployment for this study.

My Work Colleagues: Notably, Mr Christo Cloete for suggesting to have a look at *Passive Coherent Location* a few years ago and his assistance in the analysis and interpretation of the data collected during the field deployments. Mr Dembe Nenzhelele that assisted with the field deployments and lastly, Mr Jacques Cilliers and Mr Willie Nel for their valuable suggestions and inputs to my research.

I would also like to acknowledge the support of the following organisations:

The Council for Scientific and Industrial Research (CSIR): For supporting my studies and further, allowing me to work on my studies while being paid a wage.

The Armaments Corporation of South Africa (Armscor): For supporting this research and invaluable funding provided.

Peralex Electronics: Who provided the ComRad3 receiver hardware that played a significant role in the success achieved with this thesis. Notably, Mr Francois Louw and Mr Alex Bassios; as well as Mr Jean-Paul da Conceicao, Mr Robert Fowler, Mr Jean Wessels and Mr Adriaan Zeeman who assisted with the field deployments at various times.

GEW Technologies: Who also provided hardware for the field deployments, especially during the early days of this research drive. Notably, Mr Hennie Venter and also Mr Michal Kotze for his assistance during the field deployments.

Contents

List of Figures

List of Tables

List of Abbreviations

2-D	2-Dimensional.
3-D	3-Dimensional.
AAF	Auto Ambiguity Function.
ADC	Analogue to Digital Converter.
ADS-B	Automatic Dependence Surveillance - Broadcasting.
AGL	Above Ground Level.
AMSL	Above Mean Sea Level.
ARD	Amplitude/Range/Doppler.
ARGUS 3D	Air Guidance and Surveillance 3-D.
ATC	Air Traffic Control.
Az	Azimuth.
BAE	British Aerospace.
BOT	Bearing Only Tracking.
CAF	Cross Ambiguity Function.
CCRLB	Cumulative CRLB.

CFAR	Constant False Alarm Rate.
CFIM	Cumulative FIM.
CGLS	Conjugate Gradient Least Squares.
CH	Chain Home.
CPI	Coherent Processing Interval.
CR	Commensal Radar.
CRLB	Cramèr-Rao Lower Bound.
CSIR	Council for Scientific and Industrial Research.
CUT	Cell Under Test.
CW	Continuous Wave.
DAB	Digital Audio Broadcast.
DE	Differential Equation.
DF	Direction Finder.
DOPLOC	Doppler Phase Lock.
DOVAP	Doppler Velocity and Positioning System.
DPI	Direct Path Interference.
DTV	Digital Television.
DVB-T	Digital Video Broadcast - Terrestrial.
ECA	Extensive Cancellation Algorithm.
EKF	Extended Kalman Filter.
ERP	Effective Radiated Power.

FFT	Fast Fourier Transform.
FIM	Fisher Information Matrix.
FM	Frequency Modulation.
FMCW	Frequency Modulated Continuous Wave.
GDOP	Geometric Dilution Of Precision.
GEW	Grintek Ewation Technologies.
GN	Gauss Newton.
GOCA-CFAR	Greater Of Cell Averaging CFAR.
GPS	Global Positioning System.
GPSDO	GPS Disciplined Oscillator.
GSM	Global System Mobile.
IEKF	Iterated Extended Kalman Filter.
IF	Intermediate Frequency.
IQ	In phase/Quadrature.
IVE	Instrumental Variable Estimator.
LML	Least Mean Lattice.
LMS	Least Mean Squares.
LoS	Line of Site.
LPDA	Log Periodic Dipole Antenna.
LS	Least Squares.
MAP	Maximum a-Posteriori.

MIMO	Multiple Input Multiple Output.
MLE	Maximum Likelihood Estimator.
MMSE	Minimum Mean Square Error.
MVU	Minimum Variance Unbiased.
NLMS	Normalised Least Mean Squares.
OFDMA	Orthogonal Frequency Division Multiple Access.
PARADOP	Passive Ranging Doppler System.
PBR	Passive Bistatic Radar.
PCL	Passive Coherent Location.
PDF	Probability Density Function.
PDOP	Position Dilution Of Precision.
PFA	Probability of False Alarm.
PHD	Probability Hypothesis Density.
PoD	Probability of Detection.
PR	Primary Radar.
PSLR	Peak to Side Lobe Ratio.
RCS	Radar Cross Section.
REF	Row Echelon Form.
RF	Radio Frequency.
RGNF	Recursive Gauss Newton Filter.
RLMS	Recursive Least Mean Squares.

RLS	Recursive Least Squares.
RMS	Root Mean Square.
RMSE	Root Mean Square Error.
ROI	Region of Interest.
RREF	Reduced Row Echelon Form.
SAR	Synthetic Aperture Radar.
SCA	Sequential Cancellation Algorithm.
SECOR	Sequential Correlation Ranging.
SINR	Signal to Interference plus Noise Ratio.
SNR	Signal to Noise Ratio.
SPASUR	Space Surveillance System.
SSR	Secondary Surveillance Radar.
SVD	Singular Value Decomposition.
T-R	Transmitter - Receiver.
TDOA	Time Difference of Arrival.
TMA	Target Motion Analysis.
TV	Television.
UCT	University of Cape Town (South Africa).
UKF	Unscented Kalman Filter.
UMTS	Universal Mobile Telecommunications System.
US	United States.

UTM	Universal Transverse Mercator.
VDOP	Velocity Dilution Of Precision.
VHF	Very High Frequency.
WiFi	Wireless Fidelity.
WiMAX	Worldwide Interoperability for Microwave Access.
WWII	World War II.

List of Symbols

K_d	Wave number of the exploited transmitter.
$R_{E,n}$	Range between the transmitter and target at sample n [m].
$R_{Ri,n}$	Range between the target and i^{th} receiver at sample n [m].
$R_{bi}[n]$	Ideal bistatic range measured by the i^{th} receiver at sample n [m].
T	Sample period [s].
$\Delta\mathbf{x}$	Error in the state vector estimate $\widehat{\mathbf{x}}$.
Ψ	Cross ambiguity function measuring the level of correlation between the reference and surveillance signals.
$\dot{x}_n$	Target x-velocity at sample n [m/s].
$\dot{y}_n$	Target y-velocity at sample n [m/s].
λ	Wave length of the exploited transmitter's RF carrier frequency [m].
$\mathbf{B}_{REF}$	Matrix $\mathbf{B}$ in Row Echelon Form.
$\mathbf{B}_{RREF}$	Matrix $\mathbf{B}$ in Reduced Row Echelon Form.
$\mathbf{C}$	Covariance matrix of the CRLB.
$\mathbf{I}_2$	2×2 Identity matrix.

$\mathbf{J}(\mathbf{x})$	Fisher Information Matrix for $\mathbf{x}$.
$\mathbf{J}_D(\mathbf{x})$	Fisher Information Matrix for $\mathbf{x}$ using Doppler measurements.
$\mathbf{J}_{RD}(\mathbf{x})$	Fisher Information Matrix for $\mathbf{x}$ using range-Doppler measurements.
$\mathbf{K}_n$	Filter observer gain at sample n.
$\mathbf{M}$	Observation matrix.
$\mathbf{P}_n^{-1}$	Filter covariance matrix at sample n.
$\mathbf{P}_{(n+1)/n}^{-1}$	Forward predicted filter covariance matrix from sample n to sample (n+1).
$\mathbf{P}_{n/(n-1)}^{-1}$	Forward predicted filter covariance matrix from sample (n-1) to sample n.
$\mathbf{R}_D$	Doppler measurement error covariance matrix.
$\mathbf{R}_{RD}$	Range-Doppler measurement error covariance matrix.
$\mathbf{R}$	Measurement error covariance matrix.
$\mathbf{X}_R$	Matrix of receiver positions.
$\mathbf{\Phi}(t_{n-1}, t_n)$	State transition matrix from sample $n-1$ to n.
$\mathbf{r}_n$	Vector of bistatic range measurements.
$\mathbf{s}_{cs}$	Vector of samples in the surveillance channel after DPI and clutter cancellation.
$\mathbf{v}_{b,n}$	Vector of measured bistatic velocities.
$\mathbf{w}$	Noise vector.
$\mathbf{x}_n$	Target state vector at sample n.
$\mathbf{x}_{n-1}$	Target state vector at sample $n-1$.

$\mathbf{y}_{D,n}$	Ideal Doppler measurement vector at sample n.
$\mathbf{y}_{RD,n}$	Ideal range-Doppler measurement vector at sample n.
$\mathbf{y}$	Ideal measurement vector.
$p(\widetilde{\mathbf{y}}\|\mathbf{x})$	The likelihood function of $\mathbf{x}$.
$\det(\mathbf{B})$	The determinant of matrix $\mathbf{B}$.
$\overline{\mathbf{M}}$	Linearised Observation matrix.
ρ_n	Spearman rank correlation coefficient.
σ_R^2	Variance of the errors in the bistatic range measurements.
σ_f^2	Variance of the errors in the frequency measurements.
$\sigma_{p,n}$	2-D Position Dilution of Precision at sample n [m].
$\sigma_{v,n}$	2-D Velocity Dilution of Precision at sample n [m/s].
τ	Matched filter/Correlation delay [s].
$\mathbf{s}_r$	Vector of samples received from the reference antenna.
$\mathbf{s}_s$	Vector of samples received from the surveillance antenna.
$\widehat{\mathbf{x}}_{(n+1)/n}$	Forward predicted state vector from sample n to sample (n+1).
$\widehat{\mathbf{x}}$	Estimate of the target state vector $\mathbf{x}$.
$\widetilde{\mathbf{y}}_{D,n}$	Noise corrupted Doppler measurement vector.
$\widetilde{\mathbf{y}}_{RD,n}$	Noise corrupted range-Doppler measurement vector.
$\widetilde{\mathbf{y}}$	Noise corrupted measurement vector.
f_d	Bistatic Doppler shift [Hz].
$f_{di}[n]$	Bistatic Doppler shift measured by the i^{th} receiver at sample n [Hz].

k	Number of spatially separated receivers.
n	Sample number.
$rk(\mathbf{B})$	The rank of matrix $\mathbf{B}$.
t_n	Time at sample n [s].
t_{n-1}	Time at sample $n-1$ [s].
t	Continuous time as an independent parameter of a function.
x_n	Target x-coordinate at sample n [m].
x_{n-1}	Target x-coordinate at sample $n-1$ [m].
y_n	Target y-coordinate at sample n [m].
y_{n-1}	Target y-coordinate at sample $n-1$ [m].

Chapter 1

Introduction

1.1 Introductory Remarks

The aim of this thesis is to investigate whether commercial aircraft can be detected and tracked by measuring only the Doppler shift of the target at low cost. From the title, the reader might think that the concept of "Doppler only tracking" using multiple receivers, is a known concept as space surveillance systems were already based on this concept in the 1960's. However, only recent developments over several research fields made it possible to overcome the difficulties experienced in the past and only made such systems feasible for air-surveillance today, both in a cost effective and technical way.

To place the novelty of this thesis in context, this chapter is structured as follows. In Section 1.2, high level background information is presented on; 1.) Commensal[1] Radar (CR), 2.) Historical multistatic systems, and 3.) Evolution of state estimation theory. Lastly, the section concludes with a formal motivation for the research conducted in this thesis. In Section 1.3, the problem description is formulated and in Section 1.4 the scope and objective are presented. The contri-

[1] The term Commensal, commonly used in bioscience, describe a sensor system that utilises emissions of other systems, for example the FM radio band, to sense, but without affecting in any way the operation of the host emitter(s).

butions are listed in Section 1.5 and lastly, the chapter concludes in Section 1.6 with an overview of the remainder of the thesis.

1.2 Background and Motivation

1.2.1 Background

Understanding the context and novelty of this thesis largely depends on the underlying knowledge of the following three topics; 1.) CR, 2.) historical multi-static systems and 3.) estimation theory. Therefore, the intention at this stage is to provide a high level overview of the respective achievements under each topic. A more detailed overview follows in Chapter 2.

1.2.1.1 Commensal Radar

CR, also known as Passive Coherent Location (PCL) or Passive Bistatic Radar (PBR)[1] is a class of radar system that makes use of non-cooperative sources of illumination, such as commercial broadcast and communication signals, in order to detect and track objects/targets. For example, presented in Figure 1.1 is a single transmitter $\mathbf{x}_E$, two CR receivers, $\mathbf{x}_{R1}$ and $\mathbf{x}_{R2}$ and a single target. The distance between the transmitter and target is given as A, the distance between the target and $\mathbf{x}_{R1}$ is given as B and the distance between $\mathbf{x}_E$ and $\mathbf{x}_{R1}$ is given as L_1, known as the baseline.

In a classic CR, using receiver $\mathbf{x}_{R1}$ as an example, the Time Difference Of Arrival (TDOA) between the direct path (reference signal and along $L1$) and reflected path (surveillance signal along $A+B$) is measured by the CR. With the baseline length known, the CR then calculates the bistatic range, given as $A+B$. The bistatic range is illustrated by the ellipsoid in Figure 1.1, in which $\mathbf{x}_E$ and $\mathbf{x}_{R1}$ are the foci points of the ellipse. Hence, at this stage the target's position cannot be resolved with only a single bistatic range measurement. One method to resolve the target's position, is to use multiple geographically separated receivers and use

a method known as multilateration. This is illustrated by Figure 1.1, in which the target location is given by the intersection point between the bistatic range of receiver $\mathbf{x}_{R1}$ and the bistatic range of receiver $\mathbf{x}_{R2}$. Furthermore, notice that the actual number of intersections between the two ellipsoids are 4. Therefore, three additional, but incorrect target positions are registered that is commonly known as "ghost targets". This this phenomenon is not considered in this thesis. Another method to resolve the target's position, is for example to measure the bearing, θ_1 along the reflected path B at receiver $\mathbf{x}_{R1}$. The target position is then resolved by using the bistatic range and bearing information.

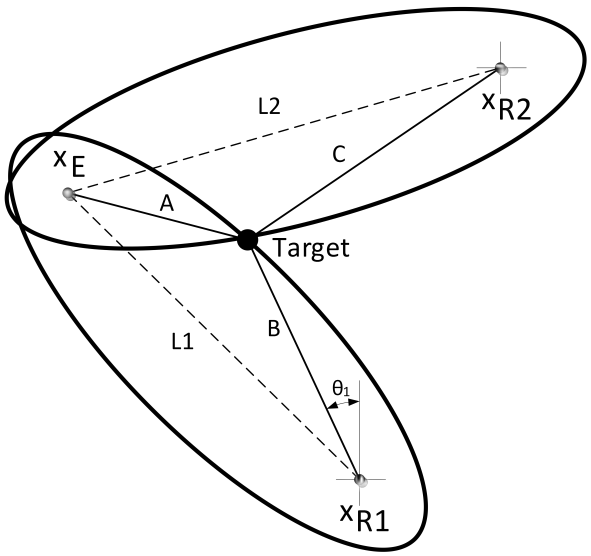

Figure 1.1: A multistatic CR configuration, consisting of a single transmit node, $\mathbf{x}_E$ and two receiver nodes, $\mathbf{x}_{R1}$ and $\mathbf{x}_{R2}$. The target position is resolved by either determining the intersection of the two bistatic range estimates or, the intersection between a single bistatic range and bearing estimate of the surveillance signal.

CR is not a new concept and is known from as early as the 1930's, in fact CR was actually used as a concept demonstrator to prove the radar concept by means of the Daventry experiment [2]. This lead to the development of the well known Chain Home (CH) system, developed by the British, to detect German aircraft

over the English channel during World War II (WWII). Like most radars used in air defence networks during the early 1930's, CH was also a Continuous Wave (CW) radar system and bistatic in nature to achieve the necessary isolation between the radar transmit and receive mode. However, the Germans were the first to develop a full functional CR system during WWII [2], called Kleine Heidelberg. It operated as a passive bistatic receiver and used the CH radar as the illuminator of opportunity to detect aircraft over the southern part of the North Sea [3]. With the development of the synchroniser in 1936 [4], bistatic radar gave way to monostatic radar due to the elimination of the geometric complexities introduced by a separate transmitter and receiver site. In addition, the monostatic principle also made it possible for shipborne and aircraft radar applications as smaller components were developed. Bistatic radar systems were considered again during the early 1950's when some interesting properties of the scattered radar energy were discovered by Siegel [4]. In fact, he was the first to describe the technology as "bistatic" in his report. The next resurgence of CR only came in the 1980's and the 1990's as a result of the development work of a CR system by Lockheed Martin, called Silent Sentry [1], as well as pioneering work by Griffiths and Long [5] and Howland et al. [6].

Since 2000, interest in CR by universities, research institutes and industry are fuelled mainly by the technology achievements made in the field of digital electronics. Today, powerful computers and fast, high-dynamic range digitisers are available on the market for relatively low prices. In return, this allowed for the attractive properties of CR to be exploited for commercial as well as military use. Probably the most attractive feature in CR is that it has the potential to be a cost effective persistent surveillance system. This is a result of several factors. Some of which include the absence of a transmitter subsystem and associated power consumption, no need for dedicated spectrum allocation and typically do not consist of any moving parts. Furthermore, these radars are able to operate covertly given that they only consist of receiver infrastructure, are highly mobile and are believed to have resistance to low observable targets due to the lower carrier frequencies and bistatic nature. As a result, companies such as Thales, Airbus (and formerly Cassidian), British Aerospace (BAE) and Selex, as well as

many academic and research institutions are or have in the past, invested large efforts into studying the capability of CR technology.

Amongst other research activities in the field of CR (see Chapter 2 for a more detailed overview of CR literature) established research includes a long list of evaluated illuminators opportunity. Some of which Frequency Modulation (FM) radio [7, 8], Analogue Television [5, 6] and Digital Video Broadcasting - Terrestrial (DVB-T)[9, 10], are regarded as favourable high powered illuminators of opportunity. Other, low power emissions such as WiFi [11], GSM [12], WiMAX [13] and UMTS [14] were also reported in literature to be successful for CR target detections, but with the range only limited to a couple of kilometres or even metres, depending on the target of interest. From the high powered illuminators, FM radio are reported to provide a good long range detection capability. However, due to the low bandwidth content of these signals, the range resolution is low and accordingly, the target position estimation is inaccurate.[2] On the other hand, DVB-T emissions are high bandwidth signals[3] that result in an attractive target position accuracy due to an increased range resolution, but are limited in range to a few 10's of kilometres. Accordingly, the research trend in developed nations are slanted mostly toward the utilisation of DVB-T for shorts range, high target position accuracy applications and exploit FM radio for long range detections with a reduced target position accuracy. As a result, multiband systems are currently being developed that makes use of FM, Digital Audio Broadcasting (DAB) and DVB-T that provides good short and long range detection capabilities with a varying degree of target accuracy [15].

1.2.1.2 Historical Multistatic System

Multistatic systems using Doppler measurements have a long history and also dates back to WWII where these systems were mostly used in missile tracking and aerospace research. The earliest systems operated only in transponder mode, for example the Doppler Velocity and Positioning System (DOVAP) which was

[2] Inaccurate in the scope of this thesis refers to position errors larger than 1.5 km's.
[3] The bandwidth of DVB-T signals are in the order of 7.6 MHz.

developed during WWII and later adapted for the United States (US) army to track ballistic missiles. DOVAP operated with a ground based CW interrogator, 36.8 MHz and transponder on the missile under test. In the order of 20 receiver stations was placed around the missile launch site and the Doppler tracking was initialised during missile launch, but signal interruptions led to annoying re-initialisation problems for Doppler only tracking.

The VHF Passive Ranging Doppler System (PARADOP) was the first bistatic passive ranging Doppler system as no transponder was fitted on the missile, therefore only tracking the skin return of the missile. It used newly developed phase locked loops (for that era) that compensated for the loss in Signal to Noise Ratio (SNR) compared to the transponder systems. Follow up systems, for example Doppler Phase Lock (DOPLOC) also used phased locked loops and was able to track in both skin mode and transponder mode from only a single receiver site.[4]

Also exploiting the phase lock loop technology was the Space Surveillance System (SPASUR), however instead of Doppler measurements, bearing measurements were made at each station for triangulation purposes. It was able to track non-cooperative satellites and remained the survivor of the multistatic triangulation systems. It operated with 3 ground based, 1 MW, CW illuminators along with 7 receiver stations and operated at a frequency of 217 MHz.

From 1960, the Doppler systems were replaced by the monostatic monopulse tracking radars, for example the AN/FPS-16 radar, and to this date remains the primary instrumentation for space surveillance. Lastly, Sequential Correlation Ranging (SECOR), was the first range-only multilateration system used for missile tracking. The system operated with a ground based Frequency Modulated Continuous Wave (FMCW) interrogator, a transponder on the missile and 3 or more receiver stations with very long base lines (500 nmi). For a more in depth discussion on the system mentioned above, see Scavullo and Paul [16].

[4] In the case of using this approach to track a target, the target is required to move in a predictable manor over a significant period of time, like for example a satellite in orbit.

1.2.1.3 Estimation Theory Evolution

State estimation theory, commonly referred to as tracking filters, was invented by Gauss in 1809 [17]. The application at the time was to obtain the best estimate of orbital parameters for asteroids by using least square estimates in combination with a Gauss Probability Density Function (PDF) approximation. It was only until Aitkin [18], replaced the least squares method with the weighted least square method to derive what is currently known as the Gauss Aitken filter minimum variance algorithm. Shortly after this, Swerling published the first recursive filter in 1958 [19], which is based on a recursive minimum variance variant of the Gauss Aitkin filter, and named it the Swerling filter. Shortly after this, Kalman published his filter and today, commonly known as the Kalman filter [20]. The Kalman filter is essentially also a Swerling filter, thus also a recursive minimum variance method, but with the equations ordered differently [21].

In a recent book Morrison [21], he points out the earlier work of Gauss and argues the place of the Gauss Newton (GN) filter, which have seemed to be "forgotten" due to the popularity of the Kalman filter. Morrison also states that limited processing power in 1960s caused Gauss filters to lack the recursive filters, however with current computer technology, this limitation seems to be breached. Also, with very attractive properties, such as virtually no initialisation requirements, a strong argument is made to use this filter in applications such as CR. The newest addition to the GN filter family is the recursive format, called the Recursive Gauss Newton Filter (RGNF) [22]. All of the advantages associated with the GN filter are inherited by the RGNF, but with less computation complexity.

1.2.2 Motivation

Developing nations cannot afford expensive Air Traffic Control (ATC) radars, and more importantly, have difficulty with the logistic costs of around the clock support, since there is a shortage of skilled technicians. The result is very poor ATC in most of Africa due to the lack of aircraft location data and in particular,

the lack of en route monitoring has also resulted in tragedies. For example, a crash just after take-off and close to the end of the runway; days of fruitless search was conducted to locate the crash site due to the lack of aircraft position information and as a result, many survivors died needlessly from sustained injuries.

Currently, CR technology is known not to be mature enough to replace active radars, although significant time and research effort has been invested in the technology. However, there are many benefits associated with CR technology. Probably the most attractive feature is the cost effective nature of the system due to the absence of a transmitter subsystem and associated power consumption. No need for dedicated spectrum allocation and typically no moving parts also add to the ability of these systems to operate covertly and accordingly have a dual use of military as well as civilian application. Furthermore, these systems are also believed to have resistance to low observable targets due to the lower carrier frequencies (considering FM radio) and bistatic nature.

Therefore, as mentioned above, one method to circumvent the high associated cost with ATC, is to explore the possibility of using CR for ATC purposes in scenario's where it makes sense. For example, benefits such as adding safety to small landing strips within the African context is specifically seen as a potential benefit where conventional ATC radars are not economically viable. Developing nations are currently well equipped with high powered FM transmitters and it is expected that these emitters will be well maintained for the foreseeable future. Furthermore, as seen from the literature provided on CR, FM radio has been proven to be an exploitable waveform of opportunity for air-surveillance purposes [23, 7, 24] and therefore considered the primary illuminator to exploit for this thesis. Together with FM radio, cell phone technology is also well established in developing countries with excellent coverage in most areas and equally well maintained due to the commercial value associated with this infrastructure. In return, this would then allow for a cost effective network of CR receiver nodes to be deployed over the region where air-surveillance is required [25].

Recent advances made in the field of digital electronics, as well as Global Po-

sitioning System (GPS) technology also allowed for a cost effective networked implementation of the system. Powerful computers and high dynamic range digital receivers now overcome the limitations experienced in the 1960's and as a result make the technology considered back then, a much more feasible and cost effective solution presently. Modern day GPS technology has the ability to synchronise geographically separated receivers around the world down to a few parts per billion accuracy at relative low cost. In fact, a current trend in surveillance techniques is to employ many low cost, low power sensors connected in a network [26, 27, 28]. Lastly, the development of the RGNF is also seen as a important milestone as it allows for a flexible, non-processing intensive filter implementation that promises to resolve the filter initiation problems experienced since the 1960's.

Although digital audio and video broadcast technology are imminent, even in developing countries, FM radio is believed to survive for a long time since the digital signals are unreliable in terms of propagation, especially for mobile users in cities or in hilly terrain. CR technology is also quite capable of using new transmitters of opportunity and the system can be designed to accommodate these if and when they become available.

1.3 Problem Description

The research intent of this thesis is to propose a low cost ATC system within the developing countries context, both from a procurement as well as maintenance perspective. A system is envisioned that harvests emissions from all the FM broadcast sites in a particular area using receivers placed at optimal positions in a geographical region. In this fashion, a multiple receiver approach is used that allows for a cost effective target location estimation. An inherent complication in exploiting FM for CR purposes is the low bandwidth content of FM broadcast signals that results in a very low range resolution. Exploiting a single FM radio channel, the typical range resolution would at best be 1.5 km for favourable broadcasting content and in the worst case scenario, where "silence"

is broadcasted, the range resolution could typically be several 10's of kilometres. In the case of using range multilateration, the resulting Geometric Dilution of Precision (GDOP) effect leads to insufficient target position accuracy for ATC purposes. The logical approach to address the insufficient target position problem would be to follow a similar approach than the developed countries, hence use DVB-T. However the lack of DVB-T infrastructure in the developing nations context, forces the use of FM broadcast emissions. An alternative approach to the problem at hand is to turn the focus to the excellent Doppler resolution achieved with a CR system. In the case of FM band CR, the typical integration time is seconds, rather than milli-seconds as in the case of conventional radars. Accordingly, the aim would then be to use multiple receiver sites and perform target tracking by using only the Doppler shift of the target measured at each site. As seen from the section on historical systems, Doppler only tracking was a well known method of tracking satellites and ballistic missiles due to the predictable movement and long latencies. However, for ATC these luxuries are not the case and make the direct use of these solution absolute for this thesis.

1.3.1 Research Hypothesis

Following the problem description above, the research hypothesis for this thesis is formulated as follows:

A Commensal Radar system can track a target with high spatial resolution, using Doppler only information in a single transmitter, multi receiver configuration, where the receivers are optimally placed.

The research questions associated with this hypothesis are:

1. How accurate can a multistatic receiver system estimate a target's position according to theory, by observing only the Doppler shift of the target?
2. Does the number of receivers influence the position estimation accuracy in point 1?

3. Does the geographical placement of the receivers influence the position estimation accuracy in point 1?

4. How does the ability to accumulate time history information influence the position estimation accuracy in point 1?

5. Could a target tracking filter track a target in Cartesian space to the same degree of accuracy than set in theory, hence point 1?

6. How is a tracking filter initialised using Doppler only measurements?

1.4 Scope and Objectives

This thesis aims to investigate and evaluate the performance of a multistatic Doppler only tracking system using FM band illuminators of opportunity. Considering the implementation of a full operational Doppler only tracking system for ATC purposes is beyond the scope of this thesis. Therefore, the scope of this thesis is outlined in Section 1.4.1 and secondly, the research objectives are listed in Section 1.4.2.

1.4.1 Scope

The author of this thesis was involved in the development of an prototype multistatic CR system that consisted of two stages. The first stage included the development of a real-time data processing chain up to and including the detection stage in bistatic range and Doppler. This was the topic of another PhD student enrolled at the University of Cape Town (UCT) [29]. The second stage included the conceptualisation of the target tracking stages and accordingly scoped to be the topic of this thesis. Furthermore, a complete consideration of all the aspects associated with a multistatic Doppler only tracking system, for example multiple targets, automated processing etc., would have expanded the scope of this study. Therefore, the following limitations are imposed on this thesis:

- A detailed consideration of a single transmitter, multiple receiver scenario is followed. All theoretical analyses presented in this thesis are based on the assumption that the target is moving in a 2-Dimensional (2-D) space with a constant velocity (note, the theory is not limited to a constant velocity, it only needs adaptation to accommodate acceleration). Evidence of tracked targets with non-constant velocities are also provided, but accordingly not benchmarked against the theoretical bound.

- A much less detailed consideration of a multiple transmitter, multiple receiver scenario is considered for this thesis.

- In the case of real-data, only a single target, with available Automatic Dependence Surveillance - Broadcasting (ADS-B) truth data is considered for tracking, which is done off-line and after the fact. Therefore, no automatic target establishment and handling of false detections are considered.

- Target tracking is based on a Probability of Detection (PoD) = 1 and assumed to have a Line of Sight (LoS) between the transmitter-to-target-to receiver. This is generally the case with high flying commercial aircraft that was considered in this thesis. In case of missing detections, interpolation was used.

- Although 3-Dimensional (3-D) experimental data is collected, only 2-D tracking is considered for validation purposes. Therefore, as all the target truth data was available, the 3-D detection data was easily transformed to a 2-D scenario.

- Only the RGNF is considered for tracking purposes in this thesis.

- Lastly, the aim of this thesis is limited to evaluating the feasibility of a Doppler only tracking system. Therefore, no optimisation is considered and would be the focus in follow on research in which the aim would to qualify Doppler only tracking for ATC purposes.

1.4.2 Objectives

Mentioned previously, the main objective of this study is to gain insight into a multistatic FM band CR system. This broad objective is broken down into the following, more focussed objectives:

Mathematical analysis: In literature a broad range of literature exists on the topic of target tracking by observing the target's; 1.) Range or 2.) Bearing or 3.) Doppler. From the three variables, the Doppler only tracking achieved the least amount of attention and more specific, very limited literature exists on considering receiver placement for CR and the additional benefits time history information could play in the Cramèr-Rao Lower Bound (CRLB).

The aim of this study is to build on the current literature in order to understand the limitations of a Doppler only tracking system. It is anticipated that such an analysis will lead to new insights that could be used to answer further research questions, for example research questions 2 to 4 as listed in Section 1.3.

Simulation verification: All theoretical concepts will be verified by simulation.

Proof of concept with a real-world experiment: To the authors knowledge, Doppler only tracking within the CR community is yet to be proven with a real-world experiment.

This study aims to compare the theoretical and simulated results with a real-word experiment. The main objective would be to plan and execute a field experiment, in which a multistatic CR system is used to detect and track a single commercial airliner over a given time period by observing only the Doppler shift.

Importantly, notice that this objective is aimed at evaluating the feasibility of Doppler only tracking for CR. Thus, no attempt would be made to qualify Doppler only tracking for ATC purposes in this thesis, but rather left as future research.

1.5 Contributions

1.5.1 Statement of Originality

The author believes that the following parts of this work constitute original contributions to the field of CR:

- Pointed out that time history information should be incorporated to the CRLB when compared to a tracking filter. In this thesis, time history information is incorporated to the CRLB in a recursive format and referred to as the Cumulative CRLB (CCRLB).
- Proved the hypothesis of Doppler only tracking with a multistatic CR system. To the author's knowledge, the results presented in this thesis are first real-world results within the CR community to display the successful tracking of a commercial airliner by observing only the Doppler shift from geographically separated receiver sites.
- First published results for comparing theoretical, simulation and measured data for Doppler only tracking.
- Pointed out the importance of keeping the observation matrix well-conditioned in Doppler only tracking and further described what factors influences the condition of the observation matrix.
- The receiver position placement analysis and the importance of receiver placement in a multistatic Doppler only tracking system.
- The feasibility analysis of using a Multiple Input Multiple Output (MIMO) configuration for Doppler only tracking.
- First published results of the RGNF applied to a real-world application.

1.5.2 Publications

The research detailed in this thesis has contributed partially or entirely to the following publications:

M. Inggs, C. Tong, A. Mishra, and F. Maasdorp, *Modelling and simulation in commensal radar system design*, Radar Systems (Radar 2012), IET International Conference on, pp. 1-5. [30]

C. Tong, F. Maasdorp, and M. Inggs, *Performance improvements using the separated reference configuration in a multi-site commensal radar system*, in International Conference on Radar, pp. 1-6, Sep 2013. [31]

F. Maasdorp, J. Cilliers, M. Inggs, and C. Tong, *Simulation and measurement of propeller modulation using FM broadcast band commensal radar*, Electronics Letters, vol. 49, pp. 1481-1482, Nov 2013. [32]

M. Inggs, C. Tong, R. Nadjiasngar, G. Lange, A. Mishra, and F. Maasdorp, *Planning and design phases of a commensal radar system in the FM broadcast band*, Aerospace and Electronic Systems Magazine, IEEE, vol. 29, pp. 5063, July 2014. [33]

F. Maasdorp, R. Nadjiasngar, and M. Inggs, *A Cramèr-Rao Analysis on Receiver Placement in a FM band Commensal Radar System based on Doppler only measurements*, in Radar Conference (Radar), 2014 International, pp. 1-6, Oct 2014. [34]

F Maasdorp, R Nadjiasngar, and M Inggs, *Target Tracking using Doppler Only Measurements in an FM Broadcast band Commensal Radar*, Electronics Letters, Accepted for publication [35]

F. Maasdorp, J. Cilliers, M. Inggs, and C. Tong, *FM band Commensal Radar Technology for the Detection of Small Aircraft and the Measurement of Propeller Modulation*, in Radar Conference (Radar), 2015 International, Accepted for publication [36]

1.6 Thesis Outline

The content of this thesis are summarised below per chapter.

Chapter 1: A brief introduction to CR is provided. The research problem is formalised to point out what the current limitations of CR are and use this as a motivation for this thesis.

Chapter 2: A more detailed survey of CR literature is presented in this chapter. This includes an overview of multistatic systems, illuminators of opportunity that is suitable for CR applications, passive tracking methods and commercially available system.

Chapter 3: An overview of the multistatic receiver deployment in the Western Cape, South Africa is presented in this chapter. The location of the 4 receivers are given, the equipment used is described in more detail and an overview of the data processing chain is presented. Lastly, the 2-D target observation scheme considered in this thesis is presented in the form of an overview of the target model, the bistatic range equation and bistatic Doppler equation. Although not considered in this thesis, insight to 3-D target tracking is presented by the inclusion of target altitude.

Chapter 4: The theoretical concepts presented in this chapter aims to establish the mathematical boundary conditions for target tracking accuracies. The short fall of excluding time history with standard Cramèr-Rao theory is highlighted and new theory is presented that does take time history information into account with the assumption that the target is moving at a constant velocity. The developed theory is verified by simulation, in which case a RGNF was used to track a target with constant velocity by observing bistatic range and Doppler information as well as Doppler only information. Lastly, the effect of target motion occurring at non constant velocities are evaluated and an analysis of using multiple transmitters/multiple receivers is also performed.

Chapter 5: The results of the field deployment are used to validate the theoretical concepts developed in Chapter 4. Target tracking results using the RGNF is presented for both range Doppler tracking and Doppler only tracking. The results presented here forms the basis of the paper by Maasdorp et al. [35].

Chapter 6: In this chapter, the developed theory of Chapter 4 are used to evaluate receiver placement combinations by means of a simulation. In return, this provides insight on the method of selecting receivers that would minimise the error performance of a Doppler only tracking system. The results presented here forms the basis of the paper by Maasdorp et al. [34].

Chapter 7: A summary of conclusions are presented in this chapter and recommendations on future research are made.

Chapter 2

Literature Review

2.1 Introduction

The goal of this chapter is to provide sufficient background information as part of the motivation for this thesis and support the novelty of the contributions claimed in the field of CR. The launch of the Sputnik-1 satellite in 1957 sparked the need to detect and track space borne objects that resulted in significant advances made in the field of estimation theory. The methods of detection and tracking also soon became apparent in other application domains, for example ballistics missile tracking and sonar passive monitoring that resulted in a vast number literature publications on these topics, as will be seen throughout this chapter. The common relationship amongst the application domains mentioned above, include the need to *detect* and *track* an object and accordingly, these are the two main topics reviewed in this chapter with the focus on CR.

In Section 2.2, an overview of the predominant work for target detection in CR is presented. At the forefront of this research are the search for suitable illuminators of opportunity and to combat the effects of Direct Path Interference (DPI) and clutter, where DPI is arguably the greatest limitation to CR. Further, improved target detection techniques are also reviewed and presented as; integration time considerations and multichannel system configurations. In Section 2.3,

an overview of estimating a target's position and velocity from noise corrupted measurements are presented. Firstly, estimation using other than frequency only measurements are reviewed and secondly, estimation based on frequency only measurements are considered, where frequency measurements refer to the detection of a target's Doppler shift as a result of relative movement between the sensor and target.[1] In Section 2.4 recent trends in CR are reviewed, a brief overview of current commercially developed CR systems are given and finally, conclusions are drawn in Section 2.5.

Before proceeding with literature review presented in Section 2.2, some background information on passive measurements and tracking are first provided, followed by defining the terminology used in this thesis to avoid any possible confusion.

2.1.1 Passive Measurements

As mentioned above, the launch of Sputnik initiated the space application to passive tracking that also flowed over into the ballistic missile and sonar applications of passive tracking. Over the years, little work has been published on passive tracking in the radar community in comparison to the sonar community. Two possible reasons for the lack of publications in the radar case include a fairly high signal processing requirement for the radar application as a result of signal interference and secondly, an active (object is emitting) target is assumed in the sonar case, that ultimately simplifies the geometry and receiver requirements for detections. However, the considerable increase in computational processing power and advancements made in the digital domain over the last few years, the required digital signal processing for air and sea surveillance applications are becoming increasingly more affordable. For these applications, the requirement would be to determine a target position from measurements that is typically corrupted with noise. In case of passive measurements, these are normally based on

[1] In the case of this thesis, although not limited to it, the receiver is assumed to be stationary and the target moving.

- Time Difference of Arrival,
- Target bearing and
- Doppler shift.

In case of CR, the TDOA between the direct path and surveillance path is a measure of the bistatic range of the target that is located on an ellipsoid, in which the foci points are the transmitter and receiver. In order to resolve the position of the target unambiguously using range measurements, at least a combination of three Transmitter-Receiver (T-R) pairs are required. Alternatively, one T-R pair can in addition to the bistatic range measurement, also make a bearing measurement on the target to resolve the target unambiguously.

Bearing only Tracking (BOT) locates and accordingly tracks a target by measuring the direction of arrival of the target reflections. To measure the target location unambiguously, either one of the following two scenarios are followed. Firstly, two receivers measures the respective bearings from two spatially separated platforms or secondly, a single receiver needs to move and measure the bearing of the target over time.

Using the Doppler shift is in effect the same as for the BOT case. Measuring the Doppler from a single site is ambiguous [37] and also requires more than one receiver to locate the target position unambiguously. However, if bearing and Doppler measurements are made from a single site, the target position can be determined unambiguously [6]. In the case of this thesis, the focus would be on using multiple receivers measuring only the Doppler shift of the target.

2.1.2 Estimation Theory

As mentioned in Chapter 1, state estimation theory is a well established field of research and dates back to the 1800's. As the theory evolved over the years, a significant amount of jargon found it's way into the field, hence making it difficult to categorise estimation theory. Therefore, in an attempt to review estimation

theory, the approach followed by Kay [38] is adopted for this thesis. Accordingly, estimators are broadly categorised under;

- Classic estimation
- Bayesian estimation, and
- Closed form solution

The first step in estimation theory is to mathematically model the data. As data is inherently random, a typical way to model it is to derive some PDF of the data. Therefore, any class of estimation based on the PDF of the data is termed classical estimation when the state vector is assumed to be deterministic, but unknown. Therefore, when the PDF of the data is known, the CRLB will give the minimum variance of an unbiased estimator. The Maximum Likelihood Estimator (MLE) is a numerical way to determine the Minimum Variance Unbiased (MVU) estimator. However, if the PDF is not known, Least Squares (LS) is used as a suboptimal estimator. As an example, the GN filter is a non-linear LS estimator whereas grid search techniques will be classified as a numerical MLE. Further, iterative techniques are mostly used where a linearised model is iterated to a point where the least square solution is close to the true state.

In the case of limiting the estimator to a range of values that is known a-priori, the deterministic nature as stated above can be relaxed and be replaced by a PDF of the range of values expected, known as joint PDFs. This type of estimator is referred to as Bayesian estimators. When the joint PDF between the range of estimates and data PDF are know a-priori, this is known as a Minimum Mean Square Error (MMSE) Bayesian estimator.[2] When the joint PDF can only be derived after, a Maximum a-Posteriori (MAP) estimator[3] is used, but results in a hit or miss scenario.

[2] Two examples of MMSE estimators are; the well known Kalman filer (under which the joint PDF's are Gaussian) and the Wiener filter (under which the joint PDF's are not Gaussian and the MMSE estimator constraint to be linear).

[3] An example of the MAP estimator is the well known particle filter.

Lastly, a closed form solution is a mathematical expression where the target state variables are directly derived from the measurements. Closed form solutions are significantly less computationally intensive than the other estimators and importantly, does not require an initial estimate. However, measurement data are usually corrupted with noise that severely degrade the estimation capability of a closed form solution. Therefore, closed form solutions are in general only useful for relatively high SNRs.

2.1.3 Terminology

In most areas of science and engineering the terminology use is not always straight forward and therefore, the following defined terms will be used in this thesis:

Bistatic is a radar configuration consisting of a single T-R pair that is spatially separated.

Multistatic is a radar configuration consisting of a single/multiple receiver(s) exploiting a single/multiple transmitter(s).

Multichannel is referred to when multiple RF channels are used to exploit a single RF carrier frequency. For example, using multiple channels to exploit a single radio station in the FM band.

Multifrequency is referred to when multiple RF channels are used to exploit multiple carrier frequencies within the same band. For example, using multiple RF channels to exploit multiple radio stations in the FM band.

Multiband aims to exploit emission over different bands, for example FM and DVB-T. This is also referred to as a hybrid system [39] that enables a single platform to perform different applications. For example, exploiting FM and DVB-T results in a platform that is capable to perform long range air-surveillance, as well as short range air-surveillance with a high degree of accuracy.

2.2 Passive Measurements

As described in Chapter 1, target detection is performed by cross correlating the direct path and the surveillance path over several range delays and matched Doppler filtering to obtain a Amplitude/Range/Doppler (ARD) map. Therefore, assuming this detection method, several important aspects are first discussed. These include the use of suitable illuminators of opportunity and the requirement of the DPI and clutter suppression in the surveillance channel. As very low signal power is reflected of the target, the requirement of extended integration times are discussed and finally, exploiting multiple channels to improve target detection are also discussed.

2.2.1 Illuminators of Opportunity

This section aims to presented a overview of individual illuminators of opportunity where the combination of illuminators are considered in Section 2.4.1.

Established research in the field of CR includes a long list of feasible illuminators opportunity that is mainly categorised in high powered illuminators of opportunity and low power illuminators of opportunity. Further, depending on the waveforms content, side lobe control is also an important consideration in CR and some space borne illuminators are also mentioned.

2.2.1.1 High Powered Illuminators

The search for high powered illuminators of opportunity attracted most of the early search for suitable illuminators of opportunity in CR. In 1986 Griffiths and Long [5] investigated the pulsed nature of analogue Television (TV) to exploit for radar purposes. Interestingly, the paper listed the two limitations at the time as; dynamic range and processing power, that received significant research over the last decade. For the first, an eight bit Analogue to Digital Converter (ADC) only gave 48 dB dynamic range, where 90 dB was required and for the second,

also realised that intensive signal processing was required to cancel the DPI and clutter in the surveillance signal.

In 1999 Howland, published results on using TV based CR to locate and track commercial airliners up to 260 km from the CR receiver. In 2005 he also published results in which he used FM radio stations to detect commercial aircraft at approximately 150 km from the receiver [7]. However, both these papers are rather discussed in Section 2.3.2 under passive tracking. Besides Howlands' paper, 2005 has seen several papers on illuminators of opportunity. Saini and Cherniakov [40] published results on the analysis of the Digital Television (DTV) ambiguity function. From the ambiguity analysis, undesirable deterministic components were identified, like the guard interval and pilot carriers and successfully suppressed by 40 dB. In 2005, Griffiths and Baker [23] published a two part paper; the first paper considered the performance prediction of CR for three illuminators of opportunity namely, FM (considered high power), DAB and GSM (low power). Possible detection ranges, assuming an 1 m^2 target, was calculated as a function of the bandwidth, integration time and transmit power. The second paper described the waveform properties of FM, DAB and GSM and concluded with an important consideration in CR; namely range and Doppler resolution in CR largely depends on two properties, the transmitted waveform properties as well as the geometry between the T-R pair. In case of the waveforms properties, their analysis included the use of the Auto Ambiguity Function (AAF) for the three respective waveforms of opportunity.

In 2007 Lauri et al. [41] presented an analysis of FM band CR. The FM waveform properties was analysed and they determined that the range resolution depends on the standard deviation and kurtosis of the modulated FM signal. They also reported that the silence period in FM severely degrades the range resolution due to the pilot carrier present in a FM signal. Lastly, they emulated an FM radio transmitter and verified the emulator with real data recordings. The emulator would later also be used to develop optimised DPI cancellation algorithms (see Section 2.2.2).

In 2009 O'Hagan [24] also performed an in depth analysis of FM band CR. Work

included an investigation of practical antenna placement to reduce DPI, receiver hardware considerations in the form of superheterodyne and direct sampling receivers, signal processing in the form of DPI and clutter suppression and lastly, target detection by means of a Constant False Alarm Rate (CFAR) detector. Further work in 2009 included a publication by Bongioanni et al. [9] that proposed a Cross Ambiguity Function (CAF) method to reduce the ambiguity peaks associated with DVB-T emissions. They exploited the fact that prior knowledge of the unwanted peaks are known through the AAF using the reference signal, prior to the CAF calculation. Accordingly, this allowed to perform the CAF with a linear filter, based on the knowledge of the ambiguity peaks, to remove the ambiguity peaks with a less computational complex solution over Saini's approach and with an additional benefit of no synchronisation required.

In 2012, Malanowski et al. [42] explored the feasibility of using FM illuminators for long range surveillance as well as for manoeuvring target detection. Experimental results demonstrated the long range detection capability with a large commercial aircraft detected at a bistatic range of 600 km, whereas the manoeuvring target detection capability was illustrated by following two manoeuvring fighter jets over the ARD map for bistatic detection ranges between 60 and 100 km. Additional long range detection results of 700 km (bistatic) was also reported on commercial aircraft in Malanowski et al. [8].

2.2.1.2 Low Powered Illuminators

Low power illuminators of opportunity also received significant research over the last decade. Tan et al. [43] was the first to investigate the feasibility of exploiting GSM for CR application in 2003. Result demonstrated that target detection ranges in GSM is limited to the low radiated power (in the order of 50 W), rather than by the range and Doppler ambiguities of the GSM waveform. These were respectively given as 86.55 km and 1733 Hz. For example, a commercial airliner flying towards the baseline at 900 km/h would have a Doppler of approximately a 1500 Hz and therefore, the detection range would rather be limited to the SNR and Signal to Interference plus Noise Ratio (SINR) in the CR. Follow up

work included the detection of sea and air targets [12] of respectively 1 km for ships and 3 km for commercial airliners. They concluded that the poor detection results were caused by the dense GSM network in Singapore as it maximised for user capacity with fairly small cell sizes (1.5 km to 2 km) and low transmission power. Therefore, in less dense environments, the cell size would be large (order of 35 km) and CR could be more suitable for surveillance purposes in such areas.[4]

In 2007, Guo et al. [44] investigated WiFi as an illuminator of opportunity for application to short range surveillance (less than 4 m). The AAF of the WiFi 802.11b beacon signal was analysed and the range and Doppler resolution established to be approx 25 m in range and 50 kHz. Results consisted of simulated and experimental data in which a moving human was detected in a anechoic chamber environment. Follow on work demonstrated the system's detection capability in an outdoor environment where a walking human was detected [45]. Although detections were observed, the effects of DPI was severe and required further research to resolve for consisted target detections.

In 2009, Falcone et al. [11] published a method to suppress the range sidelobes in a WiFi 802.11b type beacon signal, caused by the Barker code in the signal. By reducing these sidelobe levels to a Peak to Side Lobe Ratio (PSLR) of 40 dB, they demonstrated with experimental data that a motor vehicle could successfully be detected without the need of DPI and clutter suppression. Follow up work by Falcone et al. [46] included the exploitation of the 802.11g type WiFi signal, in which experimental results also demonstrated the detection of a running man following a moving car in close proximity to each other, in this case the separation distance was less than 10 m. Further, the importance of using sidelobe control, as well as reducing the effect of DPI and clutter suppression for target detections was made clear due to the low Radar Cross Section (RCS) of humans. Lastly, they also demonstrated effective Doppler side lobe control for WiFi signals as the exploited beacon signal is broadcasted at irregular intervals, hence causing Doppler ambiguities [47]. Also in 2009, Petri et al. [14] considered the use of UMTS for CR and performed an ambiguity function analysis for

[4] Note, follow up experiments with a multichannel approach did improve on these results, regardless of the low power transmissions, see Section 2.2.4.

UMTS signals, that is also an Orthogonal Frequency Division Multiple Access (OFDMA) type signal. Important outcomes from the analysis included the high range resolution properties and low sidelobe levels provided by UMTS signals. The range resolution obtained was 33 m due to the 5 MHz bandwidth of the UMTS signal and typical integration times where reported to be 0.05 ms. Further, the low sidelobe levels experienced with exploiting UMTS signals are due to the scrambling codes used by the UMTS base stations to reduce the frequency interference at the mobile stations.

In 2010, Chetty et al. [13] explored the use of WiMAX for Marine Surveillance. They performed an ambiguity function analysis for WiMAX signals, considering the 20 MHz bandwidth option. The range resolution obtained by using this option is 5.6 m and the allowable integration time around 400 ms. They further published simulation results in which the following detection ranges are possible; a 10 km detection range on large ships and a 2-5 km detection range for small or medium ships. Colone et al. [48] also published simulation results for suppressing the ambiguous peaks in the CAF when exploiting WiMAX signals. The peaks in the CAF, as in case of the DVB-T signals, were caused by the guard interval and the pilot carriers. These unwanted peaks were successfully suppressed to a PSLR of greater than 35 dB in CAF by using an inverse filter approach.

In 2011, Krysik et al. [49] were successful to detect traffic along a road using GSM as the illuminator of opportunity, in which they envisioned to be used for traffic monitoring. Further results published in 2012 included detection results of fast flying aircraft, i.e a MIG-29 and F-16, also using GSM [50]. Unfortunately, no detection ranges were reported in the latter.

In 2012, Stinco et al. [51] investigated UMTS for CR and in particular derived the average monostatic and bistatic ambiguity functions. These ambiguity functions, together with the modified CRLB were then used to evaluate the range and velocity estimation performance of a UMTS CR as function of both the waveform properties and geometry.

2.2.1.3 Space Borne Illuminators

Lastly, Space borne illuminators have also been considered for CR, for example in exploiting GPS signals were considered by Glennon et al. [52] in 2006. Further, in 2009 geosynchronous satellites used for television services and communication were considered by Palmer et al. [53]. In the latter, detection results of a train and aircraft were reported using an experimental system.

2.2.2 DPI and Clutter Suppression

Adaptive filter theory is also a broad field that is highly specialised. However, by using the frame work as set in Haykin [54], two distinct approaches are followed for adaptive filters namely, the stochastic gradient approach and the least squares approach. The stochastic gradient approach typically makes use of a transversal (tapped delay line) or lattice filter structure and an example of such a filter is the well known Least Mean Squares (LMS) algorithm. In case of the LS approach, the aim is to minimise the sum of the error squares of a number of samples, typically referred to as a batch of samples. Filtering is then operated in a recursive (Kalman filter) or non-recursive way (Gauss-Newton).

As suggested in the previous section, one of the major problems in CW bistatic radar, as well as CR is the DPI that cause the reflected signal from the target to be buried under the sidelobes of the direct path. Significant work was done in an attempt to reduce the DPI and clutter in CR.

In 2003 Saini et al. [55] published results to suppress the effects of DPI in his research with DTV, by using a mechanically rotating surveillance antenna. Besides the advantage of having the mainlobe of the surveillance antenna pointed away from the illuminator for most of the time, he introduced a delay tracking loop to cancel the DPI. Further, the rotating antenna also consisted of low cross-polarisation sidelobe levels to further reduce the DPI in the surveillance channel. These two methods resulted in a 30 - 40 dB DPI suppression over a 600 ms Coherent Processing Interval (CPI).

In 2006, Colone et al. [56] published a LS algorithm that substantially reduced the DPI and clutter in an CR. The approach followed was to search for the minimum residual signal power after cancelling the DPI and clutter returns. This was called the Extensive Cancellation Algorithm (ECA) and effectively projected the surveillance signal to two respective orthogonal subspaces, the surveillance space and disturbance space. The surveillance space was then considered to be free from DPI and clutter. However, as the ECA algorithm is a processing intensive approach for DPI and clutter cancellation, a second algorithm was also proposed, called the Sequential Cancellation Algorithm (SCA). This approach included a sequential expansion to reduce the complexity and computation load of the algorithm over the ECA method. The progressive cancellation of the strong targets in order to detect weaker targets were also described. Follow up work included a revision of the ECA algorithm in the form of the ECA Batches algorithm, as well as the ECA Batches and Stages algorithm, that was also intended to reduce the computation load over the ECA method [57].

In 2006 Malanowski et al. [58] evaluated some stochastic gradient adaptive filters to be used for DPI and clutter suppression in CR. Considering a transversal filter structure, the LMS algorithm, as well as Recursive Least Mean Squares (RLMS) algorithm were evaluated and for a lattice structure, the Least Mean Lattice (LML) predictor was considered. He compared the convergence rate as well as the computational complexity of the algorithms and concluded that the LML predictor provided the best convergence rate with the least amount of computational cost between the considered algorithms.

In 2007 Cardinali et al. [59] also compared several adaptive filters for DPI cancellation in terms of computational cost vs. cancellation capability. The LS algorithms considered was the ECA and SCA where as the stochastic gradient approach included the LMS, Normalised LMS (NLMS) and Recursive Least Squares (RLS) algorithms. In conclusion, the LMS and NLMS algorithms were found to have a slow convergence rate, but with a low computational cost and the RLS and ECA to be computational heavy algorithms with very good cancellation capability. The SCA algorithm was selected as the preferred method for the best compromise between cancellation capability and computational cost.

In 2012, Palmer and Searle [60] also reviewed some stochastic gradient methods for DPI and clutter suppression. They considered the Wiener-Hopf as the optimal algorithm, but due to being to processing intensive for real-time operation only used it as a benchmark for comparison to other algorithms. The evaluated suboptimal algorithms, that are numerically optimised for the Wiener-Hopf equation, included the steepest descent and conjugate gradient algorithms that performed near-optimal with a fraction of the computational cost. Other stochastic gradient methods considered were the LMS, RLS and Euclidean direction, with the RLS severe in computational cost, the Euclidean direction delivered good performance for short filter lengths and the LMS was suggested for applications that required a small number of Zero-Doppler range bins cancellations.

2.2.3 Integration Time Considerations

Integration time is an important concept in CR as extended integration times are typically used to increase the sensitivity and accordingly improve the target detection performance. However, having extended integration times, a concept of range-migration is of concern as the target might move over several range and Doppler bins over the given CPI. This sections gives a brief overview of recent publications on the matter at hand.

In 2006, Kulpa and Misiurewicz [61] published a paper, called stretch processing, to combat the effects of range-migration due to long integration time. He demonstrated with a simulation how stretch processing could effectively resolve range-migration. The technique was specifically implemented for range walk and mentioned that it could be extended to Doppler walk as well, but with a significant computational burden.

In 2008, Malanowski and Kulpa [62] summarised the factors than limits integration gain for CR usage. They pointed out that in the typical cross-correlation function, the bistatic range and velocity is assumed to be constant over the CPI. However, under conditions where an extended CPI is used, the bistatic range and Doppler will vary. In order to counter this, they introduced the concept

of stretching the time scale of the reference signal and modelling the motion of the target for acceleration, what they refer to as stretch processing. They then demonstrated with true measured data the need for stretch processing for integration times beyond 1 s using FM as the illuminator of opportunity. Lastly, they also mentioned that if the target motion model incorporated jerk (time derivative of acceleration), integration times of up to 10 s could be used in FM.

In 2011, Malanowski et al. [63] presented a stretch processing method to increase the integration time when exploiting DVB-T emissions. They demonstrated the feasibility of the algorithm with a simulation, as well as experimental data in which time stretching and acceleration was applied to the CAF to counter range and Doppler walk.

2.2.4 Multichannel and Multifrequency Systems

As described in Section 2.1.3, multichannel and multifrequency systems make use of more than two RF channels, that could either follow an antenna array approach for improving target detection, or exploit multiple frequencies to improve target detection or even increase the range resolution.

In 2007, Lu et al. [64] published experimental results of using a 4 channel GSM multichannel system. They demonstrated the benefit of using a multichannel system over a single channel system where air-target detection ranges increased to 6 km over previous detection results of 4 km in Tan et al.[12]. In addition to the increased target detection performance, an additional benefit includes the target bearing estimation.

In 2008, Bongioanni et al. [65] demonstrated with experimental data the benefits of exploiting multiple frequencies from a single FM transmitter. The non-coherent addition of the multifrequency approach allowed for a significant detection performance increased over the single frequency detection approach as the detection performance is more robust in terms of broadcast content and channel multipath effects. They evaluated the multifrequency approach with two prototypes, namely a superheterodyne receiver and a direct sampling receiver. The

direct sampling approach provided slightly better detection results over the superheterodyne approach as the full scale dynamic range of the ADC's were better utilised.

In 2010, Conti et al. [10] presented a paper in which a multifrequency DVB-T system was used to increase the range resolution of the CR. They considered two receiver architectures to sample 4 adjacent DVB-T channels; first a wideband approach where followed to sample all 4 channels simultaneously and secondly, sampling the 4 channels with a narrow band approach and combining the 4 channels afterwards to achieve the effect of an increased bandwidth. Simulation results were presented where they demonstrated that both architectures increased the range resolution as a multiple of the number of channels to exploit, for example exploiting 4 channels resulted in a 4 times increase in range resolution. Follow up work included a paper by Petri et al. [66] in 2011, that demonstrated the practical feasibility of the multifrequency DVB-T system of Conti et al. [10]. With an experimental setup, detection results of a commercial aircraft was presented in which the improved range resolution of exploiting multiple channels were displayed. The system exploited 3 DVB-T channels and a pre-processing algorithm was used to suppress the ambiguities of the DVB-T waveforms.

In 2011, Olsen and Woodbridge [67, 68] published results on improving the range resolution for an FM band CR by using multiple FM frequencies. Multiple radio stations broadcasted from a single transmitter are usually non-adjacently spaced to limit possible interference between radio stations. Olsen and Woodbridge suggested an architecture where these multiple non adjacent radio stations be mixed down to a base band configuration in which all the considered channels are adjacent to one another, resulting in a wider bandwidth that would improve the range resolution. However, the fluctuating signal content in an FM signal results in gaps between the channels and ultimately cause ambiguities in the CAF phase of a CR. To compensate for the gaps, Olsen and Woodbridge [67] suggested a 20 kHz filtering bandwidth of the original 160 kHz signal with a similar adjacent channel spacing. With this approach they did achieve the desired range resolution improvement, however a marginal improvement in range resolution was obtained in this way. For example, 5 channels will result in a combined bandwidth of

100 kHz, that is at best a range resolution of only 1,5 km and accordingly still a low range resolution.

Also in 2011, Greco et al.[69] investigated a method to select the "optimum" bistatic channel within a multistatic scenario for target tracking. The CRLB for each channel was calculated by considering both the geometry and waveform, in which the selection of the best channel was based on the lowest bistatic CRLB for the target velocity, or range, or a combination of the two.

Lastly, in 2013 Colone et al. [70, 71] published a two part paper series on exploiting the use of multiple frequencies and target bearing in an FM based CR system. The first paper addressed the multifrequency approach and the second exploiting target bearing information using multiple surveillance antennas.

2.3 Passive Tracking

In the previous section an overview of target detection was presented. The focus is now shifted to estimating the targets position and/or velocity from the measurement data. As mentioned previously, the measurements used in CR are bearing, TDOA and Doppler shift. Firstly, position and/or velocity estimation based on other than using only the Doppler shift is reviewed, and secondly Doppler shift only based estimation is reviewed.

The remainder of this section is covered in three sections; first individual estimation based on bearing and TDOA measurements are reviewed, secondly the combination of using bearing, TDOA and Doppler measurements are reviewed and lastly, Doppler only measurements are reviewed.

2.3.1 Bearing and TDOA Measurements

Bearing based location estimation has extensively been researched in radar, as well as in sonar and dates back to the 1960's [72]. The typical application was to determine the location of a radiating target using BOT Target Motion Analysis

(TMA). Closed form solutions have been presented by Nardone and Aidala [73] and extensive comparisons between classical estimation techniques in 2-D [74] and 3-D [75] were also performed.

Work on TDOA location techniques started in the 1970's in which the first applications considered using an airborne platform to locate a stationary radiating target [76]. Later the TDOA based location systems also received attention and promised to achieve higher measurement accuracy in a multiple receiver case due to minimising the GDOP. In 1994, Chan and Ho [77] proposed to use TDOA at multiple receiver sites with a grid search technique in 2-D, whereas Mellen et al. [78] proposed a closed form TDOA solution for resolving the location of a radiating source in 3-D space, also using multiple receivers. Torrieri [79] also investigated the performance of TDOA vs BOT, at which time the BOT was considered the most important passive location systems.

Additional care needs to be taken of two important factors in TDOA systems, namely; GDOP and "ghost targets". In 2009, Anastasio et al. [80] reported on the importance of geometry based localisation of a target in a TDOA system. With simulated results, they considered a target moving through an area of interest that was populated with multiple transmitters and receivers. For the flight path, the GDOP was then calculated at all possible receiver locations using only a combination of two transmitters at a time, in which they used Cramèr-Rao theory to select the optimal T-R pairs to minimise the target location error. Follow up work included the inclusion of a non-ideal PoD, thus less than 1 and pointed out the additional processing requirement to handle such scenarios [81].

In 2010, work from Gumiero et al. [82] extended the work of Anastasio et al. [80] to resolving the target position in 3-D, by considering 3 transmitters at a time as opposed to the two considered for 2-D target localisation. It was also shown that 3 T-R pairs could obtain the necessary 3-D position accuracy required for ATC purposes by exploiting DVB-T emissions and resolving the target's position based the bistatic range measurements, hence following a TDOA approach. Follow up work by Gumiero et al. [83] in 2011 published experimental data where the predominant aircraft routes in a Region of Interest (ROI) were derived from ADS-

B data. A selection of flight routes were then selected and the receiver position calculated based on the available FM transmitters in the area, according to the theory in Gumiero et al.[82]. 2-D target position error results were presented with the Root Mean Square Error (RMSE) varying between 580 m and 994 m, based on different selected T-R pairs. However, results were not compared to the CRLB.

As mentioned above, ghost targets are also of concern in TDOA systems when multiple targets (without transponders) needs to be located using a multistatic configuration. Resolving ghost targets in a multistatic TDOA CR system is mainly addressed in two ways; firstly more receivers result in less possible intersections of range ellipsoids and ultimately less ghost targets, as presented by Caspers [84] and secondly, improving the range resolution in a TDOA only multistatic system that would result in less range intersections and accordingly reduce the number of ghost targets [85].

2.3.2 Combined Measurements

Literature obtained from the 1990's, suggests that an improved location estimate is obtained when a combination of TDOA, bearing and Doppler measurements are used. Jauffret and Bar-Shalom [86] published on combining bearing and Doppler measurement to improve the location accuracy of a radiating source using classic estimation theory. In the paper a grid search method was used, whereas Chan and Rudnicki [87] considered the Instrumental Variable estimator (IVE). Blanc-Benon and Bienvenu [88] published results on combining TDOA and Doppler measurements of a radiating source and used a MLE iterative technique to resolve the position. Becker [89] also investigated the possibility of locating a radiating source for frequency agile radar in 2-D, using a MLE and later considered TMA for locating a constant radiating source in 3-D [90].

Besides the Kleine Heidelberg system in WWII and the Lockheed Martin development of Silent Sentry, Howland was the next person to address the CR bistatic configuration for target location and published his first results in 1997 in his PhD

[91] and also in 1999 [92]. It is worthy to note that this was the first documented, full solution of converting bistatic Doppler and coarse bearing measurements into a 2-D target state estimate using analogue TV emission as the illuminator of opportunity and an Extended Kalman Filter. The filter initialisation was done in two stages; firstly an approximate estimate was derived and secondly, this estimate was then improved by using Levenberg Marquad optimisation, but is a time consuming exercise.

In 2005, Howland et al. [7] published their results of exploiting FM broadcasting as the illuminator of opportunity. By exploiting FM emissions, they were able to measure bistatic range, bistatic Doppler and a coarse bearing of the target, but did not publish a method to resolve the target state estimation based on these three measurements. The main difference between this approach and the approach followed by Howland [92] in 1999, was the addition of the cross correlation stage between the reference signal and surveillance signal. Another important suggestion made by Howland et al. [7] was the suggestion to abandon the bearing measurements and rather resolve the target location from a multistatic approach.

In 2005, Tobias and Lanterman [93] proposed to eliminate ghost targets using a Bayesian approach and referred to the method as a Probability Hypothesis Density (PHD) filter. They implemented a particle filter which used both range and Doppler information to detect targets. An important conclusion from the work suggested that the PHD filter's performance is highly sensitive to the PoD and SNR present in the tracking scenario. Hence, this requirement presents a challenging scenario to apply the PHD filter to real radar data.

In 2007, initial work carried out by Morrison et al. [94] first tested the hypothesis of using Doppler only tracking for CR systems. Work included a simulation of a large number of receivers, 8, 16 and 24 in which it was concluded that for a large number of receivers, bearing information diminishes, and allows for efficient Doppler tracking by means of a GN filter. This conclusion directly resulted in the basic starting point of this thesis.

In 2009, another approach to resolve ghost targets was presented by Malanowski

[95]. He presented a closed form algorithm to convert bistatic range and Doppler measurements, obtained from multiple T-R pairs, to a 3-D target location. The closed form algorithm was based on spherical intersection and proved to be very efficient in resolving thousands of bistatic range intersections and eliminating ghost targets. However, as the algorithm is based on static estimations, it is very sensitive to noise and thus not as effective as tracking algorithms. In this thesis, the proposed closed form solution will be used to initialise the tracking filter. In 2012, Malanowski and Kulpa [96] extended the work of Malanowski [95] and compared spherical intersection and spherical interpolation for location accuracy. They found that spherical intersection was more adequate for the CR application and verified results with experimental data .

In 2012, Falcone et al. [97] considered jointly exploiting range and bearing measurements in a WiFi based CR, using classical estimation techniques. In an experiment, a car was used as the target, together with 3 spatially separated receiver antennas to establish 3 independent range measurements of the target and a bearing measurement. The results obtained demonstrated the improvement of target location accuracies when using range and bearing measurements as opposed to range only measurements. Further, a comparison between MLE and LS estimation techniques were performed in which case it was found that the MLE was able to exploit the range and bearing measurement more effectively in a joint fashion than in the case of the LS estimator.

2.3.3 Frequency Meaurements

Estimating the position and velocity from an object's Doppler also received some research in the past, but few in comparison to the magnitude of literature available on the previous two sections. Due to geometry, frequency measurements are broadly categorised in three sections in this thesis namely; a bistatic T-R configuration, a monostatic T-R configuration and a receiver only configuration for a radiating source.

2.3.3.1 Bistatic T-R Configuration

Determining the orbits of the early earth satellites included some of the first applications for Doppler tracking and dates back to the 1960's. R.B Patton Jr.[98] was first to attempt the tracking of a single satellite's orbits with Doppler only measurements. The measurements was taken by a ground based bistatic CW Radar in which he approximated 6 parameters assuming Keplerian motion. He approached the problem as follow; a typical Doppler versus time curve for any passing object is represented by an S-curve. He therefore used a second order differential equation in which he varied the boundary conditions of the equation until the equation matched the observed Doppler measurements, and accordingly estimated the 6 parameters used for the Keplerian motion. He achieved moderately accurate results of position and velocity, but needed to have fairly accurate initial approximations to achieve convergence. For example, the range approximation needed to be accurate to within $50 - 75$ miles and the velocity estimates accurate within $0.5 - 1$ mile/sec.

In 1961 Skolnik published a paper in which he revisited the bistatic radar configuration [99]. In the paper he demonstrated with a closed form solution that the location of a moving target could be determined by observing only the Doppler frequency measurements. He considered a single T-R pair and determined that a minimum 5 frequency measurements are required to locate the target. However, due to symmetry around the baseline, targets could not uniquely be resolved. Further, the solution was also limited to only straight line motion.

In 1970, Salinger and Brandstatter [100] published a paper, describing how an orbiting satellite's orbit and trajectory could be derived from Doppler only measurements using a Bayesian estimator, namely the Kalman filter. They pointed out that 3 receivers would be able to derive an initial position for the orbiting satellite and once initiated, real-time tracking was possible due to the recursive nature of the filter. However, filter initiation was also considered at the time, a time consuming exercise as the initial satellite position needed to be varied until the equations matched the Doppler measurements over time.

In 2010, Xiao et al. [101] considered the 2-D target observability criteria for Doppler only tracking in a multistatic radar using cooperative and non-cooperative transmitters. The work considered up to 6 transmitters, in which they concluded that 4 transmitters delivers the best results for target state observability; where after relatively small target accuracy gains are realised. Lastly, they investigated the effect of integration time on the CRLB assuming a constant velocity model.

A second paper in 2010 was that of Bishop and Smith [102] that also considered target position and velocity estimation based on Doppler measurements in a multistatic radar. The Cramèr-Rao Inequality was revisited for target parameter estimation that only characterised the target velocity estimation, and not position, on Doppler measurements. Additional work included the consideration of receiver placement in a multistatic environment.

In 2012, Nadjiasngar and Inggs [103] was able to recast the GN filter in an recursive form that retained the properties of the GN filter. Based on this development, Nadjiasngar et al. [104] also published some initial simulation results where the RGNF was used to track a target in 2-D space using a multistatic receiver placement and Doppler only measurements.

In 2013, Ristic and Farina [105] reported on using a non-linear Bayesian estimator in the form of a particle filter to estimate a target's position and velocity from Doppler only measurements using respectively 1, 2, and 4 receivers at a time. They considered the effect of false and missing detections and demonstrated the robustness of the Bernoulli particle filter's tracking capability by means of a simulation. They also pointed out the importance of choosing the correct T-R pairs in a multistatic geometry for Doppler only tracking.

2.3.3.2 Monostatic Transmitter-Receiver Configuration

Besides the Doppler tracking in a bistatic T-R configuration, Doppler only tracking in a monostatic T-R configuration was also investigated. In 1980, Levanon [106] derived an approximate closed form solution, using Taylor series expansion to determine a moving target's range, velocity and the angle between the range

vector and velocity vector, by observing radar Doppler shifts as a function of time for a monostatic radar. He determined that at least 4 measurements were required to resolve the range, velocity and angle, but position was not resolved. The solution was also limited to a constant velocity model and he further pointed out that the solution suffered under systematic errors due to the Taylor expansion approximation.

In 1982 Webster [107] revisited the work of Levanon [106] and derived an exact closed form solution for determining the target's range, velocity and angle between the range and velocity vector, using 3 consecutive Doppler measurements. As in the case of Levanon, the application was for a monostatic radar, limited to a constant velocity model and could not determine the position of the target.

In 2007 Torney [108] extended the work of Webster [107], by using multiple receivers, instead of a single receiver to resolve a target's position using only Doppler measurements. A closed form solution was presented in which 3 receivers would allow for two trajectories to be determined in 2-D and 4 would reveal a target's trajectory unambiguously in 3-D. Notice that each receiver uses three measurements of Doppler as determined by Webster [107], hence a total of 12 Doppler measurements are used to estimate the target's position and velocity in 3-D. Similar to the work presented by Webster [107], the solution is only valid for a linear motion target over three consecutive intervals.

In 2011, Shames et al. [109] considered a multistatic radar geometry in which they used polynomial optimisation to estimate the target position and velocity from Doppler only measurements. They also algebraically derived the minimum number of Doppler measurements required to unambiguously resolve the target's state vector, in which they concluded to be 5. Simulation results were also published that demonstrated the performance of the algorithm.

In 2013, Battistelli et al. [110] demonstrated an alternative approach to Doppler only tracking by combining the approaches of Webster [107] and Torney [108] in an unique way for a multistatic radar geometry. They followed a 2 stage filter approach, where the first stage included the initialisation of the observable parameters as set by Webster, namely range, velocity and relative heading an-

gle and then tracking by means of an Unscented Kalman Filter (UKF). Three receiver's sensor data were then fused in a second filtering stage as proposed by Torney, however they made use of a second UKF to determine the target's position and velocity in 2-D. Initialisation at each receiver was done by multiple hypothesis testing over a Doppler sample period of 6 measurements. Finally, they demonstrated the performance of the system with a simulation.

2.3.3.3 Radiating Source

In the last of the three categories, literature on estimating a radiating source's position and velocity from Doppler only measurements are reviewed. This application was particularly researched in the sonar and ballistic missile defence domains and commonly make use of the term differential Doppler processing. Differential Doppler processing is a known method to locate an radiating source in applications where the source centre frequency and bandwidth is unknown and relative motion between the emitting source and sensor is present.

In 1979, Schultheiss and Weinstein [111] investigated differential Doppler measurements by considering a moving radiating source and multiple stationary receiver sites. They found that differential Doppler measurements are uncoupled from the differential delay between the receiver sites and concluded that it could be used to estimate 2-D position and velocity of a radiating source with at least 5 receiver sites. However, this method could only work when the position was known a-priori.

In 1980, Weinstein and Levanon [112] followed up by proposing to track a ballistic missile's CW proximity fuse in 3-D, using a LS estimator and differential Doppler measurements from multiple receiver sites. The fact that the CW proximity fuse slowly changed over the flight justified the use of differential Doppler processing. Further, they reported the importance of having sufficiently spaced receivers to combat Doppler correlation between the respective receivers and the number of differential Doppler measurements required were directly related to the number of variables to be estimated. Lastly, they demonstrated with a numerical example what position estimation errors are expected along the projectile's track by using

a LS estimator, however, the projectiles initial position was also considered to be known. Additional work also included a comparison between different differential Doppler estimation techniques by Weinstein in 1982 [113]. He compared the; 1.) joint processing and 2.) pairwise subtraction differential Doppler techniques as the latter was known to be a more convenient method. The analysis revealed that equal performance was obtained under low SNR conditions, whereas the joint processing technique showed superior performance under high SNR conditions.

In 1987, Stratman and Rodemich [114] published an "almost closed form solution" to estimate the minimum distance between an unknown radiating projectile and a single receiver in real-time, by observing only the Doppler of the projectile. As the source frequency was unknown, they estimated the rest frequency of the source with a Fourier analysis. Further, a non-processing intensive method was proposed that matched the Doppler shifted frequencies to previously stored templates of normalised frequencies. Hence, a basic lookup scheme was used to determine the minimal range between the receiver and the source.

In 1990, Chan and Jardine [115] considered to track a radiating source from Doppler measurements using classical estimation theory. They proposed a grid search localisation technique that required to evaluate the cost function over specified grid points and choose the grid point that resulted in a minimum. They also pointed out that the techniques resulted in a large number of false detections, but compensated for this by using a Kalman filter to allow for a narrower grid search.

2.4 Modern Day State of CR

As the detection capability of CR has been proven over the last decade of research, a number of studies have also been dedicated to determine whether CR could be used to aid to an improved air-picture for ATC purposes. For example, in 2012 Macera et al. [116] described how CR could improve the air picture for co-operative as well as non-cooperative targets in ATC, respectively at high and low level altitudes within the Air Guidance and Surveillance 3-D (ARGUS

3D) programme. He described how a multi-sensor approach, consisting of a Primary Radar (PR), Secondary Surveillance Radar (SSR) and CR, could achieve an enhanced 3-D target location capability.[5]

2.4.1 MultiBand CR

The latest trend in the CR community includes research towards multiband systems. The advantage of a multiband system is that the best properties of the various illuminators is exploited by a single system and therefore, could be used for multiple applications. For example, a multi band system consisting of FM, DVB-T and DAB would have; 1.) long range cover provided by FM, 2.) high range resolution, short range cover with low elevation angles provided by DVB-T and 3.) high range resolution, short range cover with medium elevation angles provided by DAB.

In 2010 Berizzi et al. [117] described a multiband system exploiting DVB-T and UMTS. They considered hardware designs to exploit the signal concurrently, or independently and also presented experimental results for independent detections. For DVB-T, detection results of a bus travelling along a road was presented, where as for exploiting UMTS, detection results of a van travelling along a road was presented. Lastly, concurrent detections, hence using both bands was planned as future work.

In 2010, Shroeder et al. [118] presented Airbus's (formerly known as Cassidian) multiband system with some initial results. The system was able to exploit FM, DAB, and DVB-T all independently. Follow up work included the addition of a real time processing capability of all three bands as well as the instalment of the system in a mobile deployment van with a retractile mast [119]. Further, a 3-D position estimate accuracy of 500 m was reported on air targets exploiting 8 FM transmitters simultaneously. However, multiband detection fusion was set as an objective achieve in future. In a follow up paper by Edrich and Schroeder [120]

[5] For the CR section, they used an similar multifrequency approach than described in Bongioanni et al. [65].

detection results of small aircrafts were presented and several more deployment campaign were reported on with considerable more detection results using single band detections of FM, DAB and DVB-T. Similar conclusions was made in 2014 [15], with multiband fusion still to be reported on.

Other notable multiband papers include the following. Kuschel et al. [121] presented a multiband system exploiting FM, DAB, and DVB-T for application to medium air-surveillance in 2011. In 2012, Olsen and Woodbridge [122, 123] demonstrated with simulation results how FM and DVB-T could be utilised to improve range resolution. Lastly, Macera et al. [124] published a design for a multiband system that incorporates FM, DVB-T and WiFi for utilisation of long and medium range air surveillance, together with short range human surveillance.

2.4.2 Commercially Available Systems

Detailing in depth information on current passive radar systems is beyond the scope of this thesis, therefore for the sake of completeness, only the most notable passive systems available are listed in Table 2.1.

Table 2.1: Current CR systems, detailing configuration and performance.

System	Silent Sentry	Multistatic HDTV Based Radar	Homeland Alerter 100	Airbus Passive Radar	AULOS
Developer:	Lockheed Martin	SAIC, US Army	Thales	EADS	Selex
Decade:	1980-2000	2000	2000	2010	2010
Configuration:	Multistatic; Rx: 1 Tx: up to 6	Multistatic; Rx: 4 Tx:1	Multistatic; Rx: 1 Tx: unknown	Multistatic; Rx: 1 Tx: up to 8	Multistatic: Rx: 1 Tx: unknown
Transmitter Operation:	FM: Real time TV : Non-real time	HDTV: Real time	FM: Real time Upgrading to DVB-T and DAB	FM: Real time DAB: Real time DVB-T: Real time	FM: Real time DAB DAB: Real time DVB-T: Real time
Target Data:	Range, Doppler Bearing	Range, Doppler	Unknown	Range, Doppler, Bearing	Range, Doppler, Bearing
Performance: (Detection range)	100-150 km	30 km	100 km	160 km	Unknown, expected to be similar to Airbus

2.5 Discussion and Conclusion

2.5.1 Discussion

As seen from the literature, a significant body of literature has been published in CR for a different number of targets of interest. As the focus of this thesis is largely based on air-surveillance, the considerations for air-surveillance are summarised in the following key topics;

Suitable Illuminators of Opportunity. Considering only the last 30 years of development trends in CR, modern day CR research started with the quest to establish suitable illuminators of opportunity. This included not only exploring high powered illuminators, but also considering the waveforms properties of the respective transmitters. Feasible, high powered terrestrials based illuminators include; analogue TV, FM, DVB-T and DAB, whereas low power terrestrial illuminators included, WiFi, WiMAX, GSM, and UMTS. Lastly, space borne illuminators were also investigated, for example GPS and TV broadcasting services, but due to extremely low signal power, limited detection ranges were reported using these. In case of the terrestrial based transmitters, short range and long range detection ranges were reported for air surveillance, as well as short range detections of sea targets as well as human detections.

Besides, the Effective Radiated Power (ERP) considerations, the respective transmitters were also evaluated for suitable waveforms properties. Large bandwidth signals provided high range resolution in which WiFi and WiMAX provides the best range resolution properties with only a couple of metres of range resolution, but are of low ERP. Currently, DVB-T provides the best trade-off for high power and high range resolution properties, whereas FM emissions provides the worst range resolution, but are also of high ERP. Lastly, sidelobe control, in range and in Doppler, is an important consideration in most low power signals as well as DVB-T. The ambiguity peaks masks the target returns and additional processing of the

reference signal in required required prior to the CAF.

DPI and Clutter suppression. Arguably one of the most important considerations in CR is to contend with DPI and suppress clutter. Significant research methods to reduce the effect of DPI and clutter for target detection was researched. Almost all current adaptive filter cancellation techniques considered was LS type filters and stochastic gradient techniques that included trade-off studies for cancellation effectiveness vs. processing requirement. From these studies it was established that the conjugate gradient technique provides a good trade-off for cancellation capability vs. required processing power.

Improving Target Detections. In recent years, the focus in CR research shifted towards improving the target detection quality. Extending the integration gain is the first method to increase the target detection quality. However, the integration time is limited to the target velocity, but alternative CAF processing techniques were reported to compensate for extended integration times. As the focus of this thesis is on FM radio, literature suggests that integration time periods up to 10 s could be considered, but in these case a modified CAF is required.

Making use of multiple channels at the receiver to exploit a common frequency is another way to increase the target detection quality. Examples of increased target detection ranges of commercial airliners by exploiting GSM has been reported in literature to exploit this techniques. It basically involves coherent processing between the channels and a further advantage of the technique is the additional capability to exploit bearing information. An alternative way to exploit multiple channels is to exploit different frequencies broadcasted from a common transmitter and non-coherently fuse the data. This technique is typically used for illuminators in which the broadcast content determine the effective bandwidth. In such scenarios, the fusion of data will improve the target detection as it is more robust against signal content fluctuations and channel multipath.

Lastly, exploiting multiple frequencies broadcasted from a common trans-

mitter could also be used to improve the range resolution. Techniques reported to be successful for improving the range resolution included the exploitation of RF channels spaced adjacent to one another and sampled together as a wideband signal. In case of frequencies not being adjacently spaced, a RF down conversion stage is suggested to mix down the non-adjacent RF channels to being adjacent spaced in base band. This was considered for improving range resolution in FM and DVB-T, where only the DVB-T results were promising.

Bearing and TDOA Measurements. Bearing measurements has extensively been researched in the monostatic radar domain and also received considerable attention in the sonar domain. Howland et al. [7] investigated FM illuminators and considered TDOA, bearing and Doppler for tracking. An important conclusion for this study include the recommendation of using multilateration to resolve the target's position as bearing estimates were too coarse. As a result, most CR systems seek to exploit TDOA measurements and use multilateration to resolve the target location as seen from Table 2.1. For FM, most systems exploit multiple FM emitters, for example in the case of Airbus, target location accuracies of 500 m were reported by using 8 FM transmitters and fusing only TDOA measurements.

Ghost targets are of concern in TDOA systems when multiple targets (without transponders) needs to be located using a multistatic configuration. Reported methods to address this concern is to improve the range resolution and increase the number of receivers for the detection. Further, GDOP needs consideration when using BOT and TDOA with multiple receivers. Reported methods to optimise for the GDOP include a Cramèr-Rao analysis to find the optimal T-R pairs in a multiple transmitter single receiver scenario [80, 82]. However, results in which experimental data is compared to the CRLB is yet to be published.

Combined measurements. The combination of TDOA, bearing and Doppler, or subset combinations of the possible measurements, for example bearing Doppler measurements, have also been demonstrated to improve target location accuracies. Different types of Bayesian, as well as classic estima-

tion theories were considered and the preferred solution over closed form solutions that was found only useful in high SNR conditions. Cramèr-Rao theory has extensively been used for locating a radiating source using Bearing Doppler tracking. However, these simulations are yet to be compared to experimental data. Further interesting work included the consideration of using a closed form solution to eliminate ghost targets by combining range and Doppler measurements.[95].

Frequency only Measurements. In comparison to the magnitude of publications on bearing and TDOA measurements, Doppler only measurements received the least attention. For this thesis, frequency only measurements was categorised in three sections based on the transmitter-target-receiver geometry, namely 1.) receiver only configuration for a radiating source, 2.) a monostatic T-R configuration and lastly, 3.) a bistatic T-R configuration.

Doppler only tracking of an emitting source has specifically been researched in the sonar and ballistic missile defence domains. Further, the literature almost exclusively considers locating the target position by using Bayesian and classical estimation techniques, where the nonlinear relationship between Doppler and position is approximated with a linear model and iterated until a close estimate is obtained. Differential Doppler processing was used in case where estimates needed to be isolated from TDOA estimates, for example when no range information is available. It is reported that a 2-D target position and velocity estimation is possible with 4 receivers, but when the exploitation frequency is unknown, 5 receivers are required. It was also mentioned that sufficient receiver spacings is required for the Doppler estimates to be uncorrelated between receivers, but no attempt was made to determine what optimal receiver placings would be.

Considering Doppler only measurements in a monostatic T-R geometry, some closed form solutions were published. Initial solutions required 3 Doppler measurements to determine a moving targets' range, velocity and angle between the range and velocity vectors from a single receiver. Later this solutions was considered using multiple receivers where it was determined that 4 receivers would allow to unambiguously locate a target in

3-D, however it still required $3 \times 4 = 12$ Doppler measurements and is only valid for linear motion targets. Some of the latest literature suggests a 2 stage filter approach to determine the target's position and velocity from Doppler only measurements in a multistatic monostatic radar geometry using 3 receivers. The advantage with such an approach allows for the first stage filter to be initialised from a closed form solution calculation, and then used to initialise the second stage filter. In such a case, Bayesian or classical filters could be used at both stages. Lastly, a Cramèr-Rao analysis for Doppler only tracking in a monostatic radar geometry was also considered and further determined that 5 receivers were required to estimate a target's position and velocity unambiguously in 2-D.

Lastly, Doppler only measurements were also considered in a bistatic T-R geometry. A closed form solution was proposed by Skolnik that required 5 Doppler measurements to determine the target's position ambiguously around the baseline [99]. As in the case of the emitting source target location described above, the majority of the literature considering the estimation of position and velocity from Doppler measurements, are based on the classical and Bayesian estimators. The first include a LS estimation approach for tracking satellites by Doppler only measurements, however latency and convergence requirements typically occurred over a period of 20-40 minutes that is not acceptable for air-surveillance. Later, Bayesian estimation techniques were exploited that allowed for the real time tracking of satellites by means of the Kalman filter that is a much more processing efficient estimator than the LS estimators. However, initialisation of the filter was still a time consuming exercise. Besides these significant advances and some other recent contributions listed in Section 2.3.3, no real experimental data of Doppler only target tracking was found to date and compared to the CRLB for air-surveillance.

Multiband and Commercial System. The latest trend in CR is to exploit all the different types of illuminators of opportunity with a single system solution, known as a multiband system. For example long, medium range air surveillance and short range human surveillance is possible when FM,

DAB and DVB-T are exploited with a single system. These hybrid systems are currently under development, but a significant increase in signal processing power are required to realise such system and to date, no multiband fusion was demonstrated.

Lastly, an overview of CR products were presented that consisted mostly of multistatic systems that exploit multiple transmitters, rather than receivers. Typical bands exploited are FM, DAB and DVB-T and detection ranges of roughly 100 to 150 km is reported, with Airbus currently leading the race towards maturing CR technology.

2.5.2 Conclusion

The section highlighted the most important research relevant to this thesis. The gaps in the current literature were identified and it was further pointed out which gaps this thesis aims to address. As mentioned earlier, the need for a low cost ATC infrastructure in Africa, together with the potential benefits provided by CR and the work carried out by Morrison et al. [94] was the motivation for this thesis.

Therefore, based on the literature provided in this chapter, the following topics are considered for implementation of a low cost ATC system;

Selection of an Emitter. Currently, DVB-T provides the best trade-off for high power, high range resolution properties and as a result the leading most popular emitter to be exploited within Europe. Unfortunately, Africa is not well equipped with DVB-T infrastructure and the only other illuminators that would prevail till DVB-T is eventually rolled out over Africa, is FM radio broadcasting. Hence, multiband is not possible and the only selection is FM radio. One advantage of exploiting FM radio is that the FM band is low enough, 88 - 108 MHz for allowing direct sampling, that was proved to be better than the super-heterodyne receiver architecture. The results obtained in this thesis, will also prove this point.

Method of tracking. From the literature, it is a well established fact that coarse bearing estimates are obtained by exploiting FM. Therefore, discarding bearing measurements, the remaining two options to consider for this thesis are between range and Doppler.

A radar typically requires a wide bandwidth signal to make accurate range measurement. However, in the case of FM radio, the bandwidth of a single radio station is narrow and accordingly results in a low range resolution. Methods of improving the range resolution for FM radio has been suggested in literature, but results indicated that no significant increase in the range resolution was obtained. A different approach is followed in this thesis, namely to use the long integration times that is available in CR, and exploit the excellent Doppler resolution obtained for tracking purposes. Exploiting FM, integration times of 4 s seems reasonable within the ATC environment as obtained from literature. Therefore, this thesis aims to make use of a single transmitter, multiple receiver configuration, in which the respective receivers simultaneously measures only the Doppler shift of the target. Target tracking will then be performed by using only these Doppler measurements.

Processing Considerations. DPI and clutter suppression is one of the most important aspects in CR. For this thesis, the CGLS is seen as the best trade-off between cancellation capability and processing power required and accordingly used in the signal processing stages considered for this thesis. Other processing consideration will be described in Chapter 3.

Selection of a filter. As seen from the literature, estimation theory has widely been adopted to estimate position and velocity from noisy measurements. Currently, no closed form solution exist to estimate an unambiguous position in 2-D using only Doppler measurements in a bistatic T-R geometry. The relationship between Doppler measurements and position and velocity is known to be non-linear. Therefore, under such conditions an approach would be to perform a LS solution for a linear model and iterated the procedure until a close estimate is obtained, that could be accomplished with a vast number of filters.

The most popular approach for tracking in a computational efficient way is to use a recursive filter, for example the the Extended Kalman Filter (EKF) could be considered here as the Doppler equations are non-linear. However, the initial estimated needs to be fairly accurate for the filter to convergence and the filter is known to be inappropriate to track manoeuvring targets as previous estimates are also part of the estimate in a recursive filter. To be flexible from initial state estimate errors as well as target manoeuvring, the GN filter and particle filter could be considered with the draw back of high computational payload. However, Nadjiasngar recently managed to recast the GN filter into a recursive format that retains the properties of the GN filter, but as a result with a lower computational load. Further, the filter is able to guard against large estimation errors when the targets motion model deviates significantly from the actual target motion by varying it's filter memory length. Accordingly the RGNF is selected to be used in this thesis.

Filter Initialisation. As seen from the literature, significant efforts has been spend on initialising filters from measurements in general. This is also of concern in the bistatic T-R geometry case in which a filter needs to be initialised from only Doppler measurements, as no closed form solution exist to resolve the target's position unambiguously. As a result, numerous ways to initialise tracking filter were published, however all methods are some form of a time consuming exercise. In case of using an FM band CR, additional information is available in the form of a coarse bistatic range measurement, for which a closed form solution exist. The only concern with this approach is that the initial position estimate would be too coarse and result in the filter not converging. Therefore, the requirement was placed on the filter to accommodate large initialisation errors. Through the course of this thesis, it will be proved that a coarse bistatic range estimate, together with a fairly accurate Doppler estimate could be used to initiate the RGNF and successfully converge to a good estimate as time progresses. Therefore, a closed form solution is prosed to initiate the RGNF from a single measurement of bistatic range and Doppler, respectively collected at

a minimum of 3 receiver sites.

Placement of receivers. The current trend with CR system developments, specifically aimed at exploiting FM, is to make use of a single receiver, multiple transmitter scenario for target location. However, in most areas of South Africa, single high powered FM illuminators cover large service areas. Therefore, having the ability to place multiple receivers and only exploit a single transmitter is a more flexible method to optimise coverage for a region. Besides the consideration of SNR and SINR to place receivers as discussed in Inggs et al. [25], receiver placement in a multistatic Doppler only tracking system did not receive significant attention in literature. Therefore, this thesis will make use of Cramèr-Rao theory to attempt an optimised receiver placement setup.

Establish a theoretical bound. Lastly, Doppler only tracking using multiple transmitters and receivers in a bistatic T-R configuration did receive some treatment, but not adequately. For example, in addition to the effect of integration time on the CRLB, the effect of receiver placement on the CRLB needs investigation, as well as the effect of filter memory length using a recursive filter. Lastly, to the authors knowledge, no results have been published where theory has been verified by simulation and validated by measured data using a Doppler only tracking system. This is also the aim of this thesis.

Mentioned in Chapter 1, one of the main objectives of this thesis is to compare a simulated target tracking scenario with target tracking results based on real-world measured data. Therefore, in the following chapter, the field measurement campaign used to gather data for thesis are described, as well as the processing chain considered. The data gathered from this field experiment would then be used to validate the theoretical findings of Chapter 4.

Chapter 3

System Overview

3.1 Introduction

One of the key objectives of this thesis is to prove the hypothesis of Doppler only tracking in a "actual" air-surveillance environment. This in return required conducting a measurement campaign in the form of field trials. This chapter provides an overview of this deployment, in which of a multi-static CR system[1] was deployed to provide experimental proof of the hypothesis.

In Section 3.2 the geographical layout and equipment used during the trials are presented. Further, the proposed data processing for Doppler only tracking is presented in Section 3.3, the bistatic range[2] and Doppler measurement equations are presented in Section 3.4 and finally, the chapter ends with some concluding remarks presented in Section 3.5.

[1] A prototype multi-static system is currently developed as a joint collaboration between the Council for Scientific and Industrial Research (CSIR), UCT and Peralex Electronics, South Africa.

[2] As concluded in Chapter 2, bistatic range measurements are required for the initialisation of the RGNF.

3.2 Trial Layout and Equipment

3.2.1 Location and Layout

In order to detect and track commercial airliners approaching and leaving Cape Town International Airport, 4 time synchronised receivers, were deployed in and around the Western Cape region in South Africa. The geographical layout of this deployment is displayed in Figure 3.1 together with overlaid track data (ADS-B data) of an incoming airliner to the airport. As only FM broadcasting (88 - 108 MHz) was considered, the Cape Town transmitter, marked as 'T', was selected as the illuminator of opportunity due to it's favourable ERP, as well as broadcasting content, that is mostly rock music and favourable for range resolution [125]. Further, see Table 3.1 for a summary of the transmit parameters. The 4 receiver sites, marked as 'R's, were selected for favourable SNR as well as SINR [25] and consisted of a co-located architecture that is further discussed in Section 3.2.2. Photos of the "Malmesbury" and "Donkerhoek" receiver sites are shown in Figure 3.2, whereas the "Atlantic" and "Kalbaskraal" receiver sites are shown in Figure 3.3.

Table 3.1: The Cape Town transmitter parameters.

Parameter	Value
Exploited centre frequency:	89.0 MHz
Radio Station :	5 FM
Tower Height :	240 m
Exploited channel ERP :	10 kW

3.2.2 Equipment Description

As described in the previous section, each of the 4 receiver sites were equipped with a 2 channel receiver, where phase synchronisity been the two respective channels were achieved by driving both channels from a common clock source. Accordingly, two respective signals were captured, digitised and stored to disk at

Figure 3.1: The Geographical layout of the multistatic CR system in the Western Cape, South Africa. The 4 receiver nodes are marked as 'R's, the Cape Town transmitter is marked as 'T' and an incoming aircraft to Cape Town International airport is indicated with the cyan coloured line. The red overlay is the region where target tracking was considered for this thesis.

(a) (b)

Figure 3.2: A photo of (a) the Malmesbury receiver site and (b) the Donkerhoek receiver site.

(a) (b)

Figure 3.3: A photo of (a) the Atlantic receiver site and (b) the Kalbaskraal receiver site.

each receiver site that allowed for the off-line processing of the data (described in Section 3.3) and then perform the subsequent data association and tracking stages as described in Chapter 5.

Each channel was fed by a separate antenna, one facing the transmitter that captured that direct path signal and the other, facing the target surveillance area to capture the signal reflection from the target. In this thesis, the term, "reference channel", or "Ref." will refer to the channel that captures the direct path signal and "surveillance channel", or "Surv." will refer to the channel that captures the target reflection signal. With the exception of the Atlantic receiver site, directional antennas were used for both the reference and surveillance channels to maximise the respective gains towards the transmitter and the target. Considered for the directional antennas at the respective receiver sites were either a Yagi or Log Periodic Dipole Antenna (LPDA) type. These are listed in Table 3.2, together with the following additional parameters; the surveillance antenna pointing direction relative to North, the 3 dB Azimuth (Az) beam-width of the surveillance antenna and antenna height Above Ground Level (AGL). Lastly, note that the directional antenna approach with the surveillance antennas resulted in a common detection region that is referred to as the ROI. The ROI is indicated by the red overlay in Figure 3.1 and is accordingly the tracking region considered for this thesis.

For data capturing purposes, two different types of receiver hardware were used during the field trails, namely a super-heterodyne receiver and direct sampling receiver. The main difference between these two receivers are the down-mixing stage in a super-heterodyne receiver, where the RF signal are down-converted to a more convenient Intermediate Frequency (IF), prior to the sampling, digitisation and digital extraction of the signal of interest. In the case of the direct sampling receiver, the RF spectrum is directly sampled and digitised, which then also allows for the signal of interest to be digitally extracted. The direct sampling receivers used during the trials were supplied by Peralex Electronics, South Africa that is purposefully build FM band CR receivers, called "ComRad3" receivers [126]. The super-heterodyne receivers, called "MRD7050C" receivers, were supplied by Grintek Ewation Technologies (GEW), South Africa and a pur-

posefully build 2 channel Direction Finding (DF) system. Since these receivers also allowed for the extraction of narrowband data per channel, it was accordingly used for data capturing purposes. Both the MRD7050C and ComRad3 receivers, as shown in Figure 3.4, consisted of 16-bit ADCs that provided sufficient dynamic range for consistent commercial airliner detections in the ROI. Furthermore, they were also equipped GPS Disciplined Oscillators (GPSDO) to provide better phase coherency between the 2 RF channel over the CPI and also to timestamp the data to GPS time, that allowed to synchronise the data between the respective receiver sites.

Lastly, seen from the description provided above, it is evident that this thesis only considered the most common CR architecture, called the co-located architecture.[3] It is also possible to recorded the reference signal and surveillance signal at two separate receiver sites by using only a single channel receiver at each site. The implementation then allows for single channel receivers to be deployed to the respective receiver sites to record only a surveillance signal that is fed back to a common processing node for cross correlation with the reference signal [31, 127]. This is known as the separated reference architecture and although not considered for this thesis, the same processing chain considered for this thesis could also be used for the separated reference architecture.

3.3 Processing Overview

The proposed signal processing to achieve Doppler only tracking with a CR are covered next. Assuming the CR exploits FM band illuminators of opportunity, the range resolution would be low and therefore not sufficient for ATC purposes. However, long integration times would provide high resolution frequency data, in which the Doppler shift could accurately be measured. Therefore, the processing scheme under consideration estimates the target position and velocity from high resolution Doppler measurements, collected from multiple receiver sites.

[3] A co-located receiver architecture is used to respectively record a reference and surveillance signal at a single geographical location. Therefore, this architecture requires more than one RF channel per receiver.

Table 3.2: The field deployment setup configuration of each receiver in the multi-static CR system.

	Atlantic	Malmesbury	Kalbaskraal	Donkerhoek
Equipment:	MRD7050C	ComRad3	MRD7050C	ComRad3
Receiver Type:	Down Mixing	Direct	Down Mixing	Direct
Output Sample Rate:	204.8 kSps	200.0 kSps	204.8 kSps	200.0 kSps
Antenna (Surv)				
Type:	Yagi	LPDA	LPDA	Yagi
Height:	5 m	3 m	5 m	3 m
Az Direction:	55°N	135°N	70°N	330°N
Az Beamwidth:	60°	95°	180°	60°
Antenna (Ref)				
Type:	Omni	Yagi	Yagi	Yagi
Height:	10 m	3 m	6 m	3 m

In Figure 3.5, the proposed signal processing steps for a k-receiver CR are presented in the form of a block diagram and described as follows:[4]

Data Sampling: The first step of the signal processing is to sample sufficient In phase/Quadrature (IQ) data with the receiver hardware (ComRad3 or MRD7050C) at the respective receiver sites for both the reference and surveillance channels and store the data to disk.

Absolute frequency accuracy is kept over the multi-static receiver sites by each receiver's built in GPSDO that achieves a frequency stability of 3 parts per billion (ppb) [29] as a worst case scenario. Therefore, as considered in this thesis, a 4 s CPI at an RF carrier frequency of 89 MHz would result in a expected frequency accuracy of 0.178 Hz. As this result is less than the integration time frequency accuracy of 1/4 s = 0.25 Hz, absolute frequency drift is therefore not a concern in this thesis. Another important parameter to consider in a multi-static receiver system is that of accurately

[4] To achieve real-time processing of the data up to and including the "Detection" stage, was the topic of another PhD at UCT, see [29].

(a)

(b)

Figure 3.4: The receiver hardware used for the field experiment, (a) the "ComRad3" and (b) the "MRD7050C".

time stamping the IQ sampled data. In general, the requirement would be for the time stamping accuracy to be less than the sample period. In case of this thesis, the IQ data is time stamped to an accuracy of 1 μs between sites, hence less than the sample period of 5 μs (sample rate was 200 kSps).

Lastly, IQ sample alignment between the respective receiver sites is achieved in an off-line process. As mentioned above, each IQ data stream contains a timestamp that identifies the absolute time of the first IQ sample in the data stream. In return, this information is then used to time align the IQ sample data as follows; 1.) Identify the receiver site that started the recording last, by comparing the absolute time stamp of the recorded IQ data streams. 2.) Discard the first samples of the other 3 sites which are older than the first sample of the recording which was started last, in which case the IQ samples between the respective receiver sites will then be aligned to within 1 μs.

DPI/Clutter Suppression: Having sampled a CPI length of IQ samples in

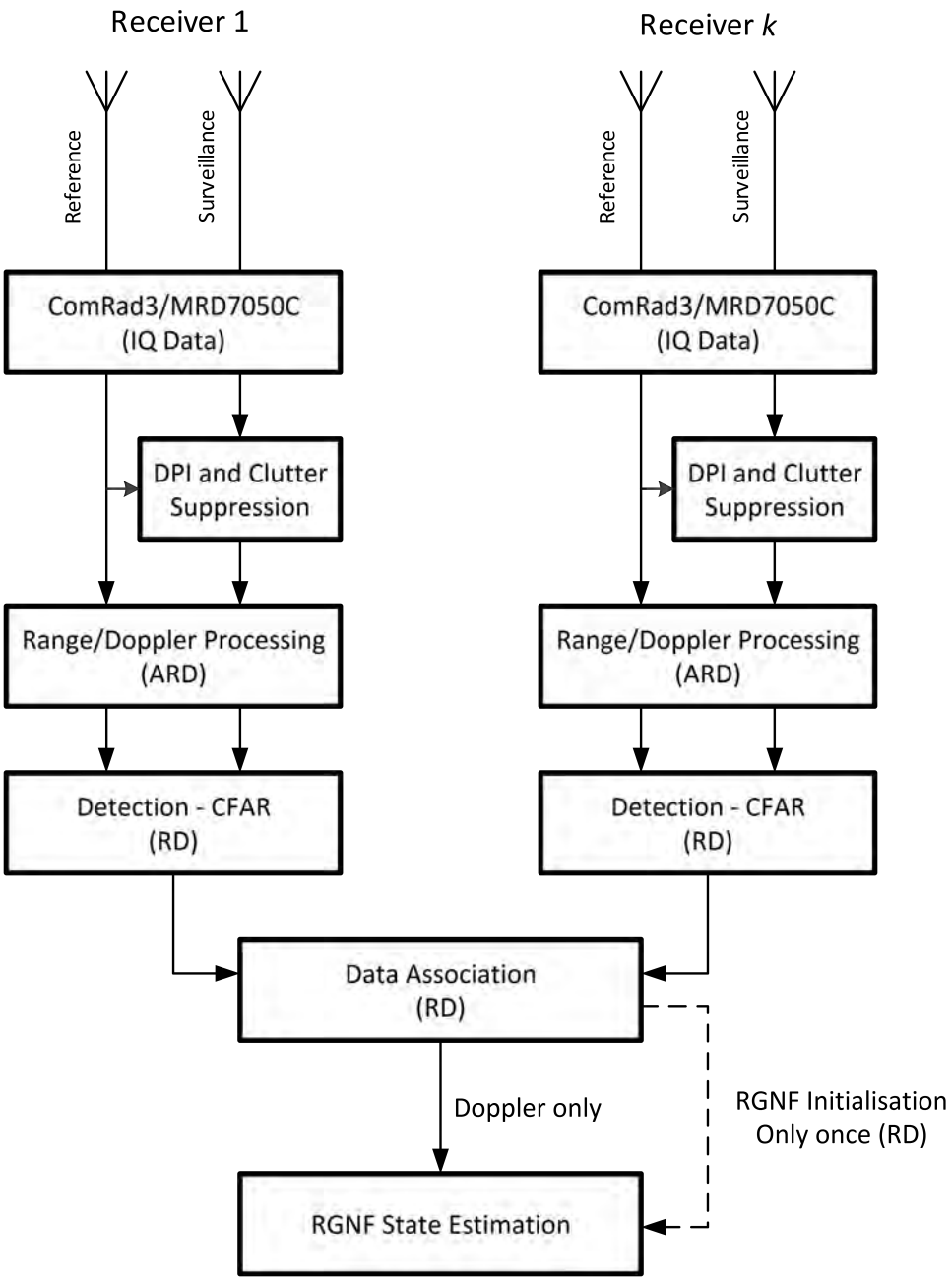

Figure 3.5: A Flow diagram showing the respective stages of the Doppler only processing chain, assuming k-receivers are deployed.

both the reference and surveillance channels, the large signal power content of the direct path, as well as clutter, needs to be suppressed in the

surveillance signal. In a CR, the target reflection power could typically be 90 dB below the power received directly from the transmitter and clutter [5], hence the requirement to suppress the DPI and clutter in the surveillance signal. Literature suggests to subtract an estimate of the DPI and clutter, modelled as $\mathbf{Ab}$, from the surveillance signal $\mathbf{s}_s$ as:

$$\mathbf{s}_{cs} = \mathbf{s}_s - \mathbf{Ab} \tag{3.1}$$

where $\mathbf{s}_{cs}$ would then theoretically be the surveillance signal that is free from DPI and clutter. As the direct path is known, matrix $\mathbf{A}$ is easily constructed by populating the individual column vectors of $\mathbf{A}$ with delayed copies of the direct path (zero delay will be the 1st column). Hence the row dimension contains the number of samples in the CPI, whereas the column dimension contains the number of range delay bins (delayed copies of the direct path) to process the data over. The last parameter, $\mathbf{b}$ represents a column vector that scales the different columns in $\mathbf{A}$ and accordingly, forms a model in which different range bins produce different clutter returns.

Considering that $\mathbf{s}_s$ contains the majority of the signal energy and $\mathbf{s}_{cs}$ is close to zero,[5] Equation (3.1) could be written as $\mathbf{Ab} = \mathbf{s}_s$ in which case $\mathbf{b}$ could be solved. However, solving this equation directly requires to find $\mathbf{A}^{-1}$ that does not exist as the number of rows and columns are not equal (row dimension much larger). Therefore, the solution would rather be, to minimise the residual signal power with a LMS approach as

$$min\big(||\mathbf{Ab} = \mathbf{s}_s||^2\big) \tag{3.2}$$

in order to solve the scaled clutter return vector $\mathbf{b}$. This value is then directly used in Equation (3.1) to calculate $\mathbf{s}_{cs}$.

In case of this thesis, the Conjugate Gradient Least Squares (CGLS) algorithm was used to calculate $\mathbf{b}$ from Equation (3.2) that provided a selectable trade-off between signal processing requirements and cancellation

[5] Importantly, notice that target echoes are Doppler shifted and therefore pseudo orthogonal to $\mathbf{Ab}$, therefore $\mathbf{Ab}$ will not cancel moving targets.

capability [29, 60].

Range-Doppler Processing: Following DPI and clutter suppression, range-Doppler processing is performed by cross-correlating the reference signal, $\mathbf{s}_r$ with the processed surveillance signal, $\mathbf{s}_{cs}$ over an user defined CPI. In literature, this is known as the CAF, given as:

$$|\Psi(\tau, f_d)|^2 = \left| \int_{-\infty}^{\infty} \mathbf{s}_{sc}(t)\mathbf{s}_r^*(t-\tau)e^{j2\pi f_d t}dt \right|^2 \tag{3.3}$$

where * denotes the complex conjugate and $|\Psi(\tau, f_d)|^2$ the ambiguity response as a function of delay time, τ and bistatic Doppler shift, f_d. Therefore, evident from Equation (3.3), amplitude values are produced as a function of delay times (that translates to range) and Doppler values in a 3-D map, hence referring to this processing stage as ARD map processing.

Equation (3.3) was implemented by performing a point-wise cross multiplication between the surveillance and reference signal[6] in the time domain, in which the resulting signal was then windowed and the Fast Fourier Transform (FFT) taken. Therefore, with τ=0, the ARD map are populated with values only along the Doppler dimension for a bistatic range equal to the base line. When τ=1, the reference channel is delayed with a single IQ data sample and therefore the next bistatic range is processed. This process of multiply-window-FFT-shift is then repeated until the ARD map is produced over the user defined number of bistatic range and Doppler bins. An example of a processed ARD map is presented in Figure 3.6 (a) in which two targets are present; the first at a bistatic range and Doppler frequency of respectively 105 km and 79.8 Hz and the second at 195 km and 101.3 Hz.

Detection: Next, a CFAR detection algorithm is applied to the ARD map in which targets are declared when the amplitude of a particular range-Doppler bin exceeds a normalised threshold. Thereby, a theoretically con-

[6] As shown in Equation (3.3) the complex conjugate of the reference signal is taken prior to multiplication

stant false alarm rate is achieved. A "Greatest Of Cell Averaging" CFAR (GOCA-CFAR) was used in which 4 guard cells and 6 reference cells were used on either side of the Cell-Under Test (CUT) in only the Doppler dimension. Lastly, the Probability of False Alarm (PFA) was set to 10^{-5}. The Doppler direction only option was chosen due to the high resolution of the Doppler dimension in the ARD map, in this case 0.25 Hz, as opposed to the $\geq$ 1.5 km range resolution that also fluctuates with the FM signal modulation bandwidth. This particularly makes target edge detection problematic in the range direction.

The corresponding CFAR detections for the ARD map presented in Figure 3.6 (a), are displayed in Figure 3.6 (b), in which the following is noticed; white range-Doppler bins represent a current CFAR detection and grey bins represent previous CFAR detections. Therefore, as time progress, previous detections of a particular target would appear as a "phosphor" trail in the CFAR map. As a current detection might span several range-Doppler bins due to the fluctuating signal content of a FM signal, a red cell is used to mark the centroid point of the detection and therefore the final detection.

Data Association: The respective target detections (red centroid values) obtained from the four different receiver sites are then associated to the same target by using the ADS-B truth data. Therefore, the data association process identifies the raw bistatic range and Doppler detections that belong to a common target. This process is covered in more detail in Chapter 5.

RGNF State Estimation: The final step in the processing chain is required to estimate the target position and velocity from the associated Doppler measurements[7] and accordingly track the target. For this purpose, the RGNF was considered for this thesis. Estimating each target track is then handled in two steps; in the first step the filter is initialised and in the second step the target track is maintained. Both these steps are briefly described below, but covered in detail in Chapter 5.

[7] In this thesis, only 2-D target tracking is considered, hence the measurements of bistatic range and Doppler in 3-D space is first transformed to detections in 2-D space. This was possible as the target's true position and velocity was known from the ADS-B truth data.

For the filter initialisation step, the target's position is estimated first by using 4 coarse, range only measurements. Only then, the initial velocity is estimated from the Doppler measurements together with the estimated position. Once the RGNF is initialised, track maintenance is kept by feeding the RGNF with only one Doppler measurement per receiver site.

3.4 Bistatic Range and Doppler Measurements

At the heart of the processing scheme presented in the previous section lies the estimation of the target's position from Doppler only measurements. Therefore, in this section measurement equations are derived for, bistatic range as a function of target position; as well as bistatic Doppler measurements as a function of target position and velocity. Further, and in support of the derivations, some associated assumptions are listed and discussed and lastly, a coordinate system was required, in which case an Universal Transverse Mercator (UTM) Cartesian coordinate system was selected.

3.4.1 Assumptions

In order to simplify the derivation of the measurement equations presented in the following sections, some simplifying assumptions are made.

Constant Velocity: The target is assumed to move at a constant velocity over the considered CPI. Considering a CPI of 4 s, as in case of this thesis, a constant velocity seems reasonable from literature [62]. However, this assumption is challenged in Chapter 5, where simulations are presented for non-constant velocity scenario's, for example target turn, but accordingly addressed.

2-D Tracking: For tracking purposes, the target height is assumed to be zero, hence only 2-D tracking is considered for this thesis. The reason for this

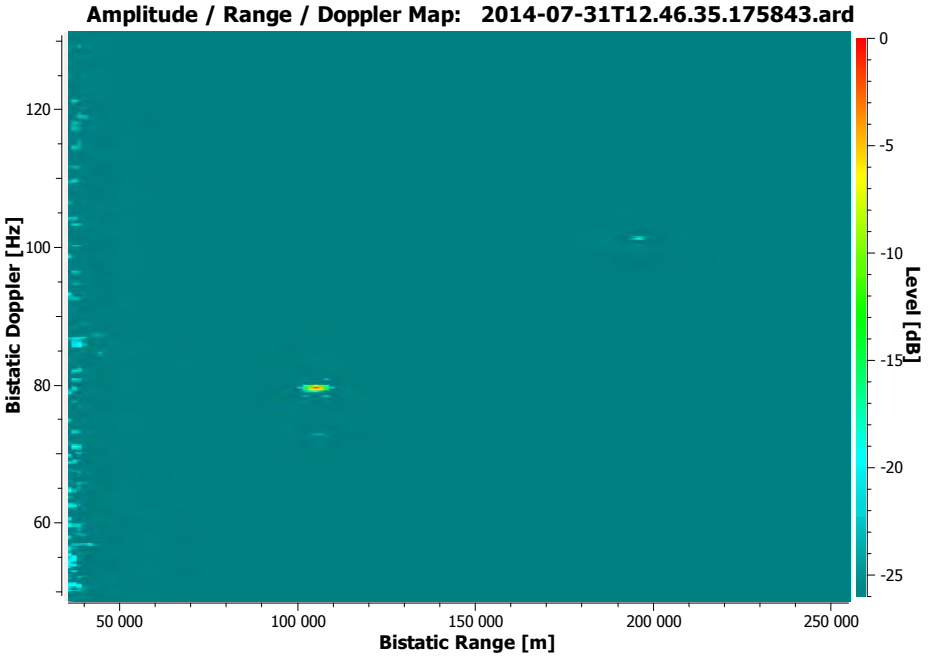

(a)

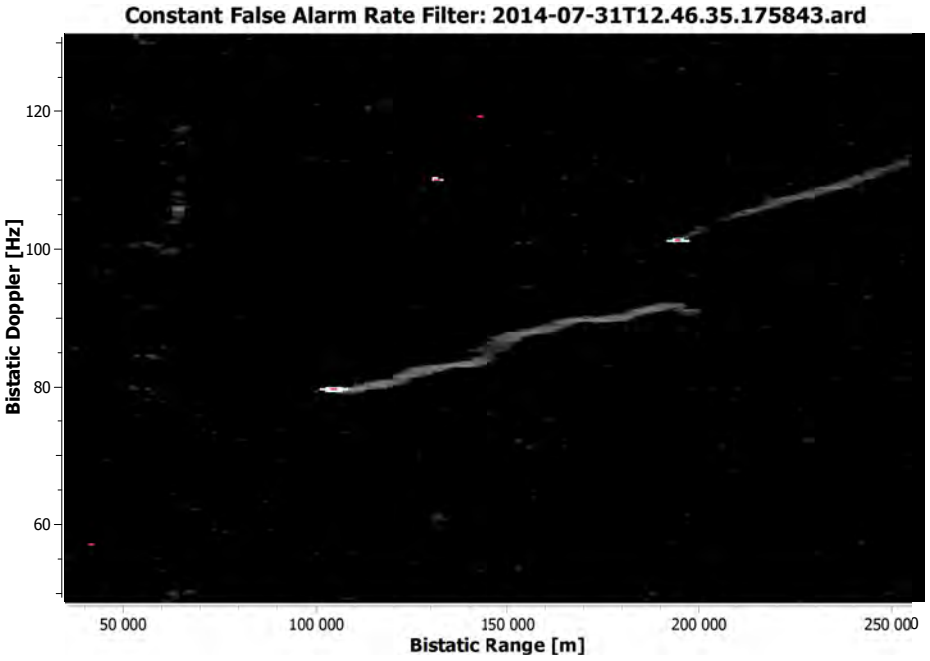

(b)

Figure 3.6: An example of two targets present in (a) the ARD map and the detection of these two targets by (b) the CFAR detector. In the CFAR map, the grey bins represent past detections, the white bins current detections and the red bins, the centroid value of the current detection.

choice will become clear in Chapter 4, but in short; 4 receivers only provides capability for 2-D tracking.

Target altitude will surely influence the tracking performance in 2-D as the target was fairly close to the transmitter-receiver setup, as seen from Figure 3.1. As ADS-B truth data of the target was available, the true difference between 2-D and 3-D bistatic range and bistatic Doppler could be calculated, hence allowing the difference to be subtracted from the 3-D measured data to obtain realistic 2-D measured data.

3.4.2 Target Model

As illustrated by Figure 3.7, a target is assumed to be moving in 2-D space in the presence of a single transmitter, k-receiver CR system. The transmitter is located at $\mathbf{x}_E = [x_E, y_E]$ where x_E and y_E are the transmitter's respective x and y-coordinates. Following this notation, the k spatially separated receivers are then respectively located at $\mathbf{x}_{R1} = [x_{R1}, y_{R1}]$ to $\mathbf{x}_{Rk} = [x_{Rk}, y_{Rk}]$ whereas the target's position is given as $\mathbf{x}_p = [x, y]$. The target is assumed to move with velocity $\mathbf{v}_{\mathrm{x}} = [\dot{x}, \dot{y}]$, where $\dot{x}$ and $\dot{y}$ are the respective velocities in the x and y directions. Therefore, at time t_n, the target's position and velocity are collectively written in state vector format as

$$\mathbf{x}_n = [x_n \, \dot{x}_n \, y_n \, \dot{y}_n]^T \tag{3.4}$$

where n is the sample number, $[\cdot]^T$ is the transpose and bold face notation is used to represent a vector.

As stated in Section 3.4.1, target motion is assumed to be linear over a single CPI that allows for the target state equations to be defined as:

$$x_n = x_{n-1} + \dot{x}_n T \tag{3.5}$$

$$y_n = y_{n-1} + \dot{y}_n T \tag{3.6}$$

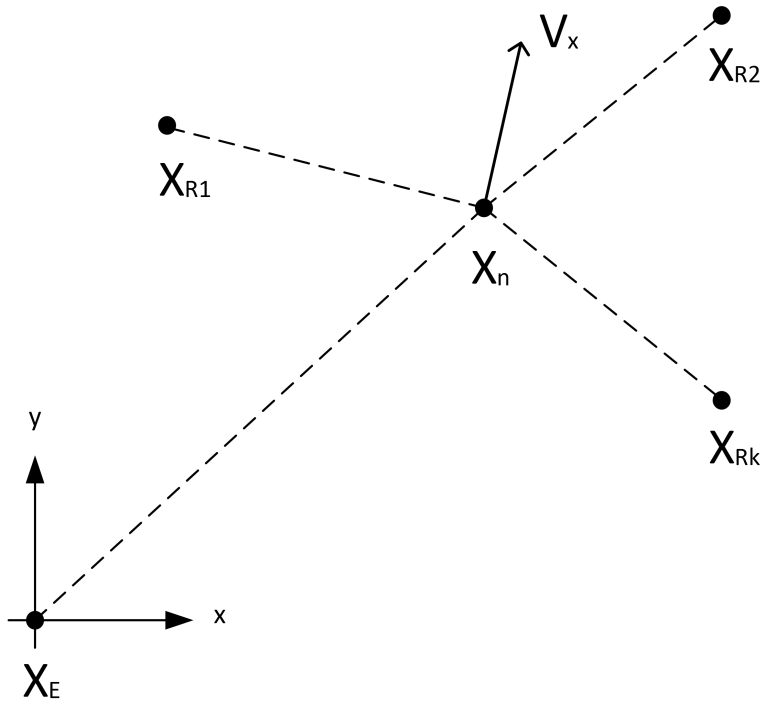

Figure 3.7: The observation model showing the target state vector $\mathbf{x}_n$, the transmitter $\mathbf{x}_E$ and the multiple receivers $\mathbf{x}_{R1}, ..., \mathbf{x}_{Rk}$. Note, the target state vector consists of the target position $\mathbf{x}_p$ and velocity $\mathbf{v}_{\mathrm{x}}$.

where T is the sample period between time t_{n-1} and t_n, x_{n-1} is the x-coordinate of the target at time t_{n-1} and $\dot{x}_n$ is the x-direction velocity component between time t_{n-1} and t_n. y is similarly defined. From the target state equations, the target state transition matrix is then written as:

$$\mathbf{x}_n = \mathbf{I}_2 \otimes \begin{pmatrix} 1 & T \\ 0 & 1 \end{pmatrix} \mathbf{x}_{n-1} = \mathbf{\Phi}(t_{n-1}, t_n)\mathbf{x}_{n-1} \tag{3.7}$$

where $\mathbf{I}_2$ is the 2×2 identity matrix, $\otimes$ is the Kronecker product, $\mathbf{x}_{n-1}$ is the target state vector at time stamp t_{n-1} and $\mathbf{\Phi}(t_{n-1}, t_n)$ is defined as the matrix representing a transition from time stamp t_{n-1} to t_n.

3.4.3 Measurement Equations

Considering the geometry as shown in Figure 3.7, the two equations that are of interest in this thesis are firstly, the bistatic range and secondly the bistatic Doppler.

The bistatic range is defined as the total path length a signal travels from the **transmitter** to the **target** to the **receiver** [128], in which case the path length from the transmitter to the target is given by

$$R_{E,n} = \sqrt{(\Delta^E_{x,n})^2 + (\Delta^E_{y,n})^2} \tag{3.8}$$

where $\Delta^E_{x,n} = x_n - x_E$, $\Delta^E_{y,n} = y_n - y_E$. The path length from the target to the i^{th} receiver, $\mathbf{x}_{Ri}$ is given by

$$R_{Ri,n} = \sqrt{(\Delta^{Ri}_{x,n})^2 + (\Delta^{Ri}_{y,n})^2} \tag{3.9}$$

where $\Delta^{Ri}_{x,n} = x_n - x_{Ri,n}$ and $\Delta^{Ri}_{y,n} = y_n - y_{Ri,n}$. Therefore, the ideal bistatic range R_{bi} measured by the i^{th} receiver at time t_n is given by

$$R_{bi}[n] = R_{E,n} + R_{Ri,n} = \sqrt{\left(\Delta^E_{x,n}\right)^2 + \left(\Delta^E_{y,n}\right)^2} + \sqrt{\left(\Delta^{Ri}_{x,n}\right)^2 + \left(\Delta^{Ri}_{y,n}\right)^2} \tag{3.10}$$

In a radar system, the Doppler shift of the target's reflected signal is related to the rate of change of the total path length the signal has travelled, hence the bistatic range as defined in Equation (3.10). Therefore, the ideal bistatic frequency shift f_d measured by the i^{th} receiver at time t_n, is given as:

$$f_{di}[n] = -\frac{1}{\lambda}\left(\frac{\mathrm{d}R_{bi,n}}{\mathrm{d}t}\right) \tag{3.11}$$

where λ is the wave length of the exploited transmitter's RF carrier frequency. By the substitution of Equation (3.10) in Equation (3.11) and taking the derivative

$(\mathrm{d}/\mathrm{d}t)$, it is trival to show that:

$$f_{di}[n] = K_d \left(\frac{\Delta^E_{x,n}\dot{x}_n + \Delta^E_{y,n}\dot{y}_n}{R_{E,n}} + \frac{\Delta^{Ri}_{x,n}\dot{x}_n + \Delta^{Ri}_{y,n}\dot{y}_n}{R_{Ri,n}} \right) \tag{3.12}$$

where $\dot{x}_n = \mathrm{d}x_n/\mathrm{d}t$, $\dot{y}_n = \mathrm{d}y_n/\mathrm{d}t$ and $K_d = -1/\lambda$ that is known as the wave number. A similar result was shown in Skolnik [99].

3.4.4 Target Altitude

In the previous section, the bistatic range and Doppler equations were derived for a 2-D case. The inclusion of target altitude to represent a 3-D scenario, could be obtained with fairly minor alterations to Equations (3.10) and (3.12). Hence, by including the target altitude, a 3-D measurement equation for bistatic range is:

$$R_{bi}[n] = \sqrt{\left(\Delta^E_{x,n}\right)^2 + \left(\Delta^E_{y,n}\right)^2 + \left(\Delta^E_{z,n}\right)^2} + \sqrt{\left(\Delta^{Ri}_{x,n}\right)^2 + \left(\Delta^{Ri}_{y,n}\right)^2 + \left(\Delta^{Ri}_{z,n}\right)^2} \tag{3.13}$$

and bistatic Doppler:

$$f_{di}[n] = K_d \left(\frac{\Delta^E_{x,n}\dot{x}_n + \Delta^E_{y,n}\dot{y}_n + \Delta^E_{z,n}\dot{z}_n}{R_{E,n}} + \frac{\Delta^{Ri}_{x,n}\dot{x}_n + \Delta^{Ri}_{y,n}\dot{y}_n + \Delta^{Ri}_{z,n}\dot{z}_n}{R_{Ri}} \right) \tag{3.14}$$

where $\Delta^E_{z,n} = z_n - z_E$, $\Delta^{Ri}_{z,n} = z_n - z_{Ri}$, z_n is the target altitude measured Above Mean Sea Level (AMSL) at time t_n, z_{Ri} is the antenna height of the surveillance antenna at the i^{th} receiver site and z_E is the antenna centre point height of the transmitter. Lastly, $\dot{z}_n$ is the z-direction velocity of the target.

3.5 Conclusions

This section mainly detailed an overview of the methodology considered for this thesis, in which an experimental prototype CR was deployed for field trials in order to capture data for the subsequent stages of data processing. The layout

and equipment used during the field trials were first reviewed. From the hardware description, as well as accompanying photos presented, it is evident that a low cost radar solution is viable with such equipment. Further, fuelled by the digital advances being made these days, as well as the trend of ever increasing processing power becoming more and more affordable, it is foreseen that the current low cost CR will become even more affordable in future.

The proposed signal processing scheme for tracking a target by using only Doppler measurements is also described. This process involves the measurement of a target's Doppler shift from several geographically separated receiver sites in order to estimate the target's position and velocity based on these measurements. These estimates would then be used to initialise[8] the RGNF and once initialised, maintain the track. As the initialisation process makes use of both high resolution Doppler measurements, as well as low range resolution range measurements, informed readers might think that this approach would result in a lack of convergence by the RGNF due to the inaccurate initial position estimate. However, in Chapter 5 this is proved not to be the case.

Lastly, the measurement equations for bistatic range and Doppler is derived for a 2-D case, as well as a 3-D case. However, only 2-D tracking is considered in this thesis as 4 receivers only allows for 2-D tracking. The reason for this will become clear in Chapter 4.

Having now derived the equation that relates Doppler only measurements to target position and velocity, the question now becomes what target position accuracy could be expected from a given a set of noise corrupted Doppler measurements. Therefore, in the following chapter the aim would be to establish a theoretical bound for the expected target tracking accuracy. In Chapter 5, this bound will then be verified by simulation and compared with the measured data obtained from the field trials as described in this chapter.

[8] The details of this initiation process are described in Chapter 5.

Chapter 4

Deriving a Lower Bound

4.1 Introduction

In the previous chapter, the practical aspects of this thesis were considered in which the focus was to gather range and Doppler measurements of a target of interest in a realistic environment. In this chapter, the focus is now shifted towards building a theoretical foundation for the multi-static Doppler only tracking system, where the main aim is to derive a lower bound on the target tracking accuracy. In support of this objective, the chapter is structured as follows. First, some mathematical background information is briefly reviewed in Section 4.2 to cover the observability and Cramèr-Rao theory that is required for the remainder of the thesis. In Section 4.3, the noise corrupted measurement equations used for this thesis are presented and in Section 4.4 the observability requirements for a Doppler only tracking CR system are derived. Following the observability criteria, mathematical equations are derived in Section 4.5 for a multi-static CR system in order to determine the theoretical accuracy such a system could achieve. In Section 4.6 the additional use of time history information is considered and equations derived to incorporate this information into current Cramèr-Rao theory. In Section 4.7, the expected target tracking accuracy (CRLB) over a 2-D surface is simulated and presented. The insights gained for these simulations are

then used as a motivation for continuing the investigations in Chapters 5 and 6. Lastly, some MIMO aspects are considered for Doppler only tracking in Section 4.8, before concluding in Section 4.9.

4.2 Background Theory

Before an attempt is made to derive a theoretical lower bound on the target tracking accuracy of a multi-static CR using only Doppler measurements, some theoretical concepts are first reviewed. These include; 1.) matrix operations, 2.) observability, that is concerned whether a set of measurements will result in an unique solution and lastly 3.) Cramèr-Rao theory that is ultimately used to determine the theoretical accuracy associated with the multi-static CR system.

4.2.1 Matrix Operations

Large portions of the work presented in this thesis involved some or other form of matrix operations and also that of solving a system of linear[1] equations. In most cases of solving a system of linear equations, the matrix inverse is required. However, the details of matrix inversion are not considered here, but the focus is rather placed on the determinant of a matrix, a function used to determine if a matrix is invertible or not. Therefore, assume matrix $\mathbf{B}$ consists of a rows and c columns and defined as:[2]

$$\mathbf{B}_{a,c} = \begin{pmatrix} b_{1,1} & b_{1,2} & \cdots & b_{1,c} \\ b_{2,1} & b_{2,2} & \cdots & b_{2,c} \\ \vdots & \vdots & \ddots & \vdots \\ b_{a,1} & b_{a,2} & b_{a,3} & b_{a,c} \end{pmatrix} \tag{4.1}$$

[1] In this thesis, all non-linear equations are approximated as linear equations. Hence, only systems of linear equations are solved.

[2] A capital letter, with bold face notation is used throughout this thesis to represent a matrix.

Then the number of rows and columns determine whether the matrix is square or not. Therefore, per definition;

Definition 1. Matrix $\mathbf{B}$ is said to be square if the number of rows a equal the number of columns c. In case $a \neq c$, the matrix is said to be non-square.

Now, let $\mathbf{B}$ be a square matrix, then the determinant of $\mathbf{B}$ is $\det(\mathbf{B}) = |\mathbf{B}|$. For example, assuming matrix $\mathbf{B}$ defined above is a 2×2 matrix, then the $\det(\mathbf{B}_{2,2}) = b_{1,1}b_{2,2} - b_{1,2}b_{2,1}$. If $\det(B) \neq 0$, $\mathbf{B}$ is called non-singular and a matrix inverse does exist. If $\det(\mathbf{B}) = 0$, $\mathbf{B}$ is singular and the matrix inverse does not exist. In case of the $\det(\mathbf{B})$ being close to zero, the matrix is said to be ill-conditioned or close to singular and lacks an unique solution. In summary, only if a matrix $\mathbf{B}$ is square and the $\det(\mathbf{B}) \neq 0$, then the inverse exist as well as an unique solution.

Another important property to consider is the effect of correlation amongst the column vectors in a matrix. Therefore, the focus is now turned to calculate the rank of a matrix;

Definition 2. The rank of matrix $\mathbf{B}$, $rk(\mathbf{B})$ is the maximum number of linearly independent column vectors in $\mathbf{B}$. If all columns are linearly independent, the matrix is said to be full column rank.

Assuming $\mathbf{B}$ is a square matrix with $a=c$, it is sufficient to only determine whether $\det(\mathbf{B}) \neq 0$, if true, the rank of the matrix is given as $rk(\mathbf{B}) = c$. However, in the case of $\det(\mathbf{B}) = 0$, the following is possible; 1.) matrix $\mathbf{B}$ could be a non-square matrix, or 2.) two, or more columns are correlated in $\mathbf{B}$. Under these conditions, Singular Value Decomposition (SVD) could be used to determine the $rk(\mathbf{B})$. However, a more simplistic solution, for the material presented in this thesis, is to compute $rk(\mathbf{B})$ using Gauss-Jordan elimination. Gauss-Jordan elimination is the process of using elementary row operations to reduce $\mathbf{B}$ to its Reduced Row Echelon Form (RREF).

Definition 3. A matrix is said to be in Row Echelon Form (REF) if 1.) all non-zero rows are above any rows with all zeros 2.) the first non-zero entry from the left, also called the pivot, of the various rows follow a staircase pattern in

which the pivot of the $a + 1^{st}$ row is to the right of pivot entry of the a^{th} row. 3.) All entries in a column below the pivots are zero.

As an example, matrix $\mathbf{B}$ with $a = 3$ and $c = 5$, in REF would be:

$$\mathbf{B}_{REF} = \begin{pmatrix} 3 & b_{1,2} & b_{1,3} & b_{1,4} & b_{1,5} \\ 0 & 0 & 4 & b_{2,4} & b_{2,5} \\ 0 & 0 & 0 & 1 & b_{3,5} \end{pmatrix} \tag{4.2}$$

Definition 4. A matrix $\mathbf{B}$ is said to be in RREF if; 1.) matrix $\mathbf{B}$ is in REF and 2.) every pivot in $\mathbf{B}_{REF} = 1$ and is the only non-zero entry in it's column.

For example, by applying Definition 4 to $\mathbf{B}_{REF}$ defined in Equation (4.2), it will reduce to it's RREF as:

$$\mathbf{B}_{RREF} = \begin{pmatrix} 1 & b_{1,2} & 0 & 0 & b_{1,5} \\ 0 & 0 & 1 & 0 & b_{2,5} \\ 0 & 0 & 0 & 1 & b_{3,5} \end{pmatrix} \tag{4.3}$$

Therefore, when a matrix is in it's RREF, one property of the matrix is that only the pivot columns are linearly independent, therefore we can immediately see which columns are correlated. Also, the number of pivots will equal the rank of the matrix. Therefore, by counting the number of pivots in $\mathbf{B}_{RREF}$, which is 3, will result in $rk(\mathbf{B}_{RREF}) = 3$.

Up to this point, only non-singular and singular matrices were considered, thus the determinant of a matrix was either non-zero or zero. However, non-zero determinant also implies a value close to zero, but not zero. In such cases, SVD is used to obtain the singular values for a matrix.

Definition 5. The singular values of a matrix are defined as the positive square roots of the eigenvalues of the matrix. A property of the singular values is that the ratio of the largest number to the smallest number gives the condition of a matrix. Accordingly, the condition of a matrix is a measure of accuracy of it's numerical inverse.

In summary; 1.) A square non-singular matrix will be full rank and the det($\mathbf{B}$)$\neq$ 0. 2.) A singular matrix will be non-full rank and the det($\mathbf{B}$) = 0. 3.) When a matrix is non-full rank, it is either non-square, or it suffers from row/column correlation. 4.) In the case of row/column correlation, the matrix will be reduced to it's RREF identify the columns that are linearly dependant. Lastly, in the case where the inverse of an almost singular matrix is required, the matrix will be referred to as ill-conditioned and the condition of the matrix will be used to determine the accuracy of the inverse.

4.2.2 Measurement Notation

Suppose a single measurement y, in the measurements space depends on c unknown parameters in the parameter space, given by $\mathbf{x} = [\mathrm{x}_1, \mathrm{x}_2, \cdots, \mathrm{x}_\mathrm{c}]^T$. Then this dependency is mathematically expressed as

$$y = g(\mathbf{x}) \tag{4.4}$$

where $g(\cdot)$ is either a linear or non-linear function[3]. Expanding function $g(\cdot)$ to a k-vector function, Equation (4.4) then becomes

$$\mathbf{y} = \mathbf{g}(\mathbf{x}) \tag{4.5}$$

where $\mathbf{g} = [g_1(\mathbf{x}), g_2(\mathbf{x}), \cdots, g_k(\mathbf{x})]^T$ in which $g_1(\mathbf{x})$ to $g_k(\mathbf{x})$ are given by Equation (4.4) and accordingly, $\mathbf{y}$ would also be a vector of length k. Therefore, an ideal set of k measurements, given as $\mathbf{y} = [y[1], y[2], \cdots, y[k]]^T$, is said to be dependant/related to the parameter space $\mathbf{x}$, through the functions defined in $\mathbf{g}(\cdot)$. As matrix notation is commonly used in linear algebra, the above equations are now transformed to matrix notation. Assuming all k-functions in $\mathbf{g}(\cdot)$ are

[3] In this thesis, the measurements are considered to be bistatic range or Doppler measurements and the parameters to be estimated are the target position and velocity. For example, as seen from Chapter 3, the function between bistatic Doppler and position is non-linear, and therefore $g(\cdot)$ will be a non-linear function.

linear, then Equation (4.5) is equivalently written in matrix notation as

$$\mathbf{y} = \mathbf{M}\mathbf{x} \tag{4.6}$$

where $\mathbf{M}$ is of dimension $k \times c$ and known as the observation matrix, in which the entries of $\mathbf{M}$ are given by the coefficients of the linear functions defined in $\mathbf{g}(\cdot)$. Now, let the vector of errors in $\mathbf{y}$ be called the noise vector $\mathbf{w}$, where

$$\mathbf{w} = [w[1], w[2], \cdots, w[k]]^T \tag{4.7}$$

and $w[1]$ to $w[k]$ will be normal distributed random variables with zero mean and variance σ^2. Then the noise-corrupted observation equation is given by

$$\widetilde{\mathbf{y}} = \mathbf{M}\mathbf{x} + \mathbf{w} \tag{4.8}$$

where $\widetilde{\mathbf{y}}$ represents the noise-corrupted measurements[4]. The aim would then be to obtain an estimate, denoted as $\widehat{\mathbf{x}}$, of the parameter space $\mathbf{x}$ by observing the noise measurements $\widetilde{\mathbf{y}}$. This is known as the classical estimation problem.

Lastly, as mentioned before, in most cases $g(\cdot)$ is a non-linear function. In order to cope with non-linear functions, a method called local linearisation [21] is used to linearise the non-linear function by taking the partial derivative of the function with respect to the parameter space, hence

$$\overline{\mathbf{M}} = \frac{\partial \mathbf{y}}{\partial \mathbf{x}} = \frac{\partial \mathbf{g}(\mathbf{x})}{\partial \mathbf{x}} \tag{4.9}$$

where the matrix entries, $m_{i,j}$ of the resultant linearised matrix are given by

$$m_{i,j} = \left.\frac{\partial g_i(x_1, \cdots, x_c)}{\partial x_j}\right|_{\overline{\mathbf{x}}} \qquad \begin{matrix} 1 \leq i \leq k \\ 1 \leq j \leq c \end{matrix} \tag{4.10}$$

and the linearisation point, called a nominal point $\overline{\mathbf{x}}$, is assumed to be close to the actual true parameters $\mathbf{x}$. Hence, the greater the difference between the nominal

[4] Throughout this thesis, the use of the tilde symbol, $\widetilde{[\cdot]}$ will indicate noise corrupted measurements.

point and actual point, the less the possibility of global convergences. Therefore, assuming the function is non-linear, $\mathbf{M}$ in Equation (4.8) is replaced with the linearised observation matrix $\overline{\mathbf{M}}$ defined in Equation (4.9) and accordingly, the linearised observation equation is given as:

$$\widetilde{\mathbf{y}} = \overline{\mathbf{M}}\mathbf{x} + \mathbf{w} \tag{4.11}$$

4.2.3 Observability

An important aspect to consider in estimation theory, is to determine whether an unique solution exists for a given set of measurements, or in other words, determine whether a set of measurements is observable, or not. Hence, in the case of this thesis the question is posed; could the position of a target be resolved by only measuring the Doppler shift of the target? As the intention of this section is only to introduce the concept of observability, the question under consideration would only be answered in Section 4.4.

Observability in general is a theoretical concept that is usually assessed under ideal conditions and accordingly, the effect of noise is not considered any further under this section. However, the effect of noise will be re-introduced in the next section where it plays an important role in the assessment of target position accuracy. Assuming the ideal measurements of a target are given by $\mathbf{y}$ and non-linearly related to the parameter vector $\mathbf{x}$, as defined in Equation (4.5), then the necessary condition for global identifiability is for the observation matrix to be full rank [101]. Therefore, following the linearisation process described in the previous section, the partial derivative of $\mathbf{y}$ is taken with respect to the parameter vector $\mathbf{x}$ as:

$$\frac{\partial \mathbf{y}}{\partial \mathbf{x}} = \begin{pmatrix} \frac{\partial y[1]}{\partial \mathrm{x}_1} & \cdots & \frac{\partial y[1]}{\partial \mathrm{x}_c} \\ \vdots & \vdots & \vdots \\ \frac{\partial y[k]}{\partial \mathrm{x}_1} & \cdots & \frac{\partial y[k]}{\partial \mathrm{x}_c} \end{pmatrix} \tag{4.12}$$

The resultant matrix in Equation (4.12), called the observation matrix, is then required to satisfy the full rank criteria. Evidently, it is required that $k \geq c$, in other words, the number of measurements needs to be at least equal to the

number of parameters to be estimated. Therefore, for an unique solution to exist, the condition of

$$\det\left(\frac{\partial \mathbf{y}}{\partial \mathbf{x}}\right) \neq 0 \tag{4.13}$$

needs to be met when the observation matrix is square. Otherwise, when $k > c$, the condition of full-column rank needs to be satisfied.

4.2.4 Cramèr-Rao Lower Bound

In addition to the existence of an unique solution as discussed above, achieving the best estimation accuracy with a set of measurements are another important consideration. The CRLB gives one an idea of the best performance that an estimator can achieve based on the data available.

Continuing from the previous section, a noise corrupted measurement vector was presented in Equation (4.8), in which the noise vector was defined as $\mathbf{w}$. Therefore, the corresponding measurement error covariance matrix is given by

$$\mathbf{R} = E\left[\mathbf{w}\mathbf{w}^T\right] = diag\left[\sigma^2_{w[1]}\ ,\cdots,\ \sigma^2_{w[k]}\right] \tag{4.14}$$

where $E[\cdot]$ is the expectation or mean of a random process. Then, the likelihood function of having obtained the measurement $\widetilde{\mathbf{y}}$, given that the parameter is $\mathbf{x}$, is given by the conditional probability density function of a multi-variate Gauss distribution

$$p(\widetilde{\mathbf{y}}|\mathbf{x}) = \frac{1}{(2\pi)^{\frac{k}{2}}\sqrt{\det(\mathbf{R})}} \exp\left\{-\frac{1}{2}\mathbf{w}^T\mathbf{R}^{-1}\mathbf{w}\right\} \tag{4.15}$$

The question now becomes, how accurately the parameters $\mathbf{x}$ could be estimated given the noise corrupted measurements? It is well known that the CRLB provides a lower bound for the estimation accuracy [129, 38], assuming an unbiased estimator. The first step to determine the CRLB is to evaluate the Fisher Infor-

mation Matrix (FIM) [129], given as

$$\begin{aligned}\mathbf{J} &= E\left[\nabla_{\mathbf{x}} \ln p(\widetilde{\mathbf{y}}|\mathbf{x})(\nabla_{\mathbf{x}} \ln p(\widetilde{\mathbf{y}}|\mathbf{x}))^T\right] \\ &= -E\left[\nabla_{\mathbf{x}}\left(\left\{\nabla_{\mathbf{x}}\left[\ln p(\widetilde{\mathbf{y}}|\mathbf{x})\right]\right\}^T\right)\right] \end{aligned} \tag{4.16}$$

where $p(\widetilde{\mathbf{y}}|\mathbf{x})$ was given in Equation (4.15) and $\nabla_{\mathbf{x}}$ is the gradient with respect to the parameter vector $\mathbf{x}$, in other words, $\nabla_{\mathbf{x}} = \frac{\partial}{\partial \mathbf{x}}$. Evaluation of the gradient with respect to the log-likelihood function defined in Equation (4.15) results in

$$\nabla_{\mathbf{x}} \ln p(\widetilde{\mathbf{y}}|\mathbf{x}) = \frac{\partial \mathbf{y}^T}{\partial \mathbf{x}} \mathbf{R}^{-1}\left[\widetilde{\mathbf{y}} - \mathbf{y}\right] \tag{4.17}$$

where $\frac{\partial \mathbf{y}^T}{\partial \mathbf{x}}$ is similarly defined as in Equation (4.9) and $\mathbf{R}$ was defined in Equation (4.14). Substitution of Equation (4.17) into Equation (4.16) and taking the expectation, the FIM for $\mathbf{x}$ is then given by

$$\mathbf{J}(\mathbf{x}) = \frac{\partial \mathbf{y}^T}{\partial \mathbf{x}} \mathbf{R}^{-1} \frac{\partial \mathbf{y}}{\partial \mathbf{x}} \tag{4.18}$$

and considered to be in the final form for this thesis. Finally, the CRLB inequality then states:

$$\mathbf{C} \geq \mathbf{J}^{-1}(\mathbf{x}) \tag{4.19}$$

where $\mathbf{C}$ is a covariance matrix containing the estimation error $\Delta\mathbf{x} = \widehat{\mathbf{x}} - \mathbf{x}$ and the estimate $\widehat{\mathbf{x}}$ is assumed to be unbiased. For the remainder of the thesis, the covariance matrix $\mathbf{C} = \mathbf{J}^{-1}(\mathbf{x})$ and then, refer to $\mathbf{C}$ as the CRLB.

4.3 Measurements

The background information presented in Section 4.2 reviewed two important concepts, namely measurement space and parameter space and, more importantly, detailed the mathematical relationship between these two spaces. Moving forward from this point, the measurement equations presented in Chapter 3 (Section 3.4), for a target moving in a 2-D coordinate system, are now placed in con-

text with regards to the measurement space. First, Doppler only measurements are assumed for Section 4.3.1 and secondly, range and Doppler measurements are assumed for Section 4.3.2.

4.3.1 Doppler Only Measurements

In Section 4.2.3, the ideal measurements, $\mathbf{y}$ is expressed as a function of the parameter space $\mathbf{x}$. Following this same guideline, but with the addition of time, the measurements taken by a CR would then read as follows; at time t_n, the collection of multiple ideal Doppler measurements, $\mathbf{y}_{D,n}$ expressed as a function of the target state vector, $\mathbf{x}_n$ are given as

$$\mathbf{y}_{D,n} = [f_{di}[n] \ , \cdots , \ f_{dk}[n]]^T \tag{4.20}$$

that is of the form $\mathbf{y} = \mathbf{g}(\mathbf{x})$. Further, $f_{di}[n]$ was defined in Equation (3.12), $\mathbf{x}_n$ was defined in Equation (3.4) and k indicates the number of receivers used, hence $i = (1, 2, \cdots, k)$. The corresponding measurement error vector will then be

$$\mathbf{w} = [w_{f_{di}} \ , \cdots , \ w_{f_{dk}}]^T \tag{4.21}$$

where i is similarly defined as above and $w_{f_{di}}$ are normal distributed random variables with zero mean and variance σ_f^2. In Howland [91] the minimum frequency standard deviation, σ_f for frequency measurements are shown to be a function of only the integration period T, as $\sigma_f = \sqrt{\frac{1}{12T^2}}$. Lastly, following Section 4.2.3, the noise corrupted Doppler measurement vector is constructed by using Equations (4.20) and (4.21), as:

$$\widetilde{\mathbf{y}}_{D,n} = \mathbf{y}_{D,n} + \mathbf{w} \tag{4.22}$$

in which the measurement error covariance matrix is given by:

$$\mathbf{R}_D = E[\mathbf{w}\mathbf{w}^T] = diag[\sigma^2_{f_{di}} \ , \cdots , \ \sigma^2_{f_{dk}}] \tag{4.23}$$

4.3.2 Range Doppler Measurements

In addition to the Doppler only measurement presented in the previous section, range-Doppler measurements are collected in a similar fashion as described for the Doppler case. Thus, the collection of ideal bistatic range and Doppler measurements from k receivers, are represented as

$$\mathbf{y}_{RD,n} = [R_{bi}[n] \ , f_{di}[n] \ , \cdots \ , R_{bk}[n] \ , \ f_{dk}[n]]^T \tag{4.24}$$

where $R_{bi}[n]$ was defined in Equation (3.10) and $f_{di}[n]$ in Equation (3.12). The corresponding measurement error vector is then given as

$$\mathbf{w} = [w_{R_{bi}} \ , w_{f_{di}} \ , \cdots \ , w_{R_{bk}} \ , \ w_{f_{dk}}]^T \tag{4.25}$$

where $w_{R_{bi}}$ are normal distributed random variables with zero mean and variance σ_R^2. $w_{f_{di}}$ and σ_f^2 are similarly defined as in Section 4.3.1. Lastly, it follows that the noise corrupted measurement vector for range-Doppler measurements are given by

$$\widetilde{\mathbf{y}}_{RD,n} = \mathbf{y}_{RD,n} + \mathbf{w} \tag{4.26}$$

with a corresponding measurement error covariance matrix given by:

$$\mathbf{R}_{RD} = E[\mathbf{w}\mathbf{w}^T] = diag\left[\sigma_{R_{bi}}^2 \ , \sigma_{f_{di}}^2 \ , \cdots \ , \sigma_{R_{bk}}^2 \ , \ \sigma_{f_{dk}}^2\right] \tag{4.27}$$

4.4 Observability

Following the observability criteria presented in Section 4.2.3 and using the measurement equations derived in the previous section, the observability for a 2-D target tracking scenario is covered in this section. Firstly, the observability for Doppler only measurements are considered in Section 4.4.1, and secondly for range-Doppler measurements in Section 4.4.2.

4.4.1 Doppler Measurements

The necessary condition for observability was presented in Equation (4.13). Therefore, using this equation together with the Doppler measurement equations derived in Section 4.3, the required condition for observability becomes,

$$\det\left(\frac{\partial \mathbf{y}_{D,n}}{\partial \mathbf{x}_n}\right) \neq 0 \tag{4.28}$$

where $\mathbf{y}_{D,n}$ was defined in Equation (4.20), $\mathbf{x}_n$ is the target state vector at time t_n and

$$\frac{\partial \mathbf{y}_{D,n}}{\partial \mathbf{x}_n} = \begin{pmatrix} \frac{\partial f_{d1}[n]}{\partial x_n} & \frac{\partial f_{d1}[n]}{\partial \dot{x}_n} & \frac{\partial f_{d1}[n]}{\partial y_n} & \frac{\partial f_{d1}[n]}{\partial \dot{y}_n} \\ \frac{\partial f_{d2}[n]}{\partial x_n} & \frac{\partial f_{d2}[n]}{\partial \dot{x}_n} & \frac{\partial f_{d2}[n]}{\partial y_n} & \frac{\partial f_{d2}[n]}{\partial \dot{y}_n} \\ \frac{\partial f_{d3}[n]}{\partial x_n} & \frac{\partial f_{d3}[n]}{\partial \dot{x}_n} & \frac{\partial f_{d3}[n]}{\partial y_n} & \frac{\partial f_{d3}[n]}{\partial \dot{y}_n} \\ \vdots & \vdots & \vdots & \vdots \\ \frac{\partial f_{dk}[n]}{\partial x_n} & \frac{\partial f_{dk}[n]}{\partial \dot{x}_n} & \frac{\partial f_{dk}[n]}{\partial y_n} & \frac{\partial f_{dk}[n]}{\partial \dot{y}_n} \end{pmatrix} \tag{4.29}$$

for $i = 1, 2, \cdots, k$ receivers. Therefore, the minimum requirement for observability requires the matrix to be square, hence $k \geq c$ where k indicates the row dimension and c the column dimension. In other words, the number of Doppler measurements should at least equal the number of parameters to be estimated in the target state vector $\mathbf{x}_n$. It is therefore concluded that the minimum number of receivers required for this thesis (2-D tracking) equals 4.

From this conclusion, one can argue that 4 consecutive measurements of Doppler could also be made from a single receiver site to satisfy Equation (4.28). Therefore, with the assumption that the velocity of the target stays constant over the 4 measurements, the time dependency is dropped, $\dot{x}_n = \dot{x}$ and given that the starting position is denoted as $[x_0, y_0]$, the partial derivative would be

$$\left.\frac{\partial \mathbf{y}_D}{\partial \mathbf{x}_0}\right|_{n=1,2,3,4} = \begin{pmatrix} \frac{\partial f_{d1}[1]}{\partial x_0} & \frac{\partial f_{d1}[1]}{\partial \dot{x}} & \frac{\partial f_{d1}[1]}{\partial y_0} & \frac{\partial f_{d1}[1]}{\partial \dot{y}} \\ \frac{\partial f_{d1}[2]}{\partial x_0} & \frac{\partial f_{d1}[2]}{\partial \dot{x}} & \frac{\partial f_{d1}[2]}{\partial y_0} & \frac{\partial f_{d1}[2]}{\partial \dot{y}} \\ \frac{\partial f_{d1}[3]}{\partial x_0} & \frac{\partial f_{d1}[3]}{\partial \dot{x}} & \frac{\partial f_{d1}[3]}{\partial y_0} & \frac{\partial f_{d1}[3]}{\partial \dot{y}} \\ \frac{\partial f_{d1}[4]}{\partial x_0} & \frac{\partial f_{d1}[4]}{\partial \dot{x}} & \frac{\partial f_{d1}[4]}{\partial y_0} & \frac{\partial f_{d1}[4]}{\partial \dot{y}} \end{pmatrix} \tag{4.30}$$

where $i = 1$ receiver. The case of using a single transmitter and receiver is well

analysed by Xaio et al. [101]. They point out that under some transmitter-target-receiver geometries, although the basic 4 measurements condition is met, the condition in Equation (4.28) failed. In summary, they identified the following geometries of target motion as being unobservable:

1. $\dot{x} = 0$ and $\dot{y} = 0$
2. $\dot{x} = 0$ and $x_0 = 0$
3. $\dot{x} = 0$ and $x_0 = x_R$
4. $\dot{y} = 0$ and $y_0 = 0$
5. $\dot{x} \neq 0$, $\dot{y} \neq 0$ and $(x_0 - x_R)\dot{y} = \dot{x}y_0$
6. $\dot{x} \neq 0$, $\dot{y} \neq 0$ and $x_0\dot{y} = \dot{x}y_0$

where the transmitter and receiver positions are respectively given as $(0, 0)$ and $(0, x_R)$. These conditions were verified by simulation and accordingly, it was discovered that a condition was missed, namely

7. $\dot{x} = 0$ and $x_0 = x_R/2$

Proof that this transmitter-target-receiver geometry results in a singular observation matrix for Equation (4.30), is provided in Section 4.7.2 by means of a simulation and analytical proof is provided in Appendix B.

Lastly, the single transmitter-receiver Doppler only tracking case is not considered for this thesis due the requirement that the target motion needs to be linear over 4 consecutive measurements, as mentioned before. Therefore, given that the CPI considered in this thesis is 4 s, four consecutive measurements require the target to be linear for a period of 16 s and seen from a practical point of view as unlikely.

4.4.2 Range Doppler Measurements

In the case of using range-Doppler measurements, the measurement vector presented in Equation (4.24) are used with Equation (4.13) and accordingly yields:

$$\frac{\partial \mathbf{y}_{RD,n}}{\partial \mathbf{x}_n} = \begin{pmatrix} \frac{\partial R_{b1}}{\partial x_n} & \frac{\partial R_{b1}}{\partial \dot{x}_n} & \frac{\partial R_{b1}}{\partial y_n} & \frac{\partial R_{b1}}{\partial \dot{y}_n} \\ \frac{\partial f_{d1}}{\partial x_n} & \frac{\partial f_{d1}}{\partial \dot{x}_n} & \frac{\partial f_{d1}}{\partial y_n} & \frac{\partial f_{d1}}{\partial \dot{y}_n} \\ \vdots & \vdots & \vdots & \vdots \\ \frac{\partial R_{bk}}{\partial x_n} & \frac{\partial R_{bk}}{\partial \dot{x}_n} & \frac{\partial R_{bk}}{\partial y_n} & \frac{\partial R_{bk}}{\partial \dot{y}_n} \\ \frac{\partial f_{dk}}{\partial x_n} & \frac{\partial f_{dk}}{\partial \dot{x}_k} & \frac{\partial f_{dk}}{\partial y_n} & \frac{\partial f_{dk}}{\partial \dot{y}_n} \end{pmatrix} \tag{4.31}$$

Therefore, it is evident that at least 2 receivers are required, where each receiver is required to make a range and Doppler measurement for the minimum observability criteria to be met.

In conclusion of this section; for a single transmitter, multiple receiver scenario where 1 Doppler measurement is made per receiver site, 4 receiver sites are required to perform 2-D tracking of a target's position and velocity. In the case of range-Doppler measurements, 2 receiver sites are required.

4.5 Calculation of the Cramèr-Rao Lower Bound

The aim in Section 4.4 was to determine whether an unique solution exists from a set of measurements. In addition to this requirement, it is also of interest to know what the best possible estimate of the state vector could be, given this set of measurements. Therefore, in continuation of Section 4.2.4, the CRLB is firstly derived for Doppler only measurements and secondly for range-Doppler measurements.

4.5.1 Doppler Only Measurements

As the theoretical performance of a Doppler only tracking system is of interest in this section, Cramèr-Rao theory is used to obtain the theoretical bound. The first

step in obtaining the CRLB is to determined the FIM as given in Equation (4.18). Therefore, with the necessary substitution, the FIM for a Doppler only tracking system is given as:

$$\mathbf{J}_D(\mathbf{x}) = \frac{\partial \mathbf{y}_{D,n}^T}{\partial \mathbf{x}_n} \mathbf{R}_D^{-1} \frac{\partial \mathbf{y}_{D,n}}{\partial \mathbf{x}_n} \tag{4.32}$$

where

$$\frac{\partial \mathbf{y}_{D,n}}{\partial \mathbf{x}_n} = \begin{pmatrix} \frac{\partial f_{d1}}{\partial x_n} & \frac{\partial f_{d1}}{\partial \dot{x}_n} & \frac{\partial f_{d1}}{\partial y_n} & \frac{\partial f_{d1}}{\partial \dot{y}_n} \\ \frac{\partial f_{d2}}{\partial x_n} & \frac{\partial f_{d2}}{\partial \dot{x}_n} & \frac{\partial f_{d2}}{\partial y_n} & \frac{\partial f_{d2}}{\partial \dot{y}_n} \\ \frac{\partial f_{d3}}{\partial x_n} & \frac{\partial f_{d3}}{\partial \dot{x}_n} & \frac{\partial f_{d3}}{\partial y_n} & \frac{\partial f_{d3}}{\partial \dot{y}_n} \\ \vdots & \vdots & \vdots & \vdots \\ \frac{\partial f_{dk}}{\partial x_n} & \frac{\partial f_{dk}}{\partial \dot{x}_k} & \frac{\partial f_{dk}}{\partial y_n} & \frac{\partial f_{dk}}{\partial \dot{y}_n} \end{pmatrix} \tag{4.33}$$

and $\mathbf{R}_D$ was defined in Equation (4.23) and $\mathbf{y}_{D,n}$ defined in Equation (4.20). Following the theory presented in Section 4.2.4, the CRLB is then obtained as:

$$\mathbf{C}_n = \mathbf{J}_D^{-1}(\mathbf{x}_n) \tag{4.34}$$

where $\mathbf{C}_n$ is the covariance matrix of the estimation error, $\Delta\mathbf{x} = \widehat{\mathbf{x}}_n - \mathbf{x}_n$ at t_n and $\widehat{\mathbf{x}}_n$ assumed to be unbiased. From Levanon [130], the GDOP vector can be obtained from the CRLB as GDOP $= \sqrt{\mathrm{Tr}(\mathbf{C}_n)}$ where $\mathrm{Tr}(\cdot)$ is the trace operator. Accordingly, the 2-D Position Dilution Of Precision (PDOP) is defined as:

$$\sigma_{p,n} = \sqrt{\mathbf{C}_n(1,1) + \mathbf{C}_n(3,3)} \tag{4.35}$$

and the Velocity Dilution Of Precision (VDOP):

$$\sigma_{v,n} = \sqrt{\mathbf{C}_n(2,2) + \mathbf{C}_n(4,4)} \tag{4.36}$$

The PDOP and VDOP can therefore respectively be considered to be the minimum position and velocity errors to be expected.

4.5.2 Range Doppler Measurements

To obtain the CRLB for a range-Doppler tracking system, a similar approach to the one presented in Section 4.5.1 is followed. Firstly, the FIM is calculated by using Equation (4.18) to obtain

$$\mathbf{J}_{RD}(\mathbf{x}) = \frac{\partial \mathbf{y}_{RD,n}^T}{\partial \mathbf{x}_n} \mathbf{R}_{RD}^{-1} \frac{\partial \mathbf{y}_{RD,n}}{\partial \mathbf{x}_n} \tag{4.37}$$

where

$$\frac{\partial \mathbf{y}_{RD,n}}{\partial \mathbf{x}_n} = \begin{pmatrix} \frac{\partial R_{b1}}{\partial x_n} & \frac{\partial R_{b1}}{\partial \dot{x}_n} & \frac{\partial R_{b1}}{\partial y_n} & \frac{\partial R_{b1}}{\partial \dot{y}_n} \\ \frac{\partial f_{d1}}{\partial x_n} & \frac{\partial f_{d1}}{\partial \dot{x}_n} & \frac{\partial f_{d1}}{\partial y_n} & \frac{\partial f_{d1}}{\partial \dot{y}_n} \\ \vdots & \vdots & \vdots & \vdots \\ \frac{\partial R_{bk}}{\partial x_n} & \frac{\partial R_{bk}}{\partial \dot{x}_n} & \frac{\partial R_{bk}}{\partial y_n} & \frac{\partial R_{bk}}{\partial \dot{y}_n} \\ \frac{\partial f_{dk}}{\partial x_n} & \frac{\partial f_{dk}}{\partial \dot{x}_k} & \frac{\partial f_{dk}}{\partial y_n} & \frac{\partial f_{dk}}{\partial \dot{y}_n} \end{pmatrix} \tag{4.38}$$

and $\mathbf{R}_{RD}$ was defined in Equation (4.27) and $\mathbf{y}_{RD,n}$ defined in Equation (4.24). As in the previous section, the CRLB is then obtained by

$$\mathbf{C}_n = \mathbf{J}_{RD}^{-1}(\mathbf{x}_n) \tag{4.39}$$

where $\mathbf{C}_n$ is the covariance matrix of the estimation error, $\Delta\mathbf{x} = \widehat{\mathbf{x}}_n - \mathbf{x}_n$ at t_n and $\widehat{\mathbf{x}}_n$ assumed to be unbiased. Lastly, the minimum position and velocity errors are obtained from $\mathbf{C}_n$ by using Equations (4.35) and (4.36).

4.6 Calculation of the Cumulative Cramèr-Rao Lower Bound

As mentioned in the introduction of this chapter, the Cramèr-Rao theory presented in Section 4.5 does not account for time history information. In order to take time history measurements into account, a method called the Posterior CRLB [131, 132] could be considered. However, rather than using the Posterior CRLB, that is based on a stochastic dynamic system, a new method, called the

CCRLB is derived that is based on a deterministic dynamic system. In this case, the CCRLB would then be lower than the Posterior CRLB. Accordingly, this section is focussed towards deriving the CCRLB and a comparison between the two bounds left as future research, see Chapter 7. Once again, the respective cases of Doppler only and range-Doppler measurements are considered for the CCRLB.

4.6.1 Doppler Only Measurements

Assuming a target is moving in 2-D space, as described in Section 3.4.2 and L_x observations of the target's ideal Doppler shift are accumulated over a time interval $[t_{n-L_x+1}, t_n]$ by an multistatic CR, then the time history of observations at time t_n, are given by:

$$\mathbf{y}_{D,n} = \left[\mathbf{y}_{D,n}, \mathbf{y}_{D,n-1}, \mathbf{y}_{D,n-2}, \cdots, \mathbf{y}_{D,n-L_x+1}\right]^T \tag{4.40}$$

where $\mathbf{y}_{D,n}$ is given by Equation (4.20) at time t_n, $\mathbf{y}_{D,n-1}$ at time t_{n-1} and so forth, hence a $[k \cdot L_x \times 1]$ vector for k receivers is obtained. Before the Cumulative FIM (CFIM) is derived, a method to take the derivative of a previous measurement vector with respect to the current target state, is required. Therefore, by making use of the chain rule,

$$\frac{\partial \mathbf{y}_{n-i}}{\partial \mathbf{x}_n} = \frac{\partial \mathbf{y}_{n-i}}{\partial \mathbf{x}_{n-i}} \frac{\partial \mathbf{x}_{n-i}}{\partial \mathbf{x}_n} \tag{4.41}$$

and recalling from Equation (3.7) that due to the motion of the target, the transition from the previous state to the current state was given as $\mathbf{x}_n = \Phi(t_{n-1}, t_n)\mathbf{x}_{n-1}$, thereby

$$\frac{\partial \mathbf{x}_{n-i}}{\partial \mathbf{x}_n} = \Phi(t_n, t_{n-i}) \tag{4.42}$$

where $\Phi(t_n, t_{n-i})$ is defined as the back projection transition matrix, representing a transition from time stamp t_n to t_{n-i}. Accordingly, by the substitution of

Equation (4.42) in Equation (4.41), the following equation is obtained:

$$\frac{\partial \mathbf{y}_{n-i}}{\partial \mathbf{x}_n} = \frac{\partial \mathbf{y}_{n-i}}{\partial \mathbf{x}_{n-i}} \Phi(t_n, t_{n-i}) \tag{4.43}$$

Next, applying Equation (4.43) to (4.40), the linearisation of L_x observations becomes

$$\frac{\partial \mathbf{y}_{D,n}}{\partial \mathbf{x}_n} = \begin{bmatrix} \frac{\partial \mathbf{y}_{D,n}}{\partial \mathbf{x}_n} \\ \frac{\partial \mathbf{y}_{D,n-1}}{\partial \mathbf{x}_{n-1}} \Phi(t_n, t_{n-1}) \\ \vdots \\ \frac{\partial \mathbf{y}_{D,n-L_x}}{\partial \mathbf{x}_{n-L_x}} \Phi(t_n, t_{n-L_x+1}) \end{bmatrix} \tag{4.44}$$

and finally, the CFIM is obtained by the substitution of Equation (4.44) in (4.18) that results in

$$\begin{aligned} \mathbf{J}_D(\mathbf{x}_n) &= \frac{\partial \mathbf{y}_{D,n}}{\partial \mathbf{x}_n}^T \mathbf{R}_D^{-1} \frac{\partial \mathbf{y}_{D,n}}{\partial \mathbf{x}_n} \\ &= \sum_{i=0}^{L_x-1} \Phi(t_n, t_{n-i})^T \frac{\partial \mathbf{y}_{D,n-i}}{\partial \mathbf{x}_{n-i}}^T \mathbf{R}_D^{-1} \frac{\partial \mathbf{y}_{D,n-i}}{\partial \mathbf{x}_{n-i}} \Phi(t_n, t_{n-i}) \end{aligned} \tag{4.45}$$

where $\mathbf{R}_D$ is defined in Equation (4.23). Lastly, setting $n = L_x - 1$, the following is obtained:

$$\begin{aligned} \mathbf{J}_D(\mathbf{x}_n) &= \frac{\partial \mathbf{y}_{D,n}}{\partial \mathbf{x}_n}^T \mathbf{R}_D^{-1} \frac{\partial \mathbf{y}_{D,n}}{\partial \mathbf{x}_n} \\ &\quad + \sum_{i=0}^{n} \Phi(t_n, t_i)^T \frac{\partial \mathbf{y}_{D,i}}{\partial \mathbf{x}_i}^T \mathbf{R}_D^{-1} \frac{\partial \mathbf{y}_{D,i}}{\partial \mathbf{x}_i} \Phi(t_n, t_i) \end{aligned} \tag{4.46}$$

By comparing Equation (4.32) and Equation (4.46), it is obvious that the CFIM adds a substantial amount of information that is essential to the CRLB analysis. It is recognised that Equation (4.46) is of similar form to the inverse of the Gauss Newton filter that Nadjiasngar [103] managed to rewrite in a recursive format, thus it follows that

$$\mathbf{J}_D(\mathbf{x}_n) = \Gamma \Phi(t_n, t_{n-1})^T \mathbf{J}_D(\mathbf{x}_{n-1}) \Phi(t_n, t_{n-1}) + \frac{\partial \mathbf{y}_{D,n}}{\partial \mathbf{x}_n}^T \mathbf{R}_D^{-1} \frac{\partial \mathbf{y}_{D,n}}{\partial \mathbf{x}_n} \tag{4.47}$$

where Γ is defined as the data forgetting factor in which $\Gamma <= 1$ that effectively holds $\frac{1}{1-\Gamma}$ history samples in Equation (4.47). Further, note that Equation (4.47) is only valid for a constant time interval, .ie $t_{n-1} - t_n = -T$.

Lastly, the CCRLB is obtained by the substitution of Equation (4.47) into Equation (4.34) and the respective position and velocity errors given by Equations (4.35) and (4.36).

4.6.2 Range Doppler Measurements

Deriving the CCRLB using range-Doppler measurements is obtained in a similar manner as described in Section 4.6.1

First, the time history array is constructed over L_x range-Doppler observations as:

$$\mathbf{y}_{RD,n} = \left[\mathbf{y}_{RD,n}, \mathbf{y}_{RD,n-1}, \mathbf{y}_{RD,n-2}, \cdots, \mathbf{y}_{RD,n-L_x+1}\right]^T \tag{4.48}$$

where $\mathbf{y}_{RD,n}$ is given by Equation (4.24) at time t_n, $\mathbf{y}_{RD,n-1}$ at time t_{n-1} and so forth. Then, following the same steps as presented in Section 4.6.1, the CFIM for range-Doppler measurements is given as:

$$\begin{aligned}\mathbf{J}_{RD}(\mathbf{x}_n) = \Gamma\Phi(t_n, t_{n-1})^T \mathbf{J}_{RD}(\mathbf{x}_{n-1})\Phi(t_n, t_{n-1}) \\ + \frac{\partial \mathbf{y}_{RD,n}}{\partial \mathbf{x}_n}^T \mathbf{R}_{RD}^{-1} \frac{\partial \mathbf{y}_{RD,n}}{\partial \mathbf{x}_n}\end{aligned} \tag{4.49}$$

where $\mathbf{R}_{RD}$ is given in Equation (4.27). Lastly, the CCRLB is obtained by the substitution of Equation (4.49) in Equation (4.39) to obtain $\mathbf{C}_n$, which in return is used to obtain the respective position and velocity errors given by Equations (4.35) and (4.36).

4.7 Simulation Results: 2D Surface plots

In the previous sections, theoretical concepts were established that are primarily concerned whether a target's position could be resolved from a set of measurements and also, what possible accuracy could be expected when using **only Doppler measurements**. The aim of this section is to visualise these concepts by simulating the expected target tracking accuracy over a 2-D surface, called 2-D surface plots. From these 2-D surface plots it will become clear that an observation analysis alone is not adequate as in many regions the observation matrix is observable, but results in insufficient tracking performance. These insufficient tracking regions will be referred to as *bad geometries* and methods to circumvent these bad geometries will be covered in more detail in the subsequent chapters.

4.7.1 Setting Thresholds

As stated by *Definition 5* in Section 4.2.1, the condition of a matrix is a measure of its inversion accuracy, hence an important aspect to consider as the CRLB is obtained by taking the inverse from either the FIM or CFIM. When the condition of a matrix is close to 1, it is said to be well conditioned, an inverse exists and the inverse will be accurate. As the condition increases, the matrix will become increasingly ill-conditioned up to a point where it is singular and will therefore be non-invertible. This is usually the case when the matrix condition tends to ∞. Further, most computers make use of floating point numbers that is associated with floating point precision. The results obtained for this thesis were executed on a 64-bit system in which the floating point precision is known to be $eps = 2^{-53}$, in which $\frac{1}{eps} \approx 319$ dB would then represent the ∞ bound. Therefore, all matrices with a condition larger than 319 dB are assumed to be singular (non-invertible). As only unique solutions were considered for this thesis, pseudo inverse techniques were not used as these techniques could possibly result in non-unique solutions as well.

As mentioned earlier, having knowledge about the singularity regions within

the ROI alone are not sufficient as additional regions might exist where the singularity criteria is met, but the target accuracy is not acceptable. For this thesis, the CRLB is used for the target accuracy criteria and since the worst case range resolution for exploiting a single FM radio channel is around 3000 m, this value was used for the accuracy criteria. Therefore in summary; 1.) A region is defined singular when the condition of the observation matrix is greater than 157 dB, 2.) When the condition of the matrix is less than 157 dB, but the CRLB $>$ 3000 m, the region is defined as a *bad geometry* region and lastly, 3.) when the CRLB $<$ 3000 m, the region is defined as a *good geometry* region. Note, the 3000 m value will be assumed throughout this thesis, unless it is stated otherwise.

4.7.2 Single Transmitter Single Receiver

The simulation investigation is started by verifying the conditions under which Xiao et al.[101] determined the observation matrix to be singular, see Section 4.4.1. In addition to the singular areas described by Xiao, a visual distinction between the good and bad geometry regions are further made in this thesis.

In Figures 4.1 and 4.2, 2-D surface plots of the expected target tracking accuracy are presented for a single transmitter-receiver configuration using only Doppler measurements. The receiver was placed at $\mathbf{x}_{R1} = [5,0]$ km and the transmitter at the origin of the xy-coordinate system, hence $\mathbf{x}_E = [0,0]$ km. In the case of Figure 4.1, the target was moving with a velocity of $\mathbf{v}_{\mathrm{x}} = [100,100]$ m/s from the bottom left of the figure to the top right. To satisfy the observation criteria as set in Equation (4.30), 4 consecutive Doppler measurements were collected at the receiver and then used to calculate the CRLB with Equations (4.32), (4.34) and (4.35). The next 4 measurements were then collected, the position accuracy calculated and so forth until the flightpath reach the top right of the figure. Finally, the whole process was then repeated until all parallel flightpaths[5] were completed to form the 2-D surface plot for the CRLB.

[5] The parallel spacing between the flight paths is 500 m.

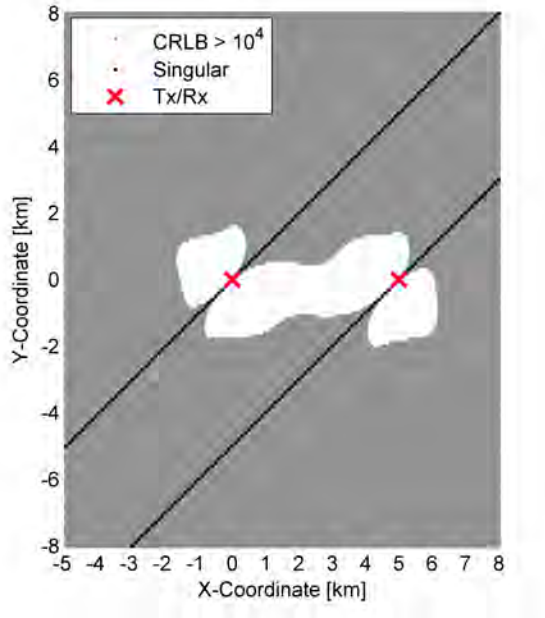

Figure 4.1: The theoretical 2-D target position accuracy for a single transmitter, single receiver scenario using only Doppler measurements. Target motion is kept constant at $\mathbf{v}_x = [100,100]$ m/s and a standard deviation of $\sigma_f = 0.2$ Hz was used to simulate the Doppler measurement errors.

In Figure 4.1, the gray areas represents the bad geometry regions and accordingly points out where the observation matrix is observable, but the expected position error[6] will be larger than 10 km. Further, the good geometry regions are represented by the white areas, the black lines indicates the areas where the observation matrix is singular and lastly, the transmitter and receiver positions are indicted by the red crosses. Two important observations are made from Figure 4.1. First, motion towards/away from the transmitter or receiver, when the velocity components are equal ($\dot{x} = \dot{y}$), result in the observation matrix being singular and confirms items 5 and 6 as set in the observation criteria list in Section 4.4.1. Secondly, the area in which the expected tracking error is less than 10 km is fairly small.

For Figures 4.2 (a) and (b), the simulation as described above, is repeated for dif-

[6] In the case of setting the CRLB to 3 km, almost the entire surface is grey. Therefore, relaxing the accuracy criteria to 10 km was required for single transmitter-receiver example.

ferent flight directions to verify the remainder of the criteria list presented in Xiao et al.[101]. In the case of Figure 4.2 (a) the target velocity is $\mathbf{v}_{\mathrm{x}} = [100,0]$ m/s, whereas in Figure 4.2 (b), $\mathbf{v}_{\mathrm{x}} = [0,100]$ m/s. Similarly to Figure 4.1, the gray region indicates bad geometry areas in which the CRLB $\geq$ 10 km.

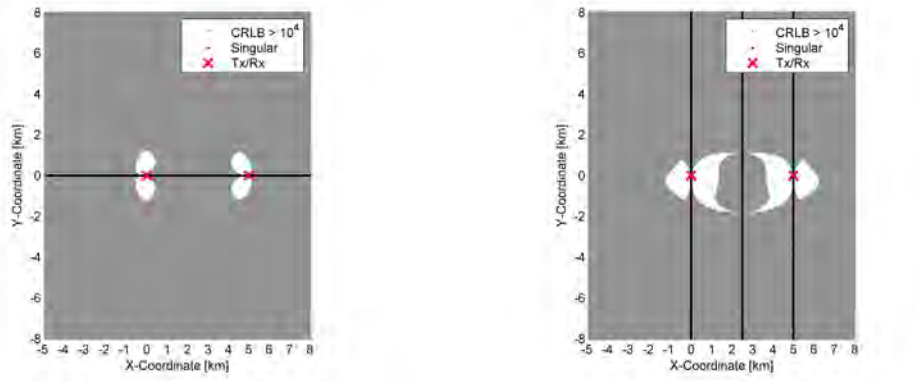

(a) (b)

Figure 4.2: The 2-D target position accuracy for a single transmitter single receiver scenario using only Doppler measurements with $\sigma_f = 0.2$ Hz. a.) Target moving at $\mathbf{v}_{\mathrm{x}} = [100,0]$ m/s, b.) Target moving at $\mathbf{v}_{\mathrm{x}} = [0,100]$ m/s.

From Figure 4.2 (a), it is evident that the observation matrix is singular when the target is travelling along the y-axis and therefore confirms criteria item 4 in Section 4.4.1. Lastly, Figure 4.2 (b) confirms criteria items 2 and 3, stating that the observation matrix will be singular when the target is moving towards/away from the transmitter or receiver when $\dot{y} \neq 0$ and $\dot{x} = 0$.

Therefore, all the observability criteria items that Xiao et al. proposed were verified, but noticing from Figure 4.2 (b), the observation matrix is also singular when the target is moving along $x = \frac{x_E}{2}$. This is easily verified by means of an example for which the following is assumed; 1.) The transmitter and receiver coordinates are $\mathbf{x}_E = [x_E,\ 0]$ m and $\mathbf{x}_{R1} = [0,\ 0]$ m respectively 2.) the target velocity is $\mathbf{v}_{\mathrm{x}} = [0,\ 1]$ m/s and 3.) the starting position is $\mathbf{x}_{p,0} = [\frac{x_E}{2}, 0]$. Using the equations derived by Xiao et al. [101], the observation matrix is calculated

to be

$$\left.\frac{\partial \mathbf{y}_D}{\partial \mathbf{x}_0}\right|_{n=1,2,3,4} = \begin{pmatrix} 0 & 0 & \frac{\partial f_{d1}[1]}{\partial y_0} & \frac{\partial f_{d1}[1]}{\partial \dot{y}} \\ 0 & 0 & \frac{\partial f_{d1}[2]}{\partial y_0} & \frac{\partial f_{d1}[2]}{\partial \dot{y}} \\ 0 & 0 & \frac{\partial f_{d1}[3]}{\partial y_0} & \frac{\partial f_{d1}[3]}{\partial \dot{y}} \\ 0 & 0 & \frac{\partial f_{d1}[4]}{\partial y_0} & \frac{\partial f_{d1}[4]}{\partial \dot{y}} \end{pmatrix} \tag{4.50}$$

where $\mathbf{x}_0 = [x_0\ \dot{x}\ y_0\ \dot{y}]^T$ and all non-zero entries in (4.50) are given by it's function description. Therefore, having two zero columns in (4.50), will result in $\det\left(\frac{\partial \mathbf{y}_D}{\partial \mathbf{x}_0}\right) = 0$ and proves that the observation matrix will be singular at $(x_0, y_0) = [\frac{x_E}{2}, y \in \mathbb{R}]$. See Appendix B for the proof of Equation (4.50).

An important observation from Figures 4.1 and 4.2 is the fairly small region of good geometry (target position error is less than 10 km) and clearly not acceptable. However, this region can easily be expanded by increasing the integration gain beyond 4 consecutive measurements as demonstrated by Xiao. However, the limitation with this approach remains the constant velocity assumption over the integration gain interval. Another option to expand the good geometry area is to make use of multiple receiver sites that is considered in the next section.

4.7.3 Multiple Receivers

This section explores the benefit of adding additional receiver sites to the single transmitter-receiver configuration that was presented in Section 4.7.2. In Figure 4.3, 2-D CRLB surface plots are presented for two different receiver placement configurations, firstly a linear receiver placement configuration in Figure 4.3 (a) and secondly, a circular receiver placement configuration in Figure 4.3 (b). In both cases the target motion is $\mathbf{v}_{\mathrm{x}}$ = [0,100] m/s and all 2-D CRLB surface plots are generated in a similar fashion as described in Section 4.7.2.

In the case of Figure 4.3 (a), all transmitter/receiver elements[7] are placed on the x-axis. The transmitter is placed at the origin of the coordinate systems, $\mathbf{x}_E$ = [0,0] km and the 4 respective respective receivers at $\mathbf{x}_{R1}$ = [-20,0] km,

[7] A minimum of 4 receivers were used as determined by the observability criteria presented in Section 4.4.1

$\mathbf{x}_{R2}$ = [-10,0] km, $\mathbf{x}_{R3}$ = [10,0] km and X_{R4} = [20,0] km. For the symmetrical circular receiver placement presented in Figure 4.3 (b), the transmitter remained at the origin of the coordinate system and the respective receivers were situated at $\mathbf{x}_{R1}$ = [20,0] km, $\mathbf{x}_{R2}$ = [0,20] km, $\mathbf{x}_{R3}$ = [-20,0] km and $\mathbf{x}_{R4}$ = [0,-20] km.

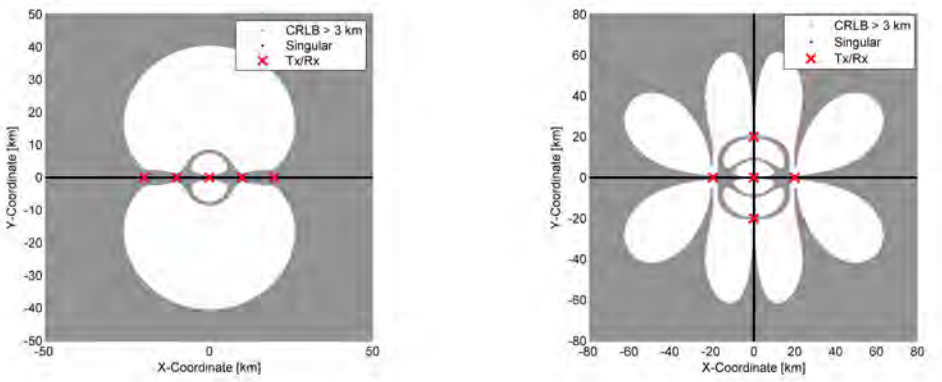

(a) (b)

Figure 4.3: The 2-D target position accuracy, based on Doppler measurements in a single transmitter, multiple receiver scenario. Target motion is kept constant at $\mathbf{v}_x$ = [0,100] m/s and the standard deviation on the Doppler measurements was σ_f = 0.2 Hz. a.) A linear receiver configuration with the transmitter located at the origin of the coordinate system. b.) A circular receiver configuration, also with the transmitter located at the origin of the coordinate system.

The most important observation from both Figures 4.3 (a) and (b) is the significant increase of the good geometry region compared to the single transmitter-receiver configuration. For the linear receiver configuration presented in Figure 4.3 (a), it is evident that the observation matrix becomes singular when the target crosses the x-axis. Further, bad geometry regions are seen around the x-axis, a circular region around the transmitter and lastly at the far ends of the axis, hence $\geq \pm 40$ km in the y-axis and $\geq \pm 20$ km in the x-axis. For the circular receiver placement presented in Figure 4.3 (b), the good geometry regions are extended in both the x and y directions compared to the linear receiver geometry, but more bad geometries are also present within this region. Also, in addition to the observation matrix only being singular when the target crosses the x-axis in the linear receiver configuration, the observation matrix is also singular when the target moves along the y-axis for a circular receiver configuration.

Next, the same circular receiver placement is considered, but the target is assumed to have velocity components in both the x and y directions. In the case of Figure 4.4 (a), the target velocity is $\mathbf{v}_x = [100,100]$ m/s and in the case of Figure 4.4 (b), the target velocity is $\mathbf{v}_x = [50,100]$ m/s.

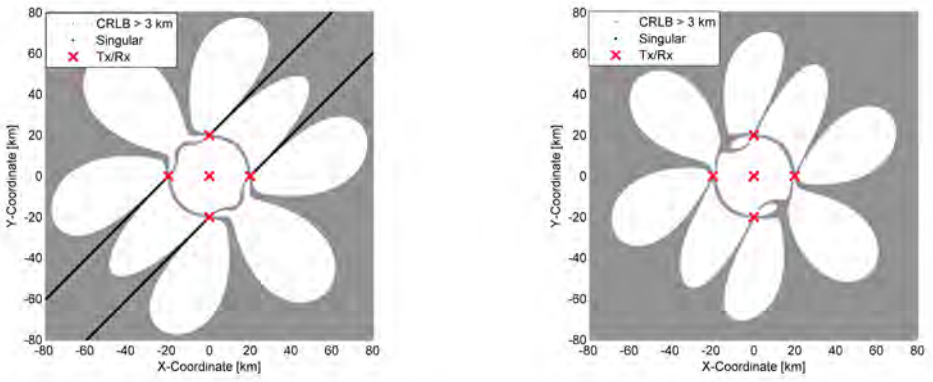

(a) (b)

Figure 4.4: The 2-D target position accuracy, based on Doppler measurements in a single transmitter, circular receiver configuration for different directions of flight motion. a.) Target moving with a velocity $\mathbf{v}_x = [100,100]$ m/s. b.) Target moving with a velocity $\mathbf{v}_x = [50,100]$ m/s.

Compared to Figure 4.3 (b), Figure 4.4 (a) illustrates that target motion in which $\dot{x} = \dot{y}$, the good geometry region slightly increased and the bad geometries inside the receiver ring are removed. Target movement towards/away from the receivers still results in the observation matrix being singular, but the singularity experienced along the x and y-axis are resolved and actually becomes a good geometry region as the target crosses it. Illustrated by Figure 4.4 (b), the observation matrix singularity is reduced to only the transmitter or receiver positions when $\dot{x} \neq \dot{y}$. However, in comparison to the $\dot{x} = \dot{y}$ case, the bad geometries slightly increased, but a fairly similar pattern remains.

Up to this point, only measurements of the target's Doppler shift were considered in the 2-D CRLB surface plot analysis. Next, range-Doppler measurements are considered and accordingly presented in Figure 4.5 for two scenarios, 1.) a linear receiver placement and 2.) a circular receiver placement, where in both cases the target velocity was $\mathbf{v}_x = [0,100]$ m/s.

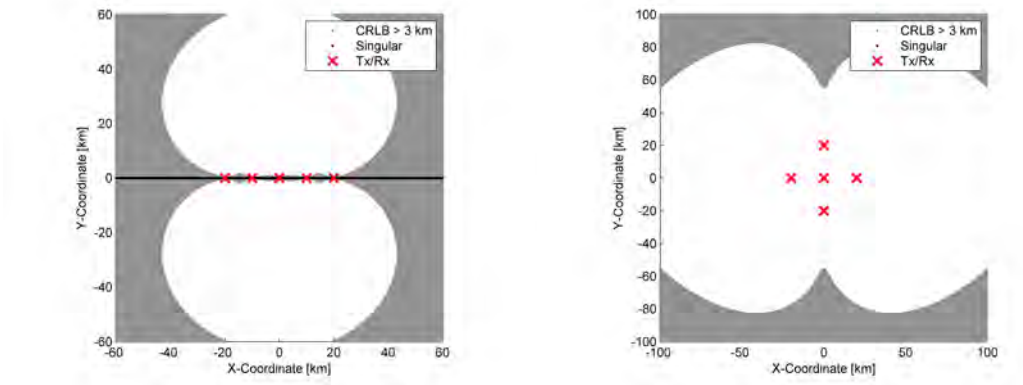

(a) (b)

Figure 4.5: The 2-D target position accuracy, based on range-Doppler measurements in a single transmitter, multiple receiver scenario. Target motion is kept constant at $\mathbf{v}_x = [0,100]$ m/s, $\sigma_f = 0.2$ Hz and the standard deviation on the range measurements was $\sigma_r = 2000$ m. a.) Linear receiver placement b.) Circular receiver placement.

Seen from both Figures 4.5 (a) and (b), the additional range measurements significantly reduced the bad geometry regions, despite the fact that the range measurements are of low resolution. This in fact means that the additional range measurements improved the observation matrix conditioning significantly. However, this will only be investigated further in Chapter 5 as the results presented in this section are only intended to point out that bad geometry regions do exist in Doppler only tracking and could be limited by considering the following; 1.) Increase the number of receivers, 2.) Receiver placement and lastly, 3.) Improve the conditioning of the observation matrix.

4.8 MIMO in Doppler Only Tracking

This section explores the option of using more than one transmitter with a multiple receiver configuration for Doppler only target tracking. From the observability criteria presented in Section 4.2.3, it was concluded that the observation matrix needs to be of full rank and accordingly lead to the conclusion that 4

Doppler measurements are required from 4 receiver sites. However, by arguing that the requirement is to obtain 4 Doppler measurements, then surely exploiting 2 transmitters with 2 receivers would also produce 4 Doppler measurements and satisfy the full rank criteria. To further investigate this option, the following two assumptions are made:

1. **Multiple Receivers** are spatially separated over a geographical area in which no two receivers occupy the same position.
2. **Ideal/perfect measurements** are assumed for this analysis.

Displayed in Figure 4.6 is a multiple transmitter, multiple receiver scenario in which the aim would be to track the target indicated by the straight line. The two transmitters are respectively labelled A and B and the 4 receivers C to F. With the assumptions made above, the transmitter to target to receiver path distance is unique to each receiver for a given transmitter and time instance. Therefore, the distance from transmitter A to target to receiver C at time t, is given as $(a[t] + c[t])$, hence according to Equation (3.11) the bistatic Doppler at receiver C is given as $f_{dC}^{A}[t] = -\frac{1}{\lambda}\frac{\partial}{\partial t}(a[t]+c[t])$. Following this notation, the ideal bistatic Doppler at the respective receiver sites are then given as follow[8]:

- Transmitter A to Target to Receiver D, $f_{dD}^{A}[t] = -\frac{1}{\lambda}\frac{\partial}{\partial t}(a[t] + d[t])$.
- Transmitter A to Target to Receiver E, $f_{dE}^{A}[t] = -\frac{1}{\lambda}\frac{\partial}{\partial t}(a[t] + e[t])$.
- Transmitter A to Target to Receiver F, $f_{dF}^{A}[t] = -\frac{1}{\lambda}\frac{\partial}{\partial t}(a[t] + f[t])$.
- Transmitter B to Target to Receiver C, $f_{dC}^{B}[t] = -\frac{1}{\lambda}\frac{\partial}{\partial t}(b[t] + c[t])$.
- Transmitter B to Target to Receiver D, $f_{dD}^{B}[t] = -\frac{1}{\lambda}\frac{\partial}{\partial t}(b[t] + d[t])$.

First a single transmitter, 4 receiver scenario is considered in which A is selected as the transmitter and C to F as the receivers. Then, 4 consecutive Doppler

[8] Not all the possible combinations of T-R pairs are listed here, but only the combinations that are used in this thesis.

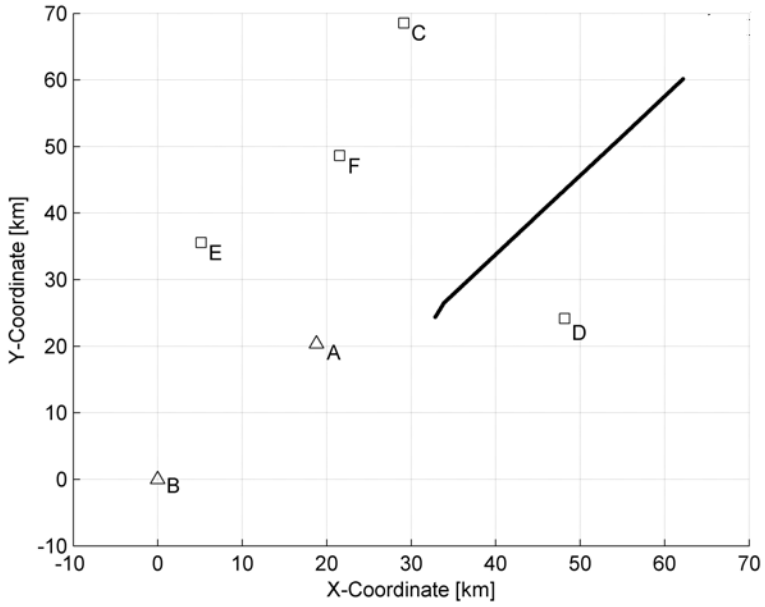

Figure 4.6: The geographical setup for a MIMO Doppler only tracking CR, displaying the positions of 2 transmitters, 4 receivers and a target flightpath. The 2 transmitters are respectively labelled 'A' and 'B' and the 4 receivers are labelled 'C' to 'F'.

measurements collected at the receivers over the time interval $t = 1$ to $t = 4$, is represented in matrix format as:

$$f_{1\text{x}4} = -\frac{1}{\lambda}\frac{\partial}{\partial t}\begin{pmatrix} (a[1]+c[1]) & (a[1]+d[1]) & (a[1]+e[1]) & (a[1]+f[1]) \\ (a[2]+c[2]) & (a[2]+d[2]) & (a[2]+e[2]) & (a[2]+f[2]) \\ (a[3]+c[3]) & (a[3]+d[3]) & (a[3]+e[3]) & (a[3]+f[3]) \\ (a[4]+c[4]) & (a[4]+d[4]) & (a[4]+e[4]) & (a[4]+f[4]) \end{pmatrix} \tag{4.51}$$

where the row dimension indicates time and the column dimension indicates space (geographically separated receivers). Through some straight forward elementary row operations, it can be shown that the matrix in Equation (4.51) can

be written into RREF as:

$$f_{1\text{x}4,RREF} = -\frac{1}{\lambda}\frac{\partial}{\partial t}\begin{pmatrix} 1 & 0 & 0 & 0 \\ 0 & 1 & 0 & 0 \\ 0 & 0 & 1 & 0 \\ 0 & 0 & 0 & 1 \end{pmatrix} \tag{4.52}$$

Thus, it immediately follows that $rk(f_{1\text{x}4,RREF}) = 4$ and proves that the Doppler measurements collected over the 4 receiver sites are not correlated. This is also consistent with the observability theory presented in Section 4.4.1.

However, when a 2×2 MIMO configuration is used, the Doppler measurements becomes correlated and as a result, the observation matrix becomes singular. This is proved next. Consider using transmitter A and B, together with receiver C and D in Figure 4.6, then the Doppler measurements in matrix form will be:

$$f_{2\text{x}2} = -\frac{1}{\lambda}\frac{\partial}{\partial t}\begin{pmatrix} (a[1]+c[1]) & (a[1]+d[1]) & (b[1]+c[1]) & (b[1]+d[1]) \\ (a[2]+c[2]) & (a[2]+d[2]) & (b[2]+c[2]) & (b[2]+d[2]) \\ (a[3]+c[3]) & (a[3]+d[3]) & (b[3]+c[3]) & (b[3]+d[3]) \\ (a[4]+c[4]) & (a[4]+d[4]) & (b[4]+c[4]) & (b[4]+d[4]) \end{pmatrix} \tag{4.53}$$

and once again, applying some straight forward elementary row operations, it can be shown that the matrix in Equation (4.53) can be written in RREF as:

$$f_{2\text{x}2,RREF} = -\frac{1}{\lambda}\frac{\partial}{\partial t}\begin{pmatrix} 1 & 0 & 0 & -1 \\ 0 & 1 & 0 & 1 \\ 0 & 0 & 1 & 1 \\ 0 & 0 & 0 & 0 \end{pmatrix} \tag{4.54}$$

Therefore, as $rk(f_{2\text{x}2,RREF}) = 3$, it is concluded that Doppler correlation between the receiver sites exist. By inspection of the matrix in Equation (4.54), it is noticed that column 4 is a linear combination of columns (2 + 3 - 1). This is easily verified to be the case as the summation of the first three columns in row 1 of Equation (4.53) is $(-[a[1]+c[1]]+[a[1]+d[1]]+[b[1]+c[1]]) = [b[1]+d[1]]$, which is indeed equal to the fourth column of row 1. Notice, this will be true for

all rows in the matrix.

Therefore, it is concluded that a MIMO like configuration in CR suffers from Doppler correlation between some of the Doppler measurements. Thus, as a rule of thumb, for the observation matrix to be observable using Doppler only information, the minimum number of transmitters and receivers required for a MIMO configuration would be:

$$N_{state} = N_t + N_r - 1 \tag{4.55}$$

where N_{state} is the number of state variables in the state vector $\mathbf{x}_n$, N_t is the number of transmitters to exploit and N_r is the number of receivers to use. In the case of 2-D tracking, 1 transmitter and 4 receiver sites are sufficient and proved that the observation matrix is non-singular. Equation (4.55) could now be used to determine the number of transmitters and receivers required to track a target's position and velocity in 3-D space using Doppler only information. For such a case, 7 or more transmitters and receivers are required, in which case 4 receiver sites and 3 transmitter sites are a possible option. Notice, using 4 receiver sites and 3 transmitter sites will result in 12 possible Doppler measurements, but only 6 will be uncorrelated.

4.9 Conclusions

This chapter detailed the theoretical concepts considered for this thesis in which the aim was to establish a lower bound for tracking accuracy. As seen from the observability criteria analysis, the linearised observation matrix needs to be of full rank to be observable. In this thesis, a single transmitter, multiple receiver configuration is considered, where each receiver is assumed to make a single Doppler measurement of the target in 2-D space. Therefore, to satisfy the full rank requirement for these conditions, a minimum of 4 receivers are required and accordingly the minimum number of receivers considered for all subsequent work.

Using Cramèr-Rao theory, a theoretical equation was derived to determine the best possible estimate of the target state from noise corrupted measurements. This is known as the CRLB and used as the lower bound for this thesis for two types of measurements, firstly Doppler only measurements and secondly, range-Doppler measurements. Further, as tracking filters, for example the RGNF, typically employ time history information, a new theoretical lower bound, called the CCRLB was also derived. Similar to the CRLB case, the CCRLB is also derived for both Doppler only measurements and range-Doppler measurements. The performance comparison between the CRLB and CCRLB will be covered in Chapter 5.

From the simulation results presented, it was concluded that the performance of a multiple receiver, Doppler only tracking system largely depends on; 1.) the number of receivers, 2.) the placement of the receivers and 3.) the conditioning of the observation matrix. By increasing the number of receivers, it was seen that the bad geometries are significantly reduced, as is the case with the conditioning of the observation matrix. These two aspects are further investigated in Chapter 5, whereas the placement of the receivers is covered in more detail in Chapter 6.

In addition to the single transmitter case, which is the primary focus of this thesis, MIMO for Doppler only tracking was also considered, hence using multiple transmitters together with multiple receivers. In the MIMO case, it is shown that Doppler correlation occurs between receivers. However, as the Doppler measurements that would cause correlation are known a-priori, only the Doppler measurements that do not cause correlation can be selected.

Having now derived a lower bound for the target state error, this lower bound can be used to benchmark the performance of any filter. Accordingly, benchmarking the performance of the RGNF against this lower bound will be the main topic of Chapter 5.

Chapter 5

Tracking with the RGNF

5.1 Introduction

In the chapters leading up to this one, theory was developed to determine the expected target tracking accuracy for a multi-static CR, where the receivers are assumed to be geographically separated. Further, an overview of the field deployment was provided and the proposed signal processing was reviewed. In this chapter, the aim is now shifted to benchmark the performance of the RGNF against the theoretical bounds derived in Chapter 4. These target tracking results are presented in two parts; first a simulation environment is considered to verify the conclusions of Chapter 4 and secondly, measurements from the field deployment are then compared to the simulation results.

In brief, this chapter consists of the following sections. Background theory on tracking filters are presented in Section 5.2, the RGNF equations are reviewed in Section 5.3 and the RGNF initialisation from bistatic range and Doppler measurements are reviewed in Section 5.4. Further, the simulated target tracking results are presented in Section 5.5, the real-data tracking results in Section 5.6 and lastly, the chapter ends with some conclusions in Section 5.7.

5.2 Background

Before the RGNF [103] is discussed, the basic elements of the filtering procedure considered in this thesis are presented in Figure 5.1. This basically involves the process of using the CR (element 2) to make noisy measurements of a moving target's state (element 1) and then use a filter (element 5) to estimate the target's state.

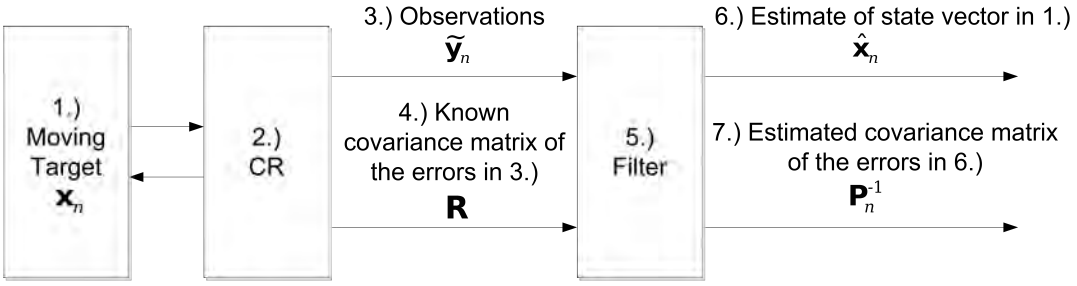

Figure 5.1: The basic elements of the filtering procedure.

Considering a more detailed description of the numbered items in Figure 5.1, each filter element is listed below and described in more detail.

1. The moving target is described with an external Differential Equation (DE) and represented by a true state vector $\mathbf{x}_n$ at time t_n. Therefore, the primary objective of the filter is to estimate this state vector.

2. The sensor element, which observes/measures the moving target that includes all the processing stages described in Chapter 3, up to and including the data association stage (see Figure 3.5). The output of the sensor are then the following two values;

3. A sequence of noise corrupted measurements/observations (bistatic range and Doppler) represented by a measurement vector $\tilde{\mathbf{y}}_n$.

4. A known measurement covariance matrix $\mathbf{R}$ of the errors in element 3, hence $\tilde{\mathbf{y}}_n$ and based on a-priori knowledge of the measurement errors.[1]

[1] This requirement forced the standard deviation analysis performed in Section 5.6.4.

5. The filter (RGNF in the case of this thesis) then uses elements 3 and 4 as input and outputs the next two elements;

6. A vector $\hat{\mathbf{x}}_n$ that is an estimate of the state vector in element 1.

7. A filter covariance matrix $\mathbf{P}_n^{-1}$, computed by the filter that is an estimate of the errors in element 6.

As shown by filter element 1 in Figure 5.1, the target position and velocity are usually represented in state vector format $\mathbf{x}_n$. Therefore, the changing state vector over time could be modelled as a DE in the following way,

$$\frac{\mathrm{d}\mathbf{x}_n}{\mathrm{d}t} = h\left(\mathbf{x}_n\right) \tag{5.1}$$

in which $h(\cdot)$ is assumed to be a linear function.[2] Observing, or measuring the DE in Equation (5.1) would then be the primary objective of the sensor and further discussed in the sections below.

5.3 The Recursive Gauss Newton Filter

The RGNF is an extension to the Gauss-Newton filter that has recently been re-organised into a recursive format [103] to allow for a computational efficient way to track targets. A brief overview of the filter algorithm is subdivided into the following sections; a section on the measurement equation, a section on defining the matrices and vectors of the RGNF and lastly, a section describing the process to cycle the filter in order to obtain an estimate of the state vector.[3]

[2] A non-linear function could also be used, but would require a more complex prediction step.
[3] For a complete description of the algorithm, see [103].

5.3.1 Measurement Equation

Observing, or measuring the DE in Equation (5.1) is mathematically expressed as

$$\widetilde{\mathbf{y}}_n = \mathbf{g}\left(\mathbf{x}_n\right) + \mathbf{w} \tag{5.2}$$

where the non-linear measurement vector, $\mathbf{g}(\cdot)$ is a vector of non-linear functions of $\mathbf{x}_n$ as defined in Equation (4.5) and $\mathbf{w}$ is a random Gauss vector with a covariance matrix $\mathbf{R}$, also previously defined in Chapter 4.

Considering the case of using Doppler only measurements collected from k-receivers sites, the non-linear measurement vector would consist of k Doppler functions, given as

$$\mathbf{g}(\mathbf{x}_n) = \left[f_{d1}[n], \cdots, f_{dk}[n]\right]^T \tag{5.3}$$

where $f_{di}[n]$ was previously given by Equation (3.12) for $i = 1$ to k receivers. Otherwise, in the case of range-Doppler measurements, the non-linear measurement vector would consist of k bistatic range and Doppler functions, given as

$$\mathbf{g}(\mathbf{x}_n) = \left[R_{b1}[n], f_{d1}[n], \cdots, R_{bk}[n], f_{dk}[n]\right]^T \tag{5.4}$$

where $R_{bi}[n]$ was previously given by Equation (3.10) and $f_{di}[n]$ the same as above.

5.3.2 RGNF Defintions

Before the RGNF algorithm is presented in the next section, all of the matrices and vectors considered are first defined. These include the following:

State Vector: The state vector of the target was presented in Equation (3.4) and defined as

$$\mathbf{x}_n = \left(x_n, \dot{x}_n, y_n, \dot{y}_n\right)^T \tag{5.5}$$

and the vector entries similarly defined as in Section 3.4.2.

Measurements: The measurement vector contains the latest set of Doppler or

range-Doppler measurements obtained from the CFAR output. Accordingly, for Doppler only measurements the measurement vector is defined as

$$\widetilde{\mathbf{y}}_n = \left(\widetilde{f}_{di}[n]\right)^T \tag{5.6}$$

where $\widetilde{f}_{di}[n]$ is the Doppler sample taken from the i^{th} receiver at time t_n. For range-Doppler measurements, the measurement vector is defined as

$$\widetilde{\mathbf{y}}_n = \left(\widetilde{R}_{bi}[n], \widetilde{f}_{di}[n]\right)^T \tag{5.7}$$

where in addition to the Doppler measurements, $\widetilde{R}_{bi}[n]$ is the bistatic range measurement at the i^{th} receiver.

Linearised Measurement Matrix: As seen in the previous section, the measurements are non-linear. Therefore, as presented in Chapter 4, Equation (4.9), at time t_n the linearised measurement matrix is obtained by taking the partial derivative of $\mathbf{g}(\mathbf{x}_n)$ in Equation (5.2) with respect to $\mathbf{x}_n$ and is of the form

$$\overline{\mathbf{M}}_n = \begin{pmatrix} m_{1,1} & m_{1,2} & m_{1,3} & m_{1,4} \\ m_{2,1} & m_{2,2} & m_{2,3} & m_{2,4} \\ m_{3,1} & m_{3,2} & m_{3,3} & m_{3,4} \\ m_{4,1} & m_{4,2} & m_{4,3} & m_{4,4} \end{pmatrix} \tag{5.8}$$

for tracking in 2-D using only Doppler measurements. The matrix entries are obtained with Equation (4.10) and given in full in Appendix A.

State Transition Matrix: As stated previously, a linear motion model is assumed for the target and accordingly, the transition matrix presented in Equation (3.7);

$$\mathbf{\Phi}(t_{n-1}, t_n) = \begin{pmatrix} 1 & T & 0 & 0 \\ 0 & 1 & 0 & 0 \\ 0 & 0 & 1 & T \\ 0 & 0 & 0 & 1 \end{pmatrix} \tag{5.9}$$

are used for the filter; with T set to the CPI.

State Prediction: The state prediction is also linear and therefore defined as

$$h(\mathbf{x}_n) = \mathbf{\Phi}\left(t_{n-1}, t_n\right)\mathbf{x}_{n-1} + \mathbf{q} \tag{5.10}$$

with $\mathbf{\Phi}\left(t_{n-1}, t_n\right)$ defined in Equation (5.9). The process noise $\mathbf{q}$ consists of normally distributed random variables with zero mean and covariance matrix $\mathbf{Q} = diag\left[\sigma_q^2\mathbf{H} \quad \sigma_q^2\mathbf{H}\right]$ where,

$$\mathbf{H} = \begin{pmatrix} \frac{T^4}{4} & \frac{T^3}{2} \\ \frac{T^3}{2} & T^2 \end{pmatrix} \tag{5.11}$$

with T set to the CPI [133]. Notice, this equation is exactly the same as previously given in Equation (3.7), except for the addition of the process noise.

Measurement Co-variance Matrix: As described in Section 5.2, the measurement covariance matrix models the expected errors in the Doppler or range/Doppler measurements. In both of these cases, the standard deviation is derived from the field deployment data. The bistatic Doppler deviation is calculated to be $\sigma_d = 0.2$ Hz and the bistatic range deviation to be $\sigma_r = 470$ m. Therefore, the measurement co-variance matrix for Doppler measurements is given as

$$\mathbf{R}_D = \sigma_d^2 \begin{pmatrix} 1 & 0 & 0 & 0 \\ 0 & 1 & 0 & 0 \\ 0 & 0 & 1 & 0 \\ 0 & 0 & 0 & 1 \end{pmatrix} \tag{5.12}$$

and for range-Doppler measurements, given as

$$\mathbf{R}_{RD} = \mathbf{I}_4 \otimes \begin{pmatrix} \sigma_r^2 & 0 \\ 0 & \sigma_d^2 \end{pmatrix} \tag{5.13}$$

where $\mathbf{I}_4$ is the 4x4 identity matrix.[4]

[4] Notice that $\mathbf{R}_{RD}$ is a 8x8 matrix.

Initial Filter Co-variance Matrix: Also described in Section 5.2, the filter co-variance matrix models the errors in the state estimate and is accordingly updated for every cycle of the RGNF. For the Gauss-Newton filter family, the choice of the initial covariance matrix is not as critical as that required by the Kalman filter [21]. Therefore, the filter co-variance matrix was initialised with the resolution expected or both the range and the velocity. For the target velocity error, 10 ms^{-1} was used and for the position error, 3000 m was used. Accordingly, the filter co-variance matrix was initialised as follows:

$$\mathbf{P}_0^{-1} = \begin{pmatrix} 9 & 0 & 0 & 0 \\ 0 & 0.0001 & 0 & 0 \\ 0 & 0 & 9 & 0 \\ 0 & 0 & 0 & 0.0001 \end{pmatrix} \tag{5.14}$$

and the definitions present a variance of 9 km^2 in position and 0,0001 km^2s^{-2} in velocity. In both cases of using Doppler and range-Doppler measurements, this initialisation was found to be adequate for tracking the target.

5.3.3 Cycling the RGNF

Next, the cycling procedure of the RGNF is considered. When a measurement $\widetilde{\mathbf{y}}_n$ is made, the filter first iterates through Equations (5.15) to (5.18) until the answer converges to an estimate $\widehat{\mathbf{x}}_n$ of the state vector $\mathbf{x}_n$ over a set number of iterations. This estimate is then used to update the filter covariance matrix $\mathbf{P}_n^{-1}$, Equation (5.19) and lastly, to respectively predict the next state estimate and filter covariance matrix presented in Equations (5.20) and (5.21).

5.3.3.1 Iteration Phase

The first step during the filter iteration phase is to update the observer gain $\mathbf{K}_n$, defined as

$$\mathbf{K}_n = \mathbf{P}_{n/(n-1)}^{-1}\overline{\mathbf{M}}_n^T \left[\mathbf{R} + \overline{\mathbf{M}}_n \mathbf{P}_{n/(n-1)}^{-1}\overline{\mathbf{M}}_n^T\right]^{-1} \tag{5.15}$$

where $\overline{\mathbf{M}}_n$ is the linearisation of function $\mathbf{g}(\widehat{\mathbf{x}}_n)$ at the estimated point $\widehat{\mathbf{x}}_n$, $\mathbf{R}$ is the measurement co-variance matrix and $\mathbf{P}^{-1}_{n/(n-1)}$ is the predicted filter covariance matrix from t_{n-1} to t_n. Next, the delta error $\delta_n\widehat{\mathbf{x}}_n$ in the state estimate is calculated as

$$\delta_n\widehat{\mathbf{x}}_n = \mathbf{K}_n\left[\widetilde{\mathbf{y}}_n - \mathbf{g}(\widehat{\mathbf{x}}_n) - \overline{\mathbf{M}}_n\left(\widehat{\mathbf{x}}_{n/(n-1)} - \widehat{\mathbf{x}}_n\right)\right] \tag{5.16}$$

where $\mathbf{g}(\widehat{\mathbf{x}}_n)$ is the non-linear vector, as defined in Equation (5.2) and evaluated for the current state vector $\widehat{\mathbf{x}}_n$. $\widetilde{\mathbf{y}}_n$ is the noise corrupted measurement input vector containing bistatic range and/or Doppler values and $\widehat{\mathbf{x}}_{n/(n-1)}$ is the previous estimated state vector, predicted to the current state. The current state vector is then updated as

$$\mathbf{x}_n = \widehat{\mathbf{x}}_n + \delta_n\widehat{\mathbf{x}}_n \tag{5.17}$$

and

$$\widehat{\mathbf{x}}_n = \mathbf{x}_n \tag{5.18}$$

at which point the iteration phase ends if a set number of iterations are met.

5.3.3.2 Update and Predication Phase

Next, the update and prediction phase are performed. In the update phase, the filter covariance matrix is updated as

$$\mathbf{P}^{-1}_n = \left[\mathbf{I} - \mathbf{K}_n\overline{\mathbf{M}}_n\right]\mathbf{P}^{-1}_{n/(n-1)} \tag{5.19}$$

where $\mathbf{I}$ is the identity matrix. The state vector is then forward predicted to t_{n+1} as

$$\widehat{\mathbf{x}}_{(n+1)/n} = \mathbf{\Phi}\left(t_n, t_{n+1}\right)\widehat{\mathbf{x}}_n \tag{5.20}$$

and the filter covariance matrix as

$$\mathbf{P}^{-1}_{(n+1)/n} = \Gamma^{-1}\mathbf{\Phi}\left(t_n, t_{n+1}\right)\mathbf{P}^{-1}_n\mathbf{\Phi}^T\left(t_n, t_{n+1}\right) + \mathbf{Q} \tag{5.21}$$

where Γ was previously defined in Chapter 4, Equation (4.47) as the forgetting factor (a value between 0 and 1) that acts as a filter memory length for previous estimates. Lastly, $\mathbf{Q}$ is the process noise covariance matrix as defined in Section 5.3.2.

5.3.4 The RGNF vs. the IEKF

At this point, an informed reader might realise that the RGNF equations presented in Section 5.3.3 are in fact very similar to the IEKF [134], with the only difference being the forgetting factor. As mentioned in Chapter 1, the RGNF used in this thesis was an evolution of the GN filter adapted for tracking by Morrison [21]. Nadjiasngar [103] adapted this filter to become recursive and showed that the IEKF is a simplified version of the RGNF, i.e. the IEKF is a non-adaptive version of the RGNF. In particular, the adaptiveness of the RGNF was shown to be superior to the IEKF approach for manoeuvring targets.

5.4 Filter Initialisation

To initiate the RGNF, a method is required to calculate the 2-D target position and velocity from the bistatic range and Doppler measurements. Malanowski [95] proposed a closed-form algorithm to solve this requirement. In brief, it was demonstrated that the bistatic range equation presented in Equation (3.10) could be rewritten in the form

$$\widehat{\mathbf{x}}_{p,n} = \left(\mathbf{X}_R^T\mathbf{X}_R\right)^{-1}\mathbf{X}_R^T\mathbf{z}_n + \left(\mathbf{X}_R^T\mathbf{X}_R\right)^{-1}\mathbf{X}_R^T\mathbf{r}_n R_{t,n} \tag{5.22}$$

where $[\cdot]^T$ denotes the transpose operator and the target position estimate is given as:

$$\widehat{\mathbf{x}}_{p,n} = \begin{bmatrix} x_n \\ y_n \end{bmatrix} \tag{5.23}$$

$\mathbf{X}_R$ is a matrix of receiver positions, given by

$$\mathbf{X}_R = \begin{bmatrix} x_{R1} & y_{R1} \\ x_{R2} & y_{R2} \\ \vdots & \vdots \\ x_{Rk} & y_{Rk} \end{bmatrix} \tag{5.24}$$

while $\mathbf{r}_n$ is a vector of bistatic range measurements, given by

$$\mathbf{r}_n = \frac{1}{2} \begin{bmatrix} R_{b1,n} & R_{b2,n} & \cdots & R_{bk,n} \end{bmatrix}^T \tag{5.25}$$

and $\mathbf{z}_n$ is an additional vector, given as:

$$\mathbf{z}_n = \frac{1}{2} \begin{bmatrix} (x_{R1})^2 + (y_{R1})^2 - (R_{b1,n})^2 \\ (x_{R2})^2 + (y_{R2})^2 - (R_{b2,n})^2 \\ \vdots \\ (x_{Rk})^2 + (y_{Rk})^2 - (R_{bk,n})^2 \end{bmatrix} \tag{5.26}$$

The only unknown in Equation (5.22) is the target range $R_{t,n}$, but is solved by means of a quadratic equation following Malanowski [95]. After the position estimate of the target is obtained using Equation (5.22), the velocity estimate is calculated using

$$\widehat{\mathbf{v}}_n = \left(\mathbf{B}_n^T \mathbf{B}_n\right)^{-1} \mathbf{B}_n^T \mathbf{v}_{b,n} \tag{5.27}$$

where $\widehat{\mathbf{v}}_n = [\dot{x}, \dot{y}]^T$ and $\mathbf{v}_{b,n}$ is a vector of measured bistatic velocities given as

$$\mathbf{v}_{b,n} = \frac{1}{K_d} \begin{bmatrix} \widetilde{f}_{d1,n}\,, & \widetilde{f}_{d2,n}, & \cdots & \widetilde{f}_{dk,n} \end{bmatrix}^T \tag{5.28}$$

and $\mathbf{B}_n$ is a matrix of coefficients given as

$$\mathbf{B}_n = \begin{bmatrix} \frac{\Delta_{x,n}^E}{R_{E,n}} + \frac{\Delta_{x,n}^{R1}}{R_{R1,n}} & \frac{\Delta_{y,n}^E}{R_{E,n}} + \frac{\Delta_{y,n}^{R1}}{R_{R1,n}} \\ \frac{\Delta_{x,n}^E}{R_{E,n}} + \frac{\Delta_{x,n}^{R2}}{R_{R2,n}} & \frac{\Delta_{y,n}^E}{R_{E,n}} + \frac{\Delta_{y,n}^{R2}}{R_{R2,n}} \\ \vdots & \vdots \\ \frac{\Delta_{x,n}^E}{R_{E,n}} + \frac{\Delta_{x,n}^{Rk}}{R_{Rk,n}} & \frac{\Delta_{y,n}^E}{R_{E,n}} + \frac{\Delta_{y,n}^{Rk}}{R_{Rk,n}} \end{bmatrix} \tag{5.29}$$

where the matrix entries of $\mathbf{B}_n$ is defined in Equations (3.8) and (3.9), hence the requirement of solving the target position first. Accordingly, Equation (5.22) is used to initiate the position and Equation (5.27) to initiate the velocity for the target state vector defined in Equation (5.5). The RGNF is then executed as described in Section 5.3.

5.5 Example Results: Simulations

It is now possible to test the performance of the RGNF against the CRLB, as well as the CCRLB in a simulation environment as discussed in Chapter 4. For the simulation scenario, a direct replica of the ROI of the field experiment is assumed, hence the placement of the receivers relative to the transmitter. First the CRLB and CCRLB are simulated over the ROI to establish both the good and bad geometry areas for a linear motion target. Then, based on this knowledge, different filter memory lengths are considered to investigate the effect of the bad geometry areas on the RGNF tracking stability. Manoeuvring targets[5] are considered in Section 5.5.4, with the focus on the CRLB and CCRLB, as strictly speaking, the CCRLB bound is only valid for linear target motion due to the linear state transition matrix. However, notice that the bound is not only limited to linear motion; it only requires the target motion model to be updated to allow for non-linear target motion and accordingly, is also set for future investigation. Following the target manoeuvring investigation, the effect of increasing the CPI length is explored in Section 5.5.5, increasing the number of receivers in Section 5.5.6 and in addition to Doppler only tracking, range-Doppler tracking are considered in Section 5.5.7. Lastly, Doppler correlation between the receivers is considered in Section 5.5.8, before this section's results is summarised and discussed in Section 5.5.9.

[5] The ability of the RGNF to vary it's filter memory length is an extremely useful feature for when targets start manoeuvring. However, adaptive filter memory length is not considered in this thesis and is left as future research.

5.5.1 Simulation parameters

In the simulations that follow, both linear and non-linear target motion are required. This is accomplished by including a heading vector in the motion model and accordingly allow to simulate a manoeuvring target. In the case of linear target motion, constant velocity with a constant heading is used and in the case of non-linear target motion, the heading vector is altered.[6] For all the simulations, the Cape Town transmitter parameters (see Table 3.1) are used and additionally, additive white Gaussian noise was added to the bistatic range and bistatic Doppler measurements. The standard deviation for the noise added to the Doppler measurement was 0.2 Hz, the standard deviation for the noise added to the bistatic range measurements was 470 m (these values will be justified in Section 5.6.4) and the process noise variance, $\sigma_q^2 = 0.1$ m^{2}s^{-4} . A PoD of 1 is assumed, the target model is simulated in a clutter free observation volume, the number of Monte Carlo runs is set to 200 and lastly, an initial target state error is simulated by adding a value of [2100, 7, 2100, -7]^T with units [m, ms^{-1}, m, ms^{-1}]^T to the true target state vector.

5.5.2 CRLB over the ROI

Following a similar approach as described in Chapter 4, a target's 2-D position accuracy is simulated for the ROI in which the field experiment took place. Therefore, the 4 receiver nodes are placed according to the geographical layout of the field trials described in Section 3.2.1, in which the configuration gives transmitter to receiver baselines of respectively 36, 54, 56 and 75 km. The expected 2-D CRLB and CCRLB of the target position accuracy are accordingly presented in Figure 5.2, where target motion is modelled to be of constant velocity and given as $\mathbf{v}_x$ = [-130, -110] with units [ms^{-1} ms^{-1}]. In the case of Figure 5.2 (a) the FIM is used to derive the CRLB and in the case of Figure 5.2 (b) the CFIM is used to derive the CCRLB. The transmitter is indicted with a white circle, the 4 receivers with white crosses and the position accuracy indicated by the colour

[6] Note, when introducing a heading change, acceleration in respectively the x and y coordinate directions are introduced that is seen as non-linear target motion.

bar to the right of each figure, in units of dB metres (a 100 m position error for example, is given as 20 dB metres).

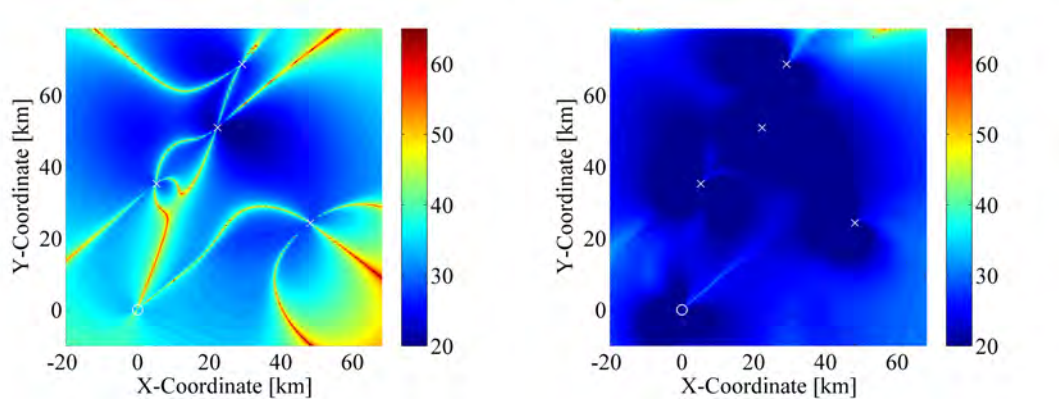

(a) (b)

Figure 5.2: 2-D surface plots using the Cape Town transmitter and the 4 receiver sites of the field deployment. The simulated flightpath direction is $\dot{x}$ = -130 ms^{-1} and $\dot{y}$ = -110 ms^{-1}, hence similar to the flight direction of an expected incoming aircraft to Cape Town International. a) The 2-D CRLB b.) The 2-D CCRLB. The colour bar to the right of each figure is in units of dB metres.

As illustrated by Figure 5.2 (a), the CRLB for the target position accuracy suggests that a number of bad geometry regions exists. In other words, if a single Doppler measurement is made from the 4 receivers sites, a significant number of regions will exist where the target's position cannot be resolved within an acceptable accuracy range. For example, an acceptable accuracy might be considered to be better than 100 m. However, as seen from Figure 5.2 (b), when the target's position estimate is based on present and past Doppler measurements from the 4 receiver sites, i.e. taking time history information into account, the estimate on the target's position is improved significantly. This is exactly what the CCRLB describes, given that the target's motion could be modelled. In the case of Figure 5.2 (b), $\Gamma = 0.9$ for the CCRLB.

5.5.3 Non-Manoeuvring Target

From the previous section, it is concluded that in many cases the target's position could not be estimated accurately using only 4 Doppler measurements, collected from 4 receiver sites (CRLB results). Further it is also shown that the bad geometry regions are significantly reduced when the CCRLB is used. Reusing the geographical scenario presented in Section 5.5.2, the RGNF is now considered to track the target's position using only Doppler measurements with a CPI of 1 s and accordingly $\sigma_f = \sqrt{0.1}$ [7]. Firstly, tracking is attempted by using a fairly short filter memory length, $\Gamma = 0.72$ (approximately 4 history samples) and secondly, the scenario is re-evaluated with the filter memory length extended to $\Gamma = 0.9$ (10 history samples). These results are respectively presented in Figures 5.3 and 5.4 and compared to the theory derived in Chapter 4. Further notice from Figures 5.3 and 5.4 (a) that the receiver positions are indicated with squares and the transmitter is located at the origin of the coordinate system.

As seen from Figure 5.3 (a), using a constant velocity target with a starting state vector of $\mathbf{x}_0 = [62000, -130, 60000, -110]^T$, the estimated target position of the RGNF (colour black) closely follows the true target track (colour blue) up to about two-thirds of the way, after which the filter estimate becomes unstable and diverged. In Figure 5.3 (b), the performance of the RGNF is bench marked against the CRLB as well as the CCRLB for $\Gamma = 0.72$. The CRLB and CCRLB are presented as blue error curves, the RGNF Root Mean Square (RMS) error as the red error curve and lastly, the RGNF co-variance matrix[7] as the black error curve, all as a function of time.

As predicted by the results presented in the previous section, Figure 5.3 (b) also clearly demonstrates the bad geometry region around t = 230 s, in which case the CRLB predicted target position errors are in excess of 10 km. At the same time, the CCRLB is able to restrict the target position error to less than 700 m, this also confirms the superior position estimation capability when time history information is considered. Another important observation made

[7] Using the RGNF co-variance matrix, P as presented in Equation (5.14), the error bound is calculated by the addition of the following matrix entries; $\sqrt{p_{1,1} + p_{3,3}}$.

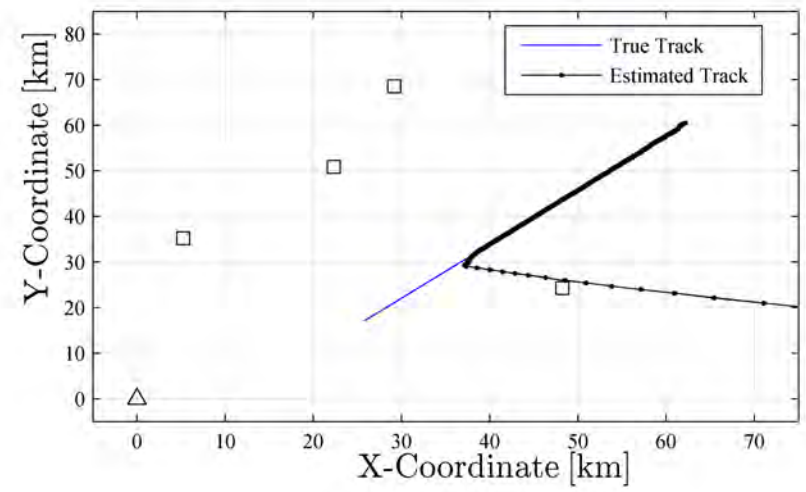

(a)

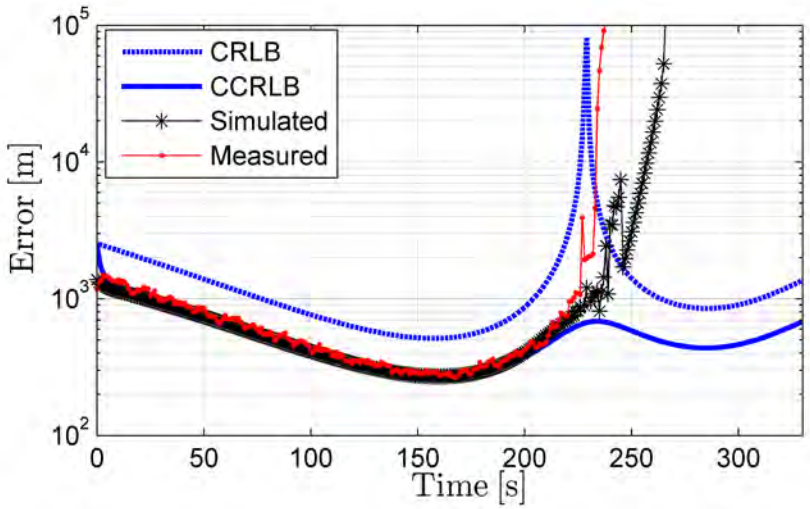

(b)

Figure 5.3: Simulated Doppler only target tracking of a non-manoeuvring target, demonstrating the effect of using a short filter memory length when the target enters a bad geometry region. a.) The true target track and estimated target track. b.) The RGNF tracking performance benchmarked to the CRLB and CCRLB.

from Figure 5.3 (b), is that both the RGNF co-variance matrix and the target RMS position error output from the RGNF closely follow the CCRLB up to

t = 230 s after which, the filter becomes unstable. This confirms the concern that a tracking filter might become unstable when the target enters a bad geometry region. In an attempt to circumvent this problem, these results are now repeated with an increased filter memory length.

As illustrated in Figure 5.4 (a), increasing the filter memory length to $\Gamma = 0.9$ resulted in the RGNF being able to successfully track the target over the entire flight path considered and it did not loose track when the target entered the bad geometry region. Further, as seen from Figure 5.4 (b), both the RGNF co-variance matrix and the target RMS position error from the RGNF once again closely followed the CCRLB, except for in the bad geometry region. More importantly, notice that the expected tracking accuracy on the target's position is in some cases better than 200 m; and that this accomplished by using only 4 receivers.

5.5.4 Manoeuvring Target

In the previous section it was confirmed that the RGNF is capable to track the position of a constant velocity target by using only the Doppler measurements and the accuracy associated with the position estimates are based on the CCRLB. In this section, the effect of non-linear target motion is investigated by introducing target heading changes in the flightpath.

The target is simulated by using the same starting position state vector as in the case of Figure 5.4, that is $\mathbf{x}_0 = [62000, -130, 60000, -110]^T$, but two medium right hand turns are introduced over the flightpath. At t = 171 s, the target starts the first heading change at a turn rate of 0.6 deg/s for a period of 50 s (30° turn) and upon the completion of the turn, returns to a constant velocity. At t = 281 s, the target starts the second turn at a turn rate of 0.4 deg/s for a duration of 50 s (20° turn), also returning to a constant velocity upon completion. The flight path for this scenario, together with the RGNF estimated position of the target using a CPI of 1 s and $\Gamma = 0.9$, are presented in Figure 5.5 (a). Once again, the estimated target track (black colour) is overlaid to the true target track (blue

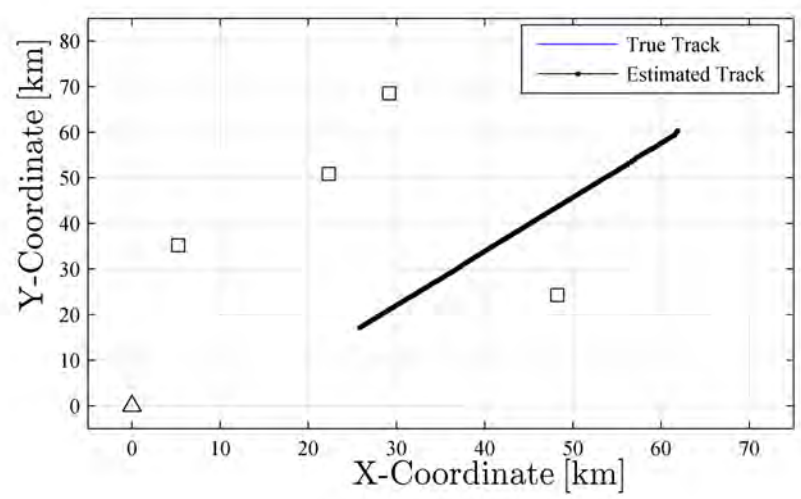

(a)

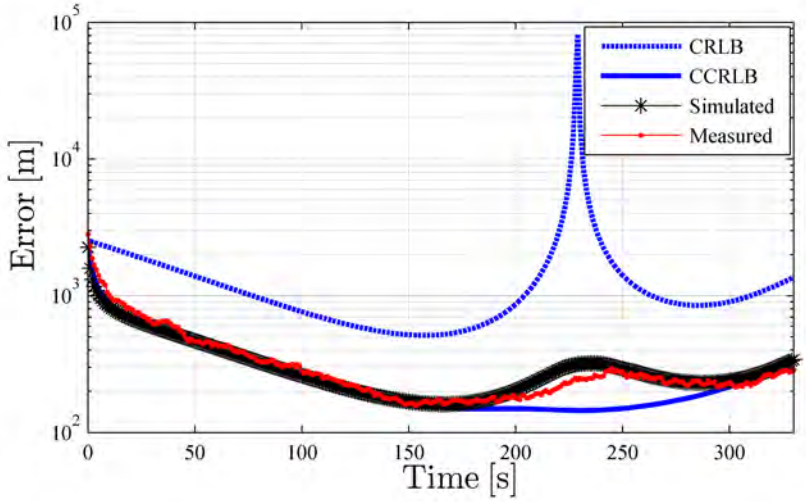

(b)

Figure 5.4: Simulated Doppler only target tracking of a non-manoeuvring target, demonstrating the effect of using a long filter memory length when the target enters a bad geometry region. a.) The true target track and estimated target track. b.) The RGNF tracking performance benchmarked to the CRLB and CCRLB.

colour) whereas the associated error curves for this scenario are presented in Figure 5.5 (b), similarly to the linear motion case.

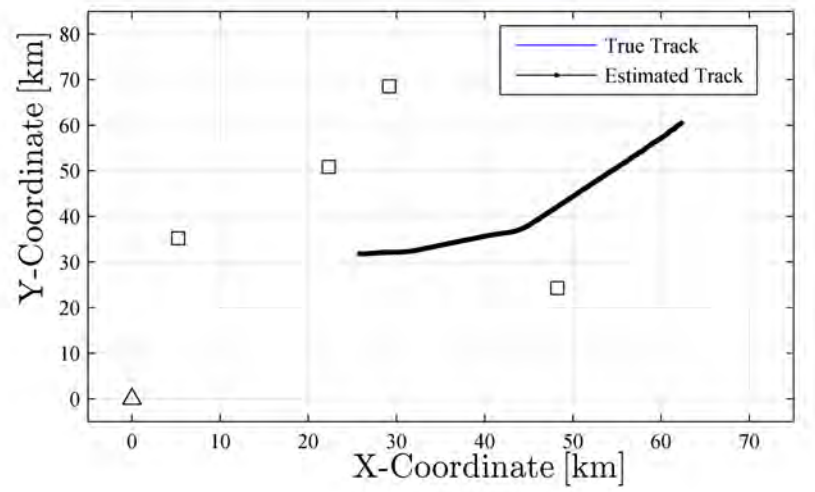

(a)

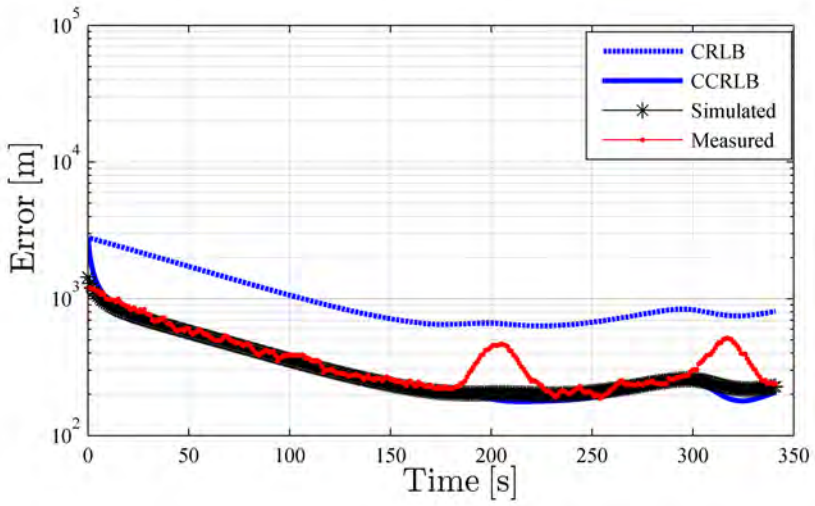

(b)

Figure 5.5: Simulated Doppler only target tracking of a flight executing two medium right hand turns. a.) The true target track and estimated target track. b.) The RGNF tracking performance benchmarked to the CRLB and CCRLB.

Notice in Figure 5.5 (b), that the RGNF is able to track the target within close proximity to the CCRLB, except for the two turns. This was expected as the RGNF employs a linear target tracking model and at best, returns a performance similar to the CRLB based on the FIM in regions where non-linear target motion

occurs, hence $\Gamma = 0$. Also notice the avoidance of the insufficient tracking region as experienced in Figures 5.3 and 5.4 due to the target's two right hand turns resulting in a trajectory being totally different to the linear target track.

Next, a more complex target trajectory is considered for tracking. As seen in Figure 5.6 (a), the flight path considered starts with an initial heading of 20° relative to North and with a starting vector of $\mathbf{x}_0 = [36000,\ 65,\ 24000,\ 190]^T$. At t = 151 s, the target enters into a turn of 2 deg/s for the interval t =[151, 290] s and upon the completion of the turn, returns to a constant velocity for the remainder of the flightpath. Once again, the estimated target track (black colour) is overlaid to the true target track (blue colour) and the associated error curves for this scenario are presented in Figure 5.6 (b).

As illustrated in Figure 5.6 (b), the RGNF is once again able to track the target within close proximity of the CCRLB for the linear motion phases of the flight track, however a deviation is observed during the long turning phase. Further as observed in Figure 5.6 (b) there are the large number of bad geometry areas that occur over the target turning phase and it is therefore concluded that the degraded target tracking performance is due to two factors over the turn phase. Firstly, the linear target tracking model used with the RGNF and secondly, the large number of bad geometry areas are encountered over the turning phase.

For the next simulation an increased CPI length is considered to reduce the standard deviation of the Doppler measurements. Therefore, using the same flight profile as described above, the CPI is increased to 4 seconds and the resulting tracking performance presented in Figure 5.7. Once again, the estimated track is overlaid to the true target track as seen in Figure 5.7 (a) and the associated error performance curves presented in Figure 5.7 (b).

As illustrated in Figure 5.7 (b), the results are once again consistent with the previous results as the estimated target position error followed the CCRLB for the linear motion phases of the flight track but are closer to the CRLB during the turning phase. Compared to the previous result, the bad geometry areas over the turn phase of the track also decreased due to the longer integration time, with a net effect of an improved tracking result. This does, however, come with

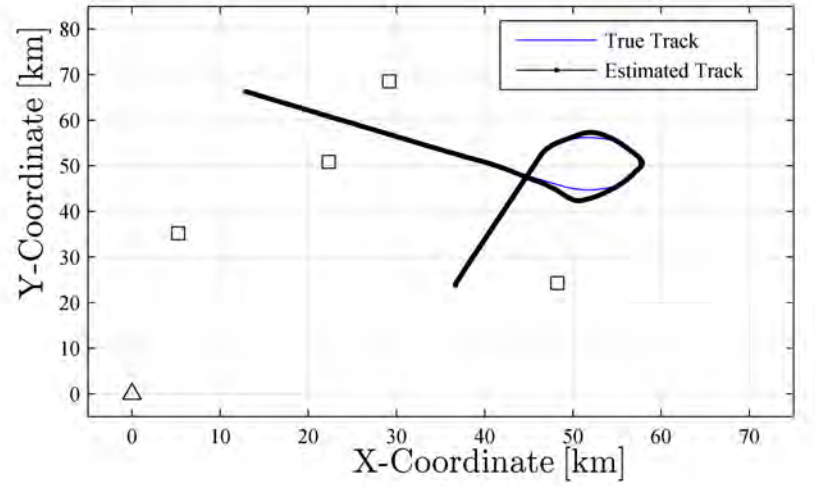

(a)

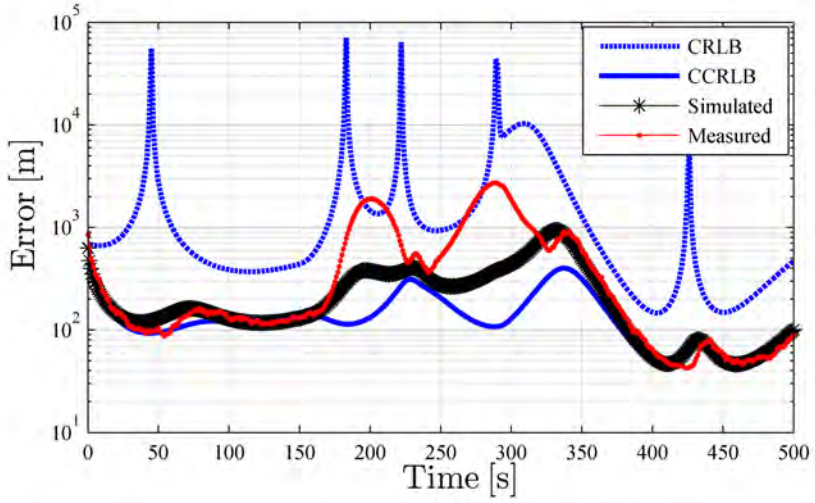

(b)

Figure 5.6: Simulated Doppler only target tracking of a flight executing a 270° medium right hand turn. a.) The true target track and estimated target track. b.) The RGNF tracking performance benchmarked to the CRLB and CCRLB.

the expense of the filter taking longer to converge back to the CCRLB after the turn due to the extended CPI. Therefore, from these results it is evident that different CPI lengths with different filter memory lengths also requires further investigation and is accordingly set as future research.

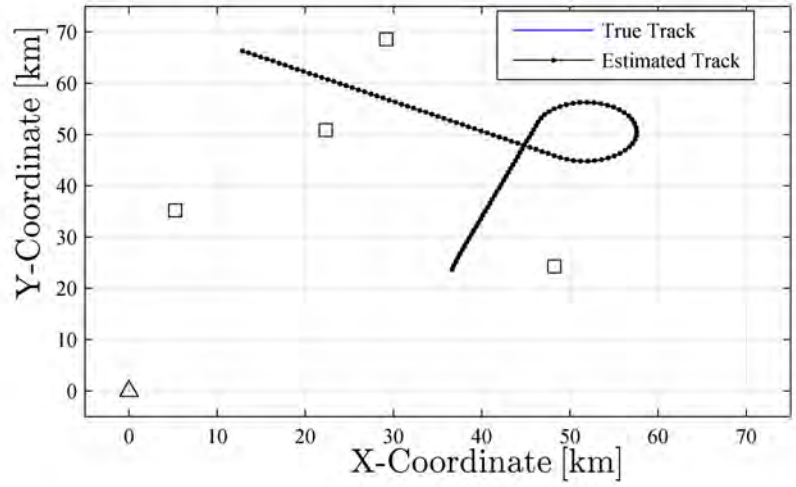

(a)

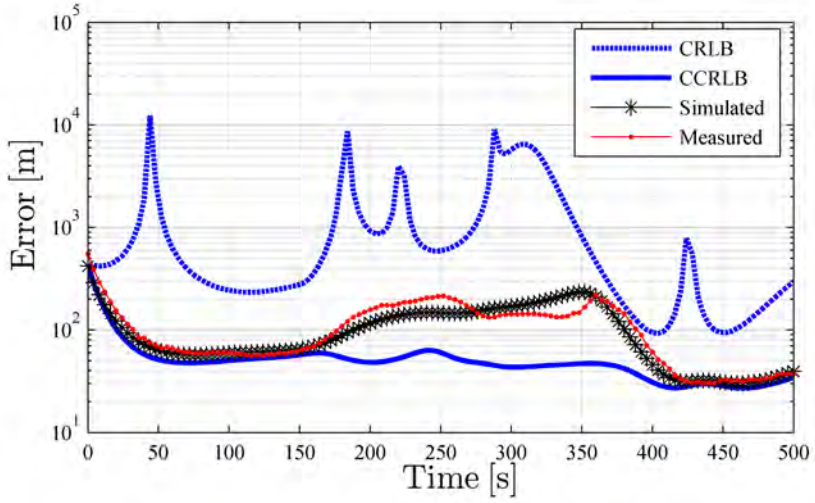

(b)

Figure 5.7: Simulated Doppler only target tracking of a flight executing a 270° medium right hand turn and using a CPI = 4 s. a.) The true target track and estimated target track. b.) The RGNF tracking performance benchmarked to the CRLB and CCRLB.

5.5.5 CPI Considerations

In Section 5.5.4 it was seen that by increasing the CPI, non-linear target motion was tracked more reliably by the RGNF as a result of the decreased standard deviation. To verify this, the linear motion target presented in Section 5.5.3 are once again considered, but the focus is now shifted to compare different CPI lengths. In Figure 5.8, CPI's of 1 and 4 seconds are considered for linear target motion and the resulting CRLB and CCRLB ($\Gamma = 0.9$) are compared.

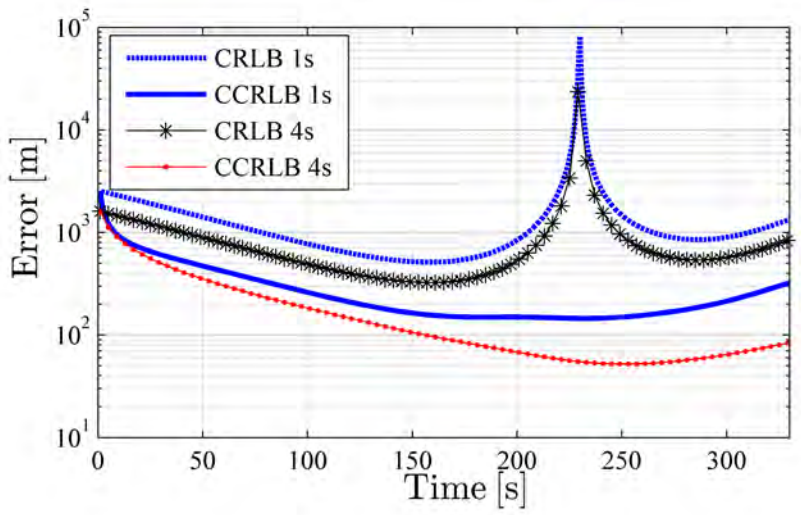

Figure 5.8: Simulated Doppler only target tracking of a non-manoeuvring flight with different CPIs.

As expected, it is seen from Figure 5.8 that by increasing the CPI, and thereby reducing the standard deviation on the Doppler measurement, results in a lower error bound on the position estimation. For the scenario presented in Figure 5.8, the CRLB position error was reduced by 40% by increasing the CPI from 1 s to 4 s and seen to be a constant difference over the duration of the flight path. However, in the case of the CCRLB, the increased CPI resulted in a slower improvement in the lower bound as compared to using a shorter CPI. This is clearly seen during the first 50 s of flight in Figure 5.8. The reason for this lies in the fact that less detections are made within a similar interval of time. For example, in a 4 second time window, using a CPI = 1 s would result in 4 detections, whereas

using a CPI = 4 s would result in only 1 detection and accordingly, the CCRLB for a CPI = 1 s is based on 4 time history measurements as opposed to 1 for a CPI = 4 s. However, when 4 detections are eventually made for the CPI = 4 s, an improved result over the CPI = 1 s is obtained. The same is also true for the results following the bad geometry region (t $\geq$ 240 s) as it is clearly seen that the CCRLB based on the CPI = 4 s is slightly delayed compared to the CCRLB based on the CPI = 1 s. Non-the-less, it is concluded that by using a CPI = 4 s, improved tracking results are obtained over using a CPI of 1 s.

Lastly, using neither a 1 s nor a 4 s CPI, the bad geometry region could be circumvented.[8] It is therefore concluded that the largest performance gain is in fact, obtained by using time-history measurements as opposed to pure integration time. Besides the CPI length consideration, notice that the CCRLB error bound predicts that a tracking accuracy within 100 m is obtainable by using only 4 receivers. This is seen as an extremely encouraging result.

5.5.6 Increased Number of Receivers

As seen in the previous sections, bad geometry regions in Doppler only tracking could be circumvented by using time history information. Another way to reduce the bad geometry regions, as briefly covered in Section 4.7, is to increase the number of receivers and is accordingly the focus of this section. As it was shown previously, that the expected tracking accuracy for a linear motion target is given by the CCRLB and that the CRLB will point out bad geometry regions, these bounds will be used to evaluate the effect of increasing the number of receiver positions within the ROI.

Reusing the receiver setup (4 receivers) and linear target motion as described in Section 5.5.3, three additional receiver positions are randomly added to the scenario to increase the total number of receivers to 7. This scenario is presented in Figure 5.9 where the original four receivers are labelled 'Rx1' to 'Rx4' and the additional 3 receivers 'Rx5' to 'Rx7'.

[8] Assuming a single Doppler measurements are obtained from the respective receiver sites.

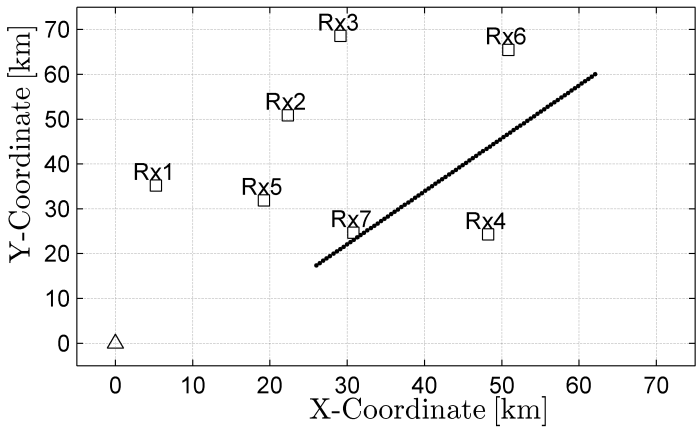

Figure 5.9: The simulation setup for a single transmitter, multiple receiver configuration, considering Doppler only target tracking of a non-manoeuvring flight with using 4, 5, 6 and 7 receiver sites.

Considering the linear motion target and multiple receiver scenario presented in Figure 5.9, the CRLB and CCRLB are evaluated for respectively 4, 5, 6 and 7 receivers and the results presented in Figure 5.10. In the case of 4 receivers, 'Rx1' to 'Rx4' are used; for 5 receivers, 'Rx1' to 'Rx5' are used and so forth up until 7 receivers. In addition, in all simulations considered in this section, the CPI = 4 s and $\Gamma = 0.9$.

As seen from the CRLB results presented in Figure 5.10 (a), with the addition of only a single receiver to the 4 receiver scenario (using 5 receivers), the bad geometry region is eliminated. Furthermore, the best target tracking accuracy was obtained by using 7 receivers and the addition of the 7^{th} receiver seems to have impacted the most on reducing the CRLB.

Similar tothe CRLB, the CCRLB results presented in Figure 5.10 demonstrate that the best target tracking accuracy is obtained by utilising 7 receivers. In this case, target position errors are as small as 50 m in the later stages of the flight path. It is interesting to note that the addition of the 5^{th} and 6^{th} receiver does not significantly improve the CCRLB. However, the addition of the 7^{th} receiver results in a significant reduction in the CCRLB. Therefore, this suggests that receiver placement has an important role to play in Doppler only tracking and

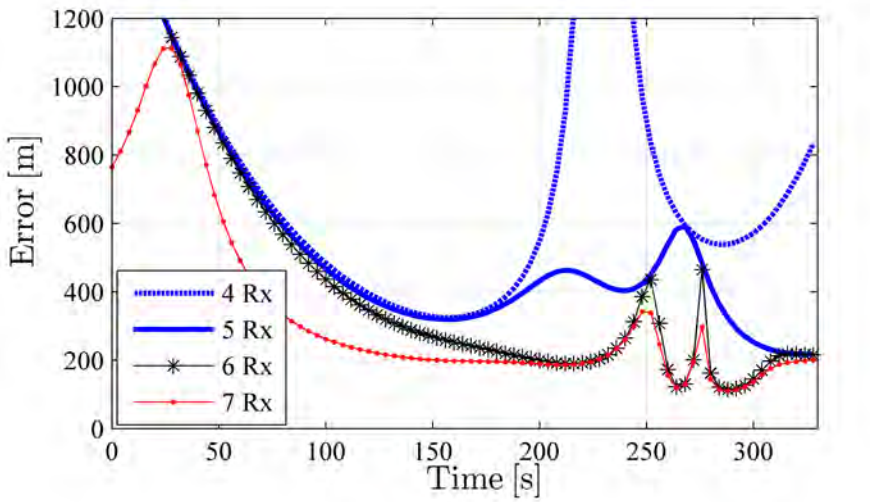

(a)

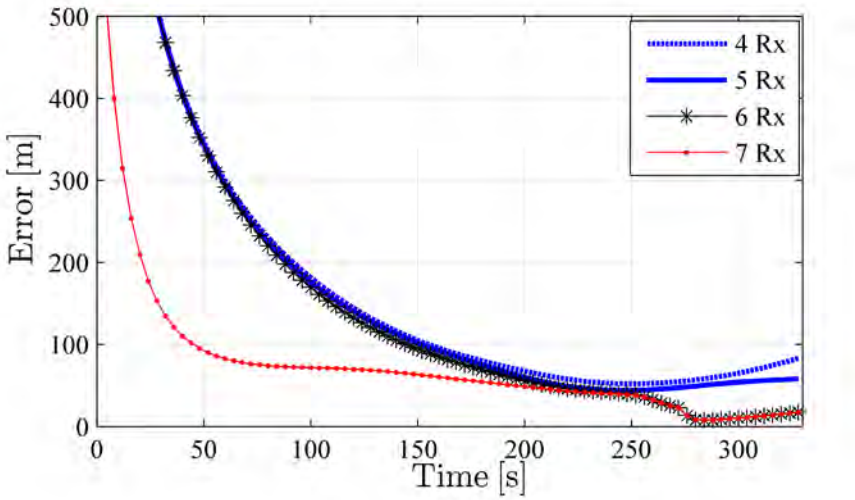

(b)

Figure 5.10: Simulated Doppler only target tracking of a non-manoeuvring flight using using 4, 5, 6, and 7 receivers. a.) The CRLB results. b.) The CCRLB results.

is further explored in Chapter 6.

5.5.7 Range and/or Doppler Simulations

Besides increasing the number of receivers to improve the conditioning of the observation matrix, bistatic range measurements could also be used for this purpose, as briefly pointed out in Chapter 4. Therefore, the focus of this section is to evaluate whether improved target position estimates could be obtained when both low resolution bistatic range measurements and high resolution Doppler measurements are utilised.[9]

Considering once again the target motion and receiver setup described in Section 5.5.3, target tracking is now considered for range-Doppler measurements, assuming a CPI = 4 s and $\Gamma = 0.9$. Again, the noise with $\sigma_r = 470$ m is added to bistatic range measurements, and for the bistatic Doppler measurements, noise with $\sigma_f = 0.2$ Hz is added. As in the case of Doppler only tracking, the results for range-Doppler tracking are presented in Figure 5.11 (a) for the CRLB, the CCRLB, the RGNF co-variance matrix and the RGNF's RMS error of the target position.

Evidently from Figure 5.11 (a), the RMS error on the target position, as output from the RGNF, closely follows the CCRLB, except for the region where the bad geometry region occurs. This is consistent with the findings up to this point. In Figure 5.11 (b), the range-Doppler tracking results are compared to the Doppler only tracking results as previously presented in Figure 5.8. As seen from the CRLB results, the bad geometry region is significantly reduced when the target position tracking is based range-Doppler measurements and not only Doppler measurements. For the CCRLB results, virtually the same performance is obtained with target tracking errors as low as 50 m seen over the flightpath. It is therefore concluded that the additional bistatic range measurements, although coarse, do substantially contribute to the conditioning of the observation matrix. However, intuitively it is believed that better ways of conditioning the observation matrix exist and set as a future investigation.

[9] Note that low range resolution and high Doppler resolution are typical of FM band CR systems.

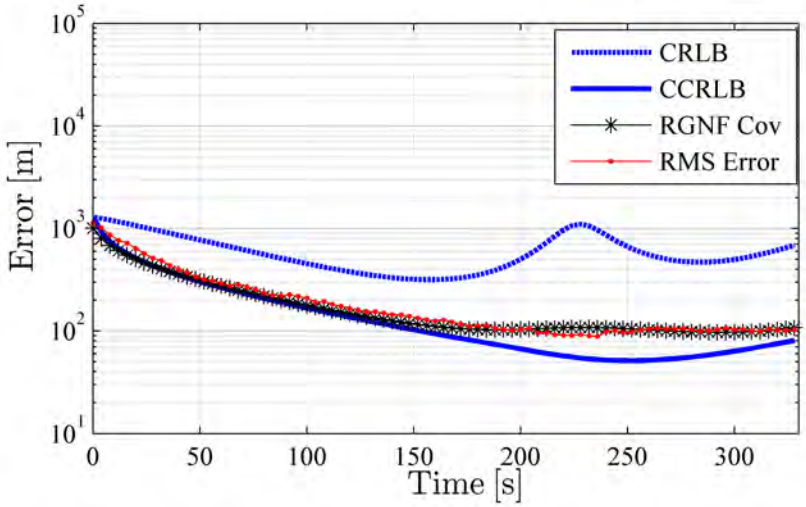

(a)

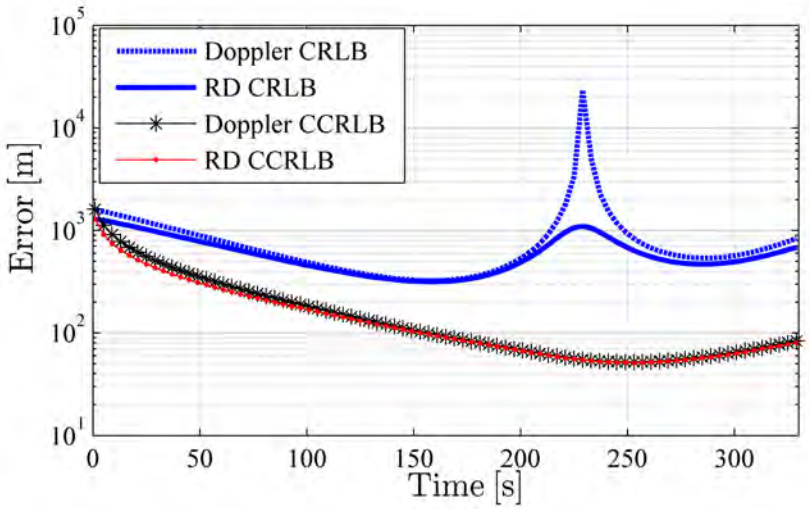

(b)

Figure 5.11: Simulated range-Doppler target tracking of a non-manoeuvring flight. (a) The RGNF tracking performance benchmarked to the CRLB and CCRLB. (b) Comparing Doppler only target tracking to range-Doppler target tracking.

5.5.8 Doppler Correlation

In Chapter 4, Section 4.7 results pointed out that the conditioning of the observation matrix is influenced by both the number of receivers and the receiver placement. Further, an observation matrix that is ill-conditioned results in bad geometry regions and a well conditioned matrix results in good geometry regions.

A common result observed in these results is that bad geometry regions are obtained in all configurations when the target is sufficiently far away from the receivers. The aim of this section is to demonstrate that this is caused by Doppler correlation between the receivers when the bistatic detection range becomes larger than the effective radius of the receiver configuration.

For the MIMO analysis presented in Section 4.8, it was shown that the Doppler measurement at a given receiver sites could be written as linear combinations of the remaining sites. This resulted in the observation matrix being non-full rank and was true for all measurements. However, the analysis required here is to show that the observation matrix becomes progressively ill-conditioned as the correlation amongst the Doppler measurements increases. For this reason the Spearman rank correlation coefficient method is considered which measures the non-linear monotonic relationship between two variables in the range of -1 and +1. A value of 0 indicates no correlation between the two variables, a value of -1 indicates that one variable is increasing and the other decreasing, and lastly +1 indicates that both variables are increasing or decreasing. Therefore, for the purpose of this analysis, +1 values would indicate a strong correlation in Doppler measurements,[10] otherwise no correlation between the sites would result in values close to zero. Further, the correlation coefficient, ρ_n between two receiver sites is calculated as:

$$\rho_n = 1 - \frac{6\sum_{j=1}^{v} d_{j,n}^2}{v(v^2-1)} \tag{5.30}$$

where v is the number of Doppler measurements the correlation is calculated over and $d_{j,n}$ is the difference between the Doppler measurements at the two re-

[10] Doppler measurements between two receiver sites are considered to be correlated when the measurements are equally decreasing or increasing between two receiver sites.

ceiver sites. For example, using the transmitter-receiver setup presented in Figure 5.12 (a) and the Doppler measurement notation described in Section 3.4.3, the Doppler difference between 'Rx1' and 'Rx2' is calculated as $d_{j,n} = f_{d1}[n + j - 1] - f_{d2}[n + j - 1]$, where $f_{d1}[n]$ and $f_{d2}[n]$ is the respective Doppler measurements at receivers 'Rx1' and 'Rx2' at time t_n. For demonstration purposes, the flight path considered for this section is assumed to start approximately in the middle of the bounding box of the receivers in Figure 5.12 (a) and then move away from the receivers with a constant velocity. The starting vector was $\mathbf{x}_0 = [20000, 65, 41000, 190]^T$. Further, using the same notation as before, the Doppler only tracking results for this flightpath are presented in Figure 5.12 (b) for the CRLB, the CCRLB, the RGNF co-variance matrix and the RGNF's RMS error of the target position.

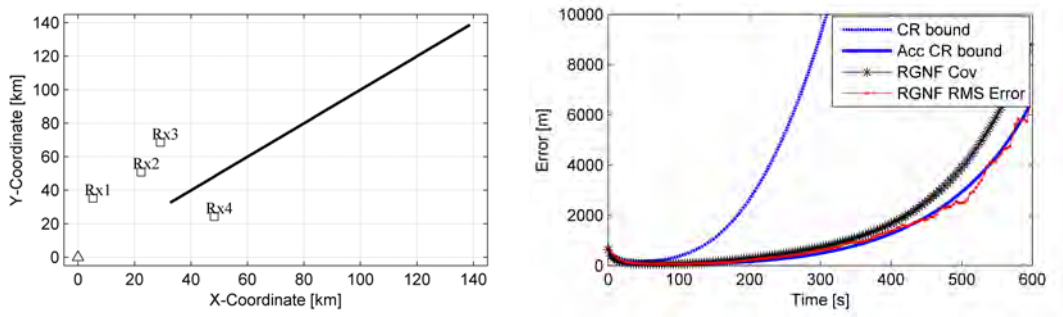

(a) (b)

Figure 5.12: Simulated Doppler only target tracking of a non-manoeuvring flight, demonstrating the effect of Doppler correlation on the tracking performance. (a) The simulation setup for a single transmitter, multiple receiver configuration and linear flight path. The flightpath started approximately in the middle of the receiver ring and moved away from the receiver towards the top right hand side of the figure. (b) The RGNF tracking performance benchmarked to the CRLB and CCRLB.

As seen from Figure 5.12 (b), the RGNF position estimation once again followed the CCRLB. Importantly, Figure 5.12 (b) also illustrates that the position accuracy becomes progressively worse as the target moves away from the receivers. The reason for this deteriorating performance lies in the fact that strong Doppler correlation is experienced amongst the receivers. This is clearly

seen in Figure 5.13 (a) in which the respective Doppler measurements from the 4 receiver sites are plotted in one figure. Further, the Spearman rank correlation coefficient method is used to determine the Doppler correlation between the 4 receiver sites. Therefore, 6 Doppler difference values are calculated between the 4 receivers sites as outlined by Equation (5.30), averaged over a window length of $v = 3$ and presented in Figure 5.13 (b) on the right axis. On the left axis, the condition of the observation matrix, $Cond(\overline{\mathbf{M}}_n)$ is shown, also as a function of time.

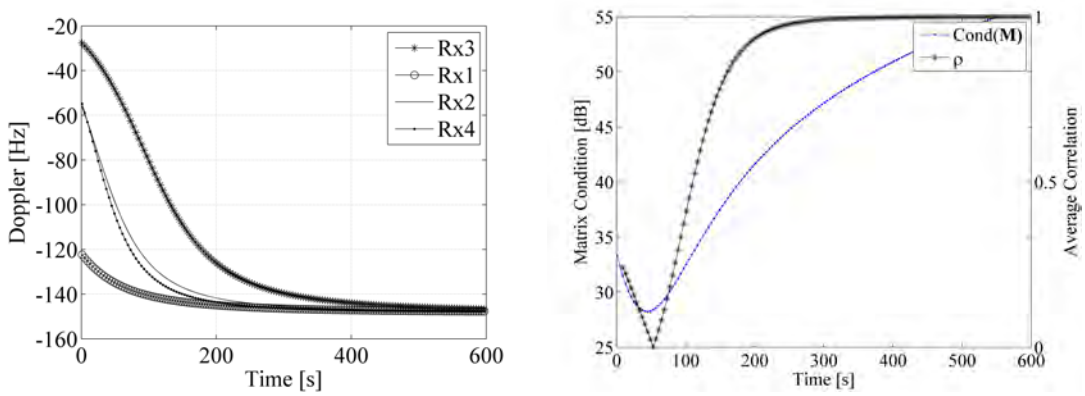

(a) (b)

Figure 5.13: Simulated results for a Doppler only tracking CR demonstrating the progressively ill-conditioning of the observation matrix as a result of Doppler correlation between the receiver sites. (a) The Doppler measurements as a function of time. (b) The observation matrix condition as a function of time (left axis), together with the average correlation between the receiver sites (right axis).

Clearly illustrated by Figure 5.13 (b), the condition of the observation matrix is dependant on the Doppler correlation. As the Doppler correlation increases, so does the conditioning of the observation matrix and vice versa. In other words, Doppler correlation amongst the receiver sites will result in an ill-conditioned observation matrix and accordingly results in inaccurate position estimates.

Lastly, it was also intended to determine a rule of thumb for when Doppler correlation becomes significant in far out tracking applications. However, as seen from the above discussion, the Doppler correlation depends on several factors, for example, the number of receivers, placement of the receivers, integration time,

standard deviation of the Doppler measurements and so forth. Therefore, it is concluded that the Doppler correlation needs to be calculated on a case by case basis for the time being and the rule of thumb investigation is set as an future investigation. However, from the results presented, it is safe to say that Doppler correlation is insignificant when the target is within the bounding box of the transmitter-receivers. For example, in Figure 5.12 (a), the target position is right bounded by the x-coordinate of 'Rx4', hence $\mathbf{x}_n <$ the x-coordinate 'Rx4'. Similarly, the y in $\mathbf{x}_n$ is top bounded by the y-coordinate in 'Rx3' and finally left and bottom bounded by the transmitter.

5.5.9 Discussion

The simulation results presented in this section demonstrated that the RGNF is able to track a target with only 4 Doppler measurements gathered from 4 geographically separated receivers. In the case of linear target motion, the RGNF tracking accuracy was shown to follow the CCRLB, that in return verified the newly developed CCRLB. In the case of non-linear target motion, the tracking accuracy could not match the CCRLB, but more importantly the filter was able to track the target through a non-linear trajectory even though a linear target motion model was implemented.

Further, initialising the RGNF with a position error of around 3 km and velocity error of around 10 ms^{-1} also appears not to effect the ability of the RGNF to converge and successfully track the target. Therefore, this should be adequate for initialisation and tracking in a real FM band CR.

From the CPI investigation, an CPI length of 4 s seems to perform the best for the tracking, especially under non-linear target motion and is therefore considered for the real measurement tracking implementation. The conditioning of the observation matrix also appears to reduce the bad geometry regions for Doppler only tracking. For the simulations presented, the results demonstrated that by increasing the number of receivers, or complementing the Doppler measurements with range measurements, although coarse; successfully reduced the bad geome-

try regions. Lastly, as seen from the Doppler correlation results, tracking of far out target using Doppler only measurements should be avoided.

Having sufficient confidence that the RGNF will be able to track a target, both under linear and non-linear motion, the RGNF is next put to the test in tracking a target from the real Doppler measurements obtained during the field trails, as described in Chapter 3.

5.6 Example Results: Real Data

In the previous section it was determined that the RGNF would be able to track a target by observing the Doppler shift of the target from 4 geographically separated receiver sites. This section now aims to establish target tracking using the real measured data from the field deployment described in Chapter 3.

In brief, this section covers the following; remarks on the target truth data is presented in Section 5.6.1, some ARD map detections are presented in Section 5.6.2 and the data association method considered for this thesis is discussed in Section 5.6.3. The standard deviation results for both the bistatic range and Doppler measurements (from the real data) are presented in Section 5.6.4, after which target tracking results are then presented in Section 5.6.5 for using only Doppler measurements and in Section 5.6.6 for using range-Doppler measurements. Finally, the highlights of this section are briefly discussed in Section 5.6.7.

5.6.1 Target Truth Data

For the purpose of calculating the CRLB and CCRLB to benchmark the performance of the RGNF against, truth data of the target is required. For the purpose of this thesis, ADS-B data is used.

Besides the obvious comparison between the RGNF estimated track and true target track (ADS-B data) in Cartesian space, the truth data is also transformed to ARD space that in return allows for a direct comparison between the range and

Doppler detections to the truth data. Furthermore, the truth data, transformed into ARD space is also used in the data association process that is described in Section 5.6.3.

Unfortunately, a limited number of aircraft were equipped with ADS-B responders during the trial period, as this is still not yet a civil aviation regulation in South Africa at the time of trial period. However, two flights, namely flight SAA333 and SAA327 were equipped with ADS-B transponders and are accordingly considered for tracking for the remainder of this chapter.

5.6.2 Bistatic Range and Doppler Detections

Following the processing steps outlined in Chapter 3, Section 3.3, range-Doppler detections were produced for the four receiver sites using a CPI of 4 s. As these range-Doppler detections are processed in less than 4 second intervals [29], the update interval for the tracking stages are also set to 4 seconds. Notice that processed range-Doppler detections for only two receivers sites are presented in this section.

Firstly, considering the Atlantic receiver site, the bistatic range detections as a function of time are presented in Figure 5.14 (a) for the time period when flight SAA333 is present in the ROI and secondly, the bistatic Doppler detections[11] are presented for the same time period in Figure 5.14 (b). Furthermore, in both figures, the target truth data from flight SAA333 is also overlaid in red.

Secondly, considering the same time period as for the Atlantic receiver, processed range-Doppler detections are also provided for the Malmesbury receiver site. Presented in Figure 5.15 (a), are the bistatic range detections as a function of time and in Figure 5.15 (b), the bistatic range rate detections, also as a function of time. Once again, the truth data for flight SAA333 is overlaid in red to both figures.

[11] Notice from Figure 5.14 (b), detections are presented as range rate. Doppler is obtained from the range rate by simply normalising the range rate to the wavelength of illuminator's carrier frequency. This is assumed throughout the thesis.

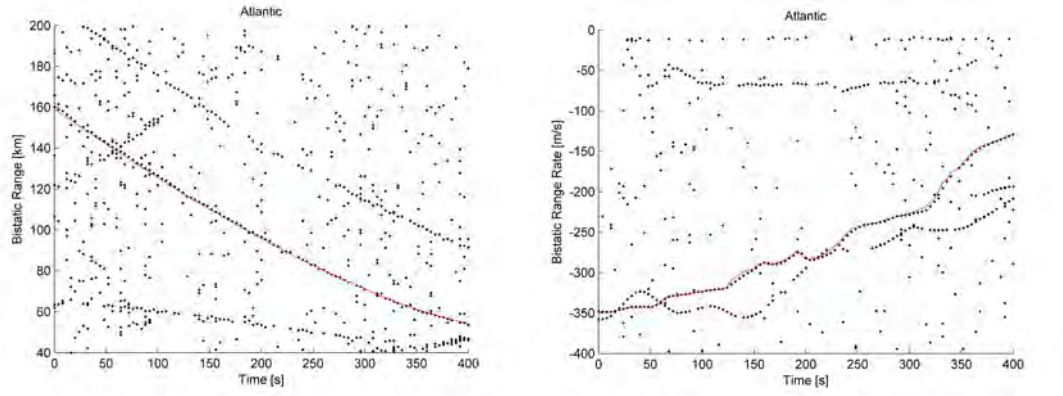

(a) (b)

Figure 5.14: Bistatic range and range rate detections at the Atlantic receiver site. Flight SAA333 truth data are overlaid in red; (a) Bistatic range detections over time and (b) Bistatic range rate detections over time.

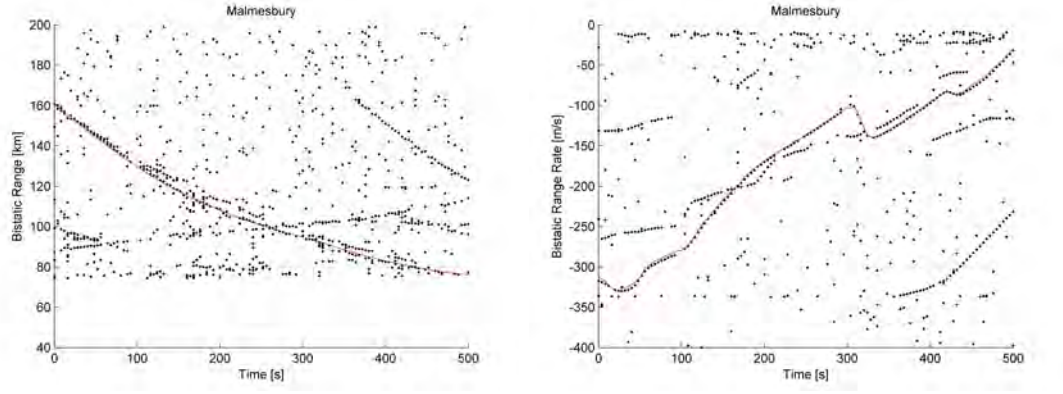

(a) (b)

Figure 5.15: Bistatic range and range rate detections at the Malmesbury receiver site. Flight SAA333 truth data are overlaid in red. (a) Bistatic range detections over time and (b) Bistatic range rate detections over time.

As seen from the range-Doppler detections, numerous aircraft detections were made at the respective receiver sites, but importantly, notice the close resemblance of truth and detection data for flight SAA333 (similar detection results was obtained for flight SAA327). Lastly, also note the fairly good probability of detection of flight SAA333 in comparison to the other flight detections. As flight SAA333 was an Airbus A340-600, hence a large commercial airliner, the SNR

detections at the receiver were most probably larger than the other comparative aircraft's SNR as a result of the larger associated Radar Cross Section (RCS) returns.

5.6.3 Data Association

As stated in Section 5.6.1, the target truth data is also used for data association purposes. First, the ADS-B track data is transformed to range-Doppler space by making use of the time-stamped ADS-B data and the known positions of the transmit-receiver pairs. Accordingly, a total of 4 transformations are made for the 4 receiver sites and for the remainder of the thesis be referred to as range-Doppler truth data. Further, also notice from the bistatic range and Doppler detections presented in Section 5.6.2 that the target detections closely followed the truth data, hence allowing this approach to be followed.

The best target association results are achieved by first comparing the range-Doppler truth data to the target detection data in the Doppler domain. Hence, the Doppler truth data is overlaid to the raw Doppler detections, in which case all the Doppler detections that lie within an error bound of ± 0.4 Hz to the Doppler truth data, are selected as potential detections. These potential detections are then compared to the associated range values of the Doppler detections in which case the single range-Doppler detection to minimise the detection error, is selected as the final detection. Accordingly, this range-Doppler detection is then associated to the flight under consideration. This process is repeated over the entire flight profile and also over the respective receiver sites, after which it can safely be assumed that all the range-Doppler detections at the various receiver sites are correctly associated to the corresponding flight profile. These range and/or Doppler detections were then considered to be the input to the RGNF;[12] with a measurement error (standard deviation) that is to be covered in Section 5.6.4.

[12] The 3-D range-Doppler detections are transformed to 2-D range-Doppler detections prior to the target tracking stage as described under "RGNF State Estimation" in Chapter 3, Section 3.3.

Table 5.1: Standard deviation results of bistatic range and bistatic Doppler for flight SAA333 and SAA327 over a 4 s CPI.

	$\sigma_f[Hz]$		$\sigma_r[m]$	
	SAA 333	SAA 327	SAA 333	SAA 327
Atlantic:	0.12	0.15	462.65	403.53
Malmesbury:	0.17	0.21	461.18	447.59
Kalbaskraal:	0.29	0.19	512.16	517.43
Donkerhoek:	0.25	0.22	494.95	435.30
Flight Average:	**0.21**	**0.19**	**482.74**	**450.96**
Average:	**0.20**		**466.85**	

5.6.4 Standard Deviation of Measured Data

As listed in Chapter 1, Section 1.4.2, one objective was to validate the theoretical and simulated data with measured data and accordingly required a standard deviation analysis of the bistatic range and bistatic Doppler measurements. Therefore, at each receiver site, a polynomial data mean is fitted to the raw detection data[13] of a particular flight and subsequently, followed by the straight forward calculation of the standard deviation. A summary of these standard deviation results are presented in Table 5.1, for flight SAA333 and SAA327 using a CPI to 4 s. These values appear to be in line with those reported of Tharmarasa [135] in which the analysis of bistatic range and Doppler measurements are also reported on.

5.6.5 Doppler Only Tracking

As all the necessary set-up and pre-processing is performed prior to this section, it is now possible to attempt target tracking with the RGNF. In the following sections, results are presented in which the RGNF was used to estimate the target position from real measured data, collected by 4 spatially separated receivers[14]

[13] Raw detection data in this context refers to either the bistatic range or bistatic Doppler detections from the CFAR detection stage in the processing chain and is already associated to a particular flight, see Section 5.6.3.

[14] Each FM band CR receiver exploited a single channel from the same FM transmitter.

over a given period of time. Firstly, Doppler only tracking is considered and secondly, range-Doppler tracking is considered in Section 5.6.6.

5.6.5.1 Example 1 : Flight SAA333

Aiming to track flight SAA333 by using Doppler only measurements and a CPI of 4 s, is considered first. In all cases of using real data, the state vector of the RGNF is initialised with the method described in Section 5.4, $\Gamma = 0.95$ and the filter co-variance matrix $\mathbf{P}_0^{-1}$ is initialised as given in Equation (5.14). Further, the filter is cycled as described in Section 5.3.3 to produce a state estimate, $\hat{\mathbf{x}}_n$ from the associated Doppler detections described in Section 5.6.3. Lastly, the standard deviation of the Doppler measurement errors was assumed to be $\sigma_f = 0.20$ Hz as determined in Table 5.1.

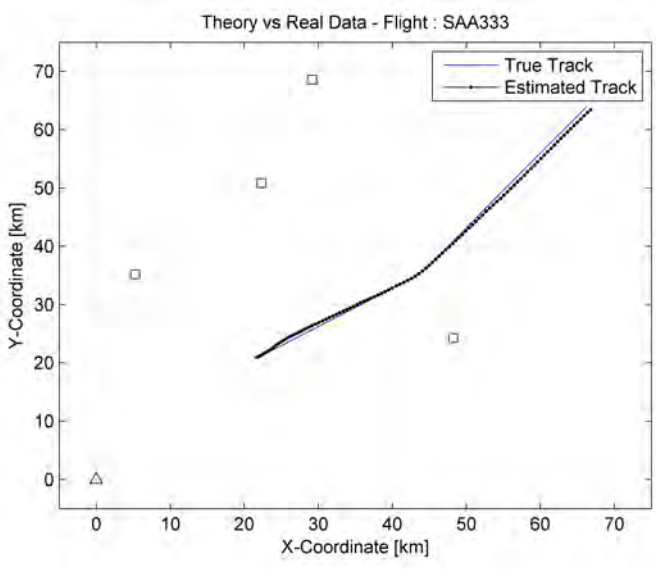

Figure 5.16: Doppler only target tracking of flight SAA333 overlaid to ADS-B truth data.

In Figure 5.16, the RGNF track estimate (colour black) for flight SAA333 is overlaid to the true track (colour blue) in a Cartesian coordinate system; referenced to the transmitter. Target motion occurs from the top right corner of the figure towards the transmitter, situated at the bottom left corner. As in the case

of the simulation section, the transmitter position is indicated by the '△' and the four receiver positions with squares.[15] Most importantly, Figure 5.16 clearly demonstrates that the RGNF is able to successfully track the target over the entire flight path considered, even though a gentle right hand turn was present in the track and the fact that the flight is non-linear. This is covered next.

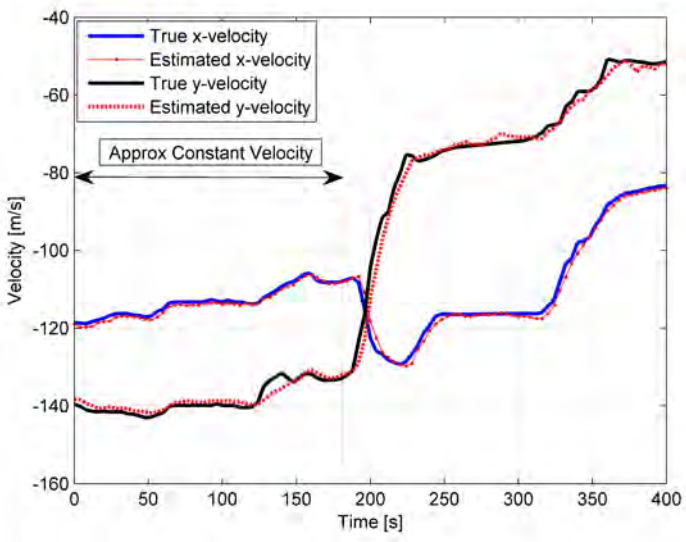

Figure 5.17: Estimated velocity of flight SAA333 overlaid to the true velocity calculated from the ADS-B data; based on Doppler only measurements.

The estimated velocity of flight SAA333 is presented in Figure 5.17 and once again overlaid to the ADS-B truth data. Importantly, notice from the figure that the estimated velocity (colour red) closely follows the true velocity (colour black and blue) and as expected, the flightpath is highly non-linear. Furthermore, in the first phase of the flight path, up to t = 180 s, the velocity in both the x and y directions slowly changes and accordingly can be seen as an "almost constant velocity" scenario. Therefore, this phase of the flight path was most suited to be compared to the theory developed in Chapter 4, as it assumes constant linear motion.[16]

[15] This is the exact same setup as used in the simulation section.

[16] In Section 5.5 theory was verified by simulation under linear motion conditions. The focus of this section is to validate the simulations to some degree, given that the flight path is non-linear.

Presented in Figure 5.18, are the theoretical, simulated and measured target position error results of flight SAA333. The simulation data is based on 200 Monte Carlo runs with an initial state error as mentioned in Section 5.5.1 and lastly, the exact same setup of the RGNF was used for the measured data as in the case of the simulation data.

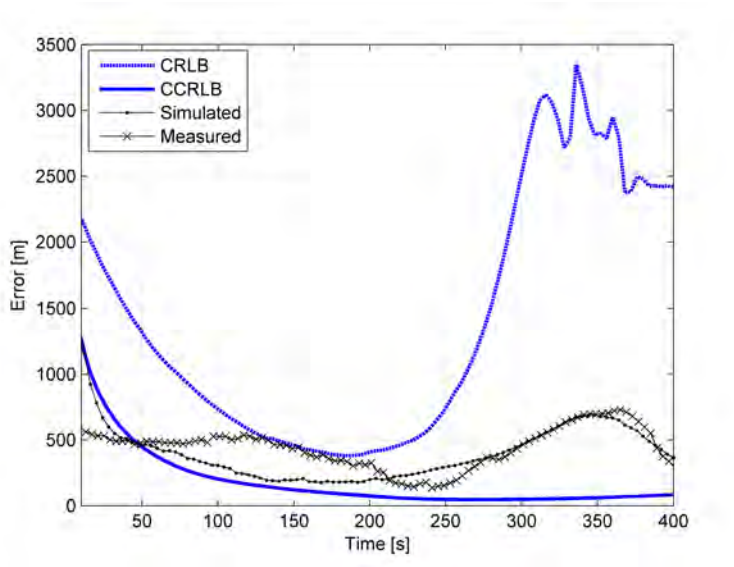

Figure 5.18: The RGNF tracking performance benchmarked to the CRLB and CCRLB for flight SAA333; based on Doppler only measurements.

As illustrated in Figure 5.18, the measured target position error follows a similar error pattern to the simulated target position error, with the exception that the RGNF takes longer to converge when using real Doppler measurements. As expected, neither the simulated nor the measured data position error follows the CCRLB as a result of the non-linear motion of the target. However, surprisingly, the performance does exceed the CRLB, hence confirming the benefit of using history Doppler measurements to improve the target position accuracy.

Further, notice from the simulation results that the RGNF follows the CCRLB in close proximity up to t = 180 s, although not as closely as in the case of perfect linear motion, after which it then diverges from the CCRLB. This suggests that the turn has more of an effect on the RGNF while being exposed to non-linear motion over an extended period of time.

Further seen in Figure 5.18, is that both the simulated and measured results start below the CCRLB at the time of initiation. As mentioned earlier, the RGNF is initialised from both range and Doppler information and in this case, the additional range information improves the initial estimate due to the Doppler only measurements emerging from a bad geometry region. As the CCRLB only assumes Doppler information, it is therefore possible to outperform the CCRLB initially, but due to the Doppler only observations that follow, it should over time diverge to be greater than the CCRLB, or equal to it at best. In the case of the simulated data, the initial error is set smaller than the theoretical expected error in order to verify the findings of the measured data. Similarly, the results diverged to be greater than CCRLB as time progresses.

In summary of the results presented here; 1.) it is encouraging to see that RGNF is able to track the target, even though the target exercised non-linear motion. 2.) The target position accuracy is seen to lie between the CRLB and CCRLB and lastly, 3.) it is observed that the CCRLB is too optimistic to predict the target position accuracy for non-linear target motion, but this result is expected. In the sections to follow, this criteria will mostly be used to build the readers confidence in these three observations.

5.6.5.2 Example 2 : Flight SAA327

Next, Doppler only tracking for a second recorded flight is considered, namely flight SAA327. Following a similar approach and setup of the RGNF as used in Section 5.6.5.1, together with a CPI of 4 s, the target position and velocity estimates are overlaid to the truth data in respectively Figures 5.19 and 5.20. Seen from Figure 5.19, the RGNF is once again successful in tracking flight SAA327, despite four turns over the flight path. These four turns are clearly seen in Figure 5.20 at time stamps $t_n = 50$ s, 310 s, 420 s and 480 s.

In the case of flight SAA327, the approximate constant velocity period is between t = 70 s and t = 300 s, as indicated in Figure 5.20 and the region in which the position estimates are expected to converge to the CCRLB. Further, notice from Figure 5.20 that the estimated velocity closely follows the truth data. However,

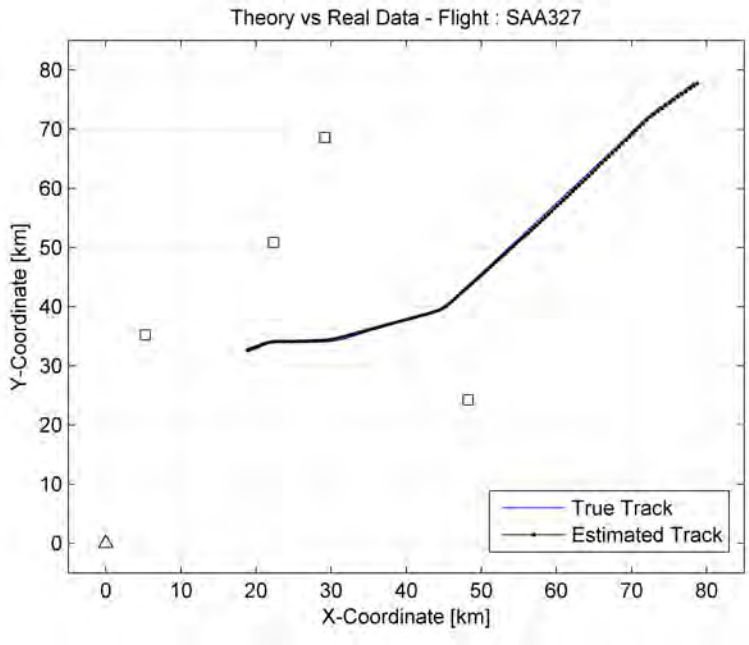

Figure 5.19: Doppler only target tracking of flight SAA327 overlaid to ADS-B truth data.

the truth data does contain over some heading errors that translates to velocity errors. This is clearly seen in Figure 5.20 as the "bumps" in the true y-velocity data, with the most noticeable being between t = 100 s and 200 s.

Presented in Figure 5.21, are the theoretical, simulated and measured target position error results of flight SAA327. Before continuing, first notice from Figure 5.21 that the CRLB suggests that target tracking is to be started while the target resides within a bad geometry region. The impact of this on the tracking is explored by means of the following three options.

The first option considered is to initialise the RGNF co-variance matrix, $\mathbf{P}_0^{-1}$ as given in Equation (5.14) and evaluate the tracking. In this case, the RGNF is unstable at initiation and made errors around 4.5 km, only to diverge back to the CCRLB at roughly t = 300 s. Given that the target resides in a bad geometry region, this result is seen as sensible as the observation matrix is ill-conditioned due to the bad geometry region. But importantly, when the target moves out of the bad-geometry region, tracking did improve and a similar result

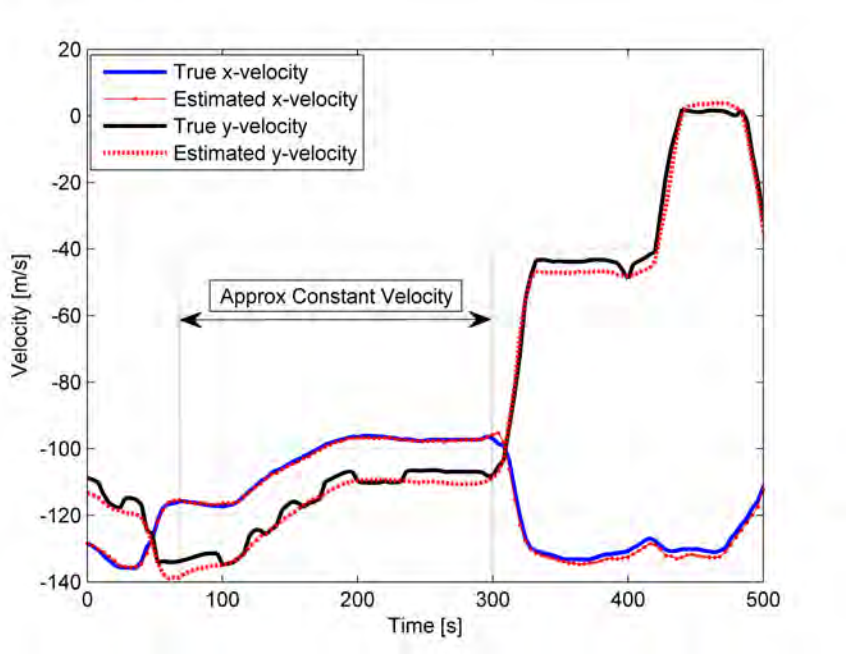

Figure 5.20: Estimated velocity of flight SAA327 overlaid to the true velocity calculated from the ADS-B data; based on Doppler only measurements.

than presented in Figure 5.21 for the later stages of tracking, is obtained.

The second option considered is to lower the variance on the position significantly in $\mathbf{P}_0^{-1}$, in which case a slower convergence rate is the penalty, or even no convergence. However, with the additional range information, luckily the state vector initialisation is sufficiently accurate, within 500 m of the true position and therefore allows $\mathbf{P}_0^{-1}$ to be initialised as;

$$\mathbf{P}_0^{-1} = \begin{pmatrix} 0.25 & 0 & 0 & 0 \\ 0 & 0.0001 & 0 & 0 \\ 0 & 0 & 0.25 & 0 \\ 0 & 0 & 0 & 0.0001 \end{pmatrix} \tag{5.31}$$

The results presented in Figure 5.21 are based on this method. From these results, importantly, notice the slight ripple effect of the RGNF estimate over the first part of the flight track as a result of the extremely confident setting on $\mathbf{P}_0^{-1}$. However, the close relationship between the simulated and measured

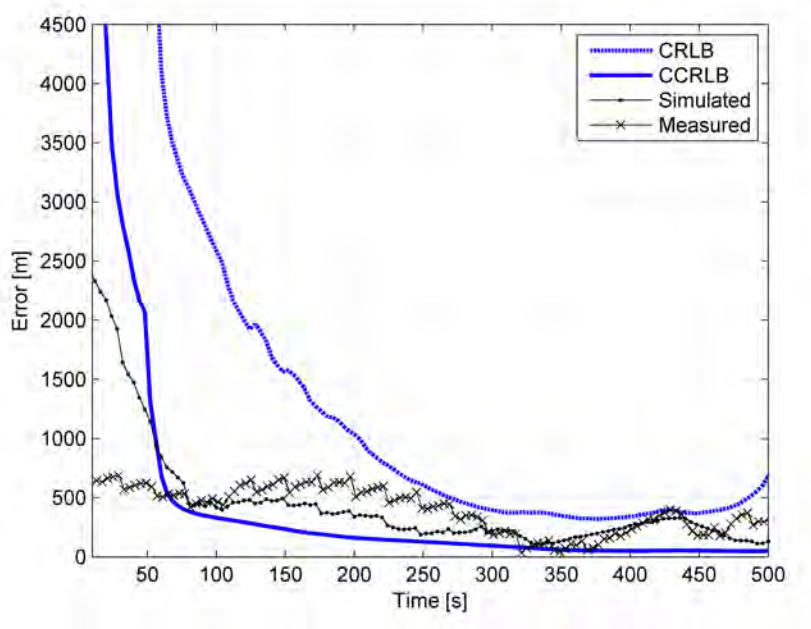

Figure 5.21: The RGNF tracking performance benchmarked to the CRLB and CCRLB for flight SAA327; based on Doppler only measurements.

results is maintained and the RGNF performance also lies between the CRLB and CCRLB. Furthermore, as seen from Figure 5.21, the flight phase between t = 70 s and t = 300 s represents an approximate linear motion time period and does indeed result in a scenario where the tracking error diverges to the CCRLB over time. Also, notice that the initial position estimation is once again lower than the CRLB at time of initiation as explained in case of flight SAA333.

The third an last option considered is to simply wait out the bad geometry region, i.e. start the tracking at t = 100 s with $\mathbf{P}_0^{-1}$ initialised to Equation (5.14). In this case, the RGNF also successfully tracks the target with a similar result as presented in Figure 5.21 for t = 100 s and onwards, but importantly without the rippling effect.

5.6.6 Range-Doppler Tracking

Following the investigation into using additional bistatic range information to condition the observation matrix, this is now tested with real measured data for flights SAA333 and SAA327. Once again, simulation results are based on 200 Monte Carlo runs, standard deviations of respectively $\sigma_r = 470$ m and $\sigma_f = 0.20$ Hz are used for the bistatic range and Doppler measurement errors and lastly, the RGNF is setup with the same parameters as considered for the Doppler only tracking presented in Section 5.6.5.

The 2-D positional error results of flight SAA333 and SAA327 are respectively presented in Figures 5.22 and 5.23. Importantly, notice that the additional range information improves the CRLB as well as the CCRLB in comparison to Figures 5.18 and 5.21 using Doppler only measurements. Once again, the measured position accuracy of the target follows the simulated results and also lie within the CRLB and CCRLB error bounds. Lastly, it is again observed that the CCRLB is too optimistic in predicting the lower bound on positional accuracy for non-linear motion targets.

5.6.7 Discussion

The main goal of this section was to prove the feasibility of Doppler only tracking by making use of real measured data. As can be seen from the results presented, this goal is clearly reached in which the target position accuracy lies between the CRLB and CCRLB due to the non-linear motion of the target. As a result, the CCRLB is too optimistic to predict the lower error bound for a non-linear motion target, but is expected as the CCRLB assumes linear target motion; although not limited to it.

Using low resolution bistatic range measurements together with high resolution Doppler measurements to initialise the RGNF is also shown to be successful, as the RGNF was able to successfully converge to the target track based on this initialisation.

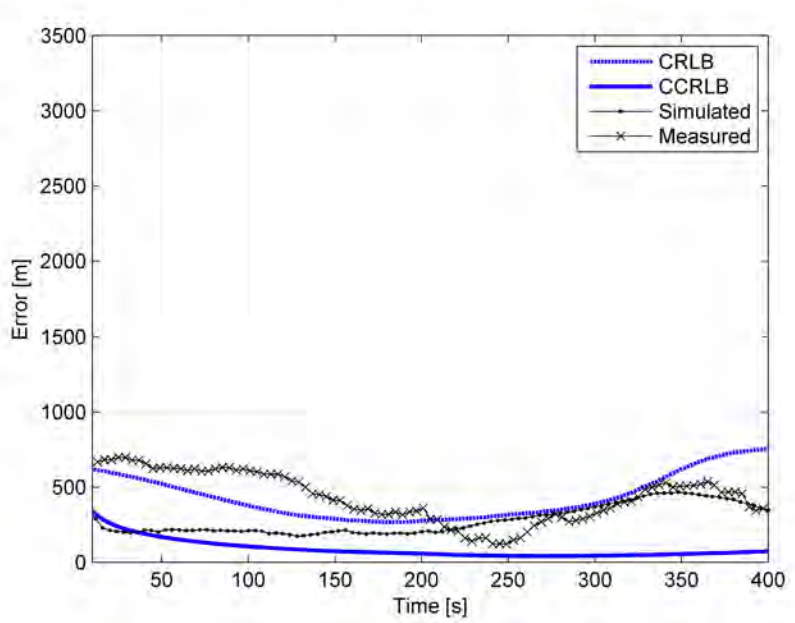

Figure 5.22: The RGNF tracking performance benchmarked to the CRLB and CCRLB for flight SAA333; based on range-Doppler measurements.

Further, with the addition of bistatic range measurements to the Doppler measurements, tracking is slightly improved and accordingly suggests that the conditioning of the observation matrix is an important aspect in Doppler only tracking. The addition of low resolution range measurements to the observation matrix is one approach, however, intuitively one would believe that other, and possibly better methods exist to accomplish this. Therefore, this investigation is set aside for future research.

The effect of Doppler walk, due to the extended period of integration times (long CPI) used in this thesis, is another aspect that needs further investigation. As an example, consider the following; assume a target is fairly close to the baseline with a bistatic angle $\beta = 120°$ and the illuminator of opportunity's frequency is

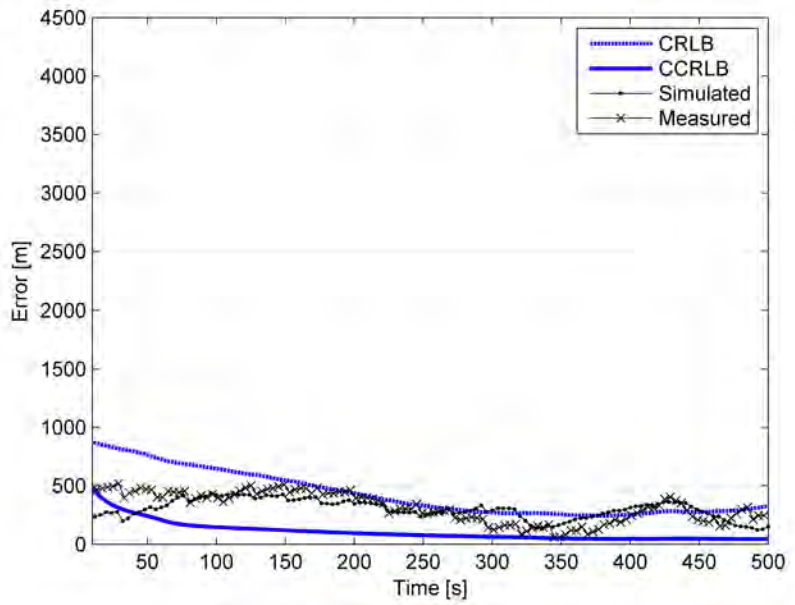

Figure 5.23: The RGNF tracking performance benchmarked to the CRLB and CCRLB for flight SAA327; based on range-Doppler measurements.

89 MHz. The bistatic velocity resolution, δv is then given as[17]

$$\delta v = \frac{\lambda}{2T\cos(\beta/2)} \tag{5.32}$$

which means that $\delta v = 0.843$ ms^{-1} for a CPI of 4 s. Therefore, any change in target velocity over the 4 s CPI that exceeds δv, will result in Doppler walk. Taking the difference between two velocity points in Figures 5.17 and 5.20, it is seen that this threshold is easily exceeded due to the aircraft being in it's approach phase to Cape Town International airport. Therefore, Doppler walk needs to be accounted for in this scenario, but for example when the aircraft is at constant cruising speed, this matter would pose less of an issue. Furthermore, evidence of Doppler walk is seen in the standard deviation results section, in which the Doppler deviation seems to under perform compared to the theoretical standard deviation given by Howland [91] as $\sigma_f = \sqrt{\frac{1}{12T^2}}$, where T is the CPI.

[17] Note, β was specifically chosen to be 120°, as at this angle the bistatic velocity resolution is equal to the range rate resolution in ARD map.

Theoretically, a standard deviation result of 0.07 Hz should be achieved for a CPI of 4 s, where only 0.2 Hz was achieved in this thesis. However, Doppler walk is a known phenomenon within the Synthetic Aperture Radar community and could also be applied to CR. Further, a paper by Malanowski et al. [62] also shows, with suitable treatment, that long CPI's (up to 10 s) can be used for FM band CR. Hence, Doppler walk is not seen as a major concern, but requires further investigation.

Lastly, also not taken into account in this thesis, is the fact that the Doppler measurements might not be an unbiased estimate under non-linear motion. Unfortunately, the ADS-B data captured during the field trials does not allow for such an investigation as the velocity measurements are not sufficiently accurate. Therefore, the CRLB and CCRLB probably needs re-investigation considering this fact, but is also set aside for future investigation.

5.7 Conclusions

The results presented in this section make use of the full-processing chain proposed for a multi-static Doppler only tracking system described in Chapter 3. Certainly, the most important result includes the fact that the proposed processing of the data is capable of first establishing a target detection in the form of the target's Doppler shift (Chapter 3), followed by transforming the detection into a target position (Chapter 4) and being able to produce a target track as time progresses with the RGNF (Chapter 5).

It is therefore concluded that the RGNF is able to track a target under linear motion conditions with only measuring the target's Doppler shift from geographically separated receivers. Under such conditions, the target position accuracy is then given by the CCRLB.

Of utmost importance in Doppler only tracking applications, is ensuring that the observation matrix is properly conditioned, as failure to do so, will result in the so called bad geometry regions. Factors that influence the conditioning of the

observation matrix is pointed out as; the number of receivers used (assuming the basic observation criteria is met), the placement of the receivers, also keeping in mind the possibility of Doppler correlation in the measurements and lastly, the use of additional information to condition the observation matrix. In this thesis range measurements are used, but intuitively one would suspect that better ways exist to accomplish this.

The simulation results was also validated by real data measurements. Under these conditions, it is concluded that the target position accuracy lies between the CRLB and CCRLB error predictions, as a result of the non-linear motion exercised by the target. Further, an investigation of evaluating the effect of bias error on the CRLB and CCRLB is also seen as necessary to advance/optimise Doppler only tracking for real data measurements. It is further concluded that the target tracking results presented for the real measured data could probably be further improved as Doppler walk (as a result of long CPI) is not considered and therefore, needs further investigation. Although Doppler walk not considered in this thesis, Synthetic Aperture Radar (SAR) processing and some other suggestions in literature could be used to address Doppler walk and accordingly, should be included in the processing chain in future.

Lastly, the receiver positions selected for the field trails were based on a SNR and DPI criteria [25]. However, it was seen in this chapter, as well as Chapter 4 that firstly, the number of receivers and secondly, the positions of the receivers influence the bad geometry regions. Therefore, one remaining question could be asked: "Could a better receiver placement have been used for the flight paths considered during the fields trials?" Accordingly, this theme is next covered in Chapter 6.

Chapter 6

Finding better receiver positions

6.1 Introduction

In Chapter 3 the planning and execution of an experimental trial was described, in which the aim was to detect and track commercial airliners by sensing the Doppler shift of the target at multiple geographically separated receivers. For these trials, the receiver placement was based on the SNR and SINR criteria presented by Inggs et al. [25]. However, as concluded from Chapters 4 and 5; the number of receivers and importantly, their placement influences the bad geometry regions as well as the CRLB and CCRLB.

Therefore, this chapter now aims to use the knowledge gained over the last two chapters in an attempt to determine whether better receiver placements could have been used for the experimental trial.[1] Accordingly, this chapter is structured as follows. In Section 6.2, the setup of a virtual receiver grid over the ROI is described and in Section 6.3, the potential tracking performance is investigated for using all the receiver positions in the virtual receiver grid. In Section 6.4, the developed theory from Chapter 4 is then considered to determine the optimal

[1] Notice, although this chapter aims to address the specific case of optimising the receiver placement for the field experiment described in Chapter 3, it could also be generalised to an universal solution for any multi-static system.

receiver placement for a reduced number of receivers (compared to all the receiver positions being utilised) and also, how this influences the tracking performance. Lastly, some conclusions are drawn in Section 6.5.

6.2 Receiver Grid Placement

Aiming to optimise the receiver placement for a typical inbound flight to Cape Town International Airport, a grid of 36 possible receiver nodes are placed over the ROI that the target is moving in. This virtual grid, together with a 2-D flight path of a typical inbound flight to Cape Town International Airport is illustrated in Figure 6.1. The 36 node receiver grid is assumed to be static and placed in a 60 km by 60 km, UTM defined rectangular shape, with a separation distance of 12 km between the grid nodes. As seen from Figure 6.1, the grid nodes are indicated with an "o", the Cape Town FM transmitter with a "△" and the target trajectory with the straight line. For the flight path, the linear motion model considered in Chapter 5, Section 5.5.3, is once again reused. In this fashion, the performance gain could easily be evaluated with a direct comparison between the results obtained in this chapter and the results obtained previously, in which optimised receiver placements where not considered.

6.3 Utilising all Possible Receivers

Before, the receiver placement investigation is considered, all possible receiver nodes are first utilised to establish the lower bound on the expected tracking performance, assuming the findings of Morrison et al. [94] holds.

For all simulations used in this chapter, the following setup parameters are considered. First, the transmitter settings presented in Chapter 3, Table 3.1 are reused here, together with the assumption that only a single radio station is exploited. Additionally, the following parameters are used in the simulation; a forgetting factor, $\Gamma = 0.9$ for the CCRLB; a standard deviation, $\sigma_f = \sqrt{0.1}$ Hz

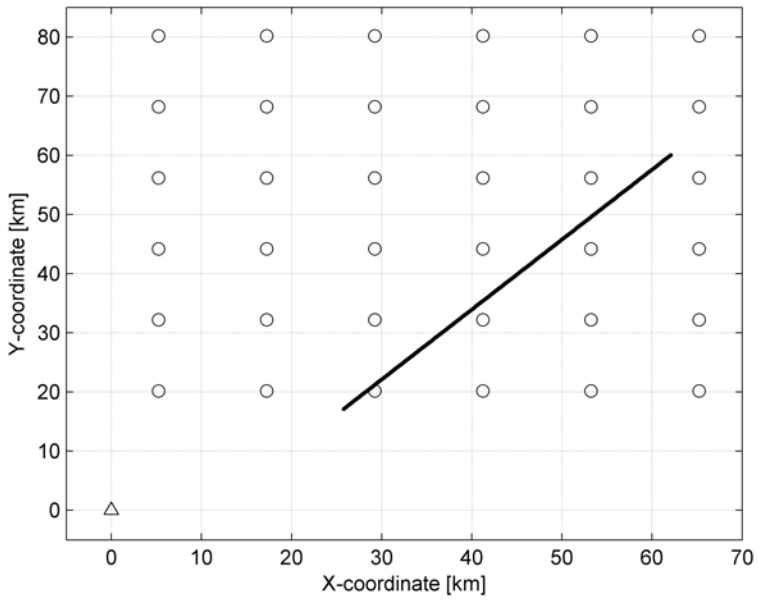

Figure 6.1: The placement of the receiver grid in the ROI, consisting of 36 possible receiver positions indicated by "o". The flight path is indicated by the straight line and the transmitter indicated by "△".

for the Doppler measurements; a CPI = 1 s and the total flight duration 330 s.

Recalling from Chapter 5, both the CRLB and CCRLB are shown to be a good representation of the actual performance delivered by the RGNF and accordingly, only these two bounds are considered for simulation in this chapter. Therefore, for the scenario presented in Figure 6.1, the CRLB and CCRLB is evaluated next utilising all 36 receiver nodes. Following the procedure as described in Chapter 4, both the FIM and CFIM are first calculated with Equation (4.32) and Equation (4.46), followed by the calculation of the CRLB and CCRLB with Equation (4.19) and lastly, the PDOP calculation by using Equation (4.35). Accordingly, the lower bound on the target position error, as predicted by the CRLB and CCRLB, are presented in Figure 6.2 in which a logarithmic scale is used on the y-axis.

From Figure 6.2 the CRLB demonstrates that the best possible position estimates of the target would have an error that varies between 60 m and 150 m over the

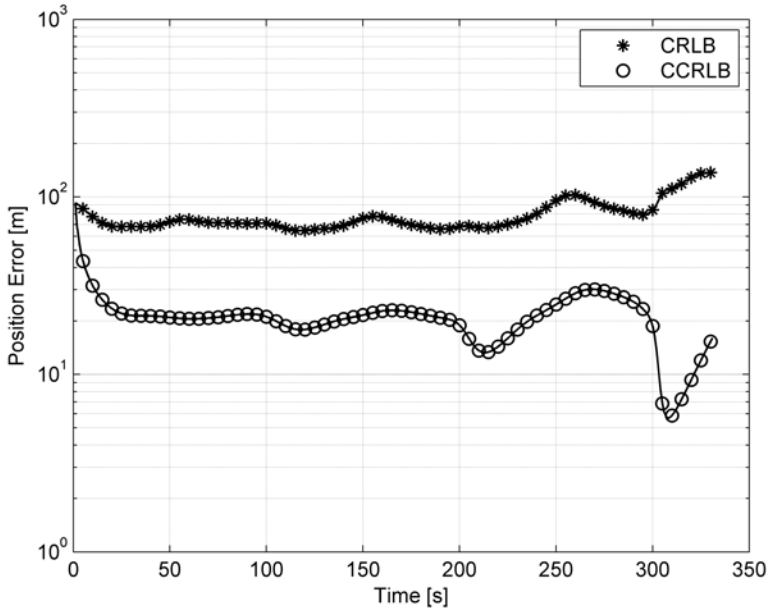

Figure 6.2: The CRLB and CCRLB performance predictions for a Doppler only tracking CR using 36 receivers.

flight path and on average, would have an error of 70 m. However, if perfect time history information is taken into account (CCRLB), this positional error is reduced to between 5 m and 30 m with an average error of approximately 20 m. Hence, from this result it is concluded that a large number of receivers enables accurate Doppler only tracking and confirms the finding of Morrison et al. [94]. The question could now be asked; "Could a reduced number of receivers achieve a similar result?" In the next section, an attempt is made to answer this question.

6.4 CRLB based selection

In Section 6.3, all possible receiver positions in the receiver grid are utilised to determine the CRLB and CCRLB. As the placement of 36 receivers might be less desirable in scenarios where operational cost and maintenance of an ATC system is the predominant drive, the effect of reducing the number of receivers

is explored in this section. Besides reducing the number of receivers, the aim would also be to select a set of receivers that would minimise the tracking errors according to the CCRLB bound. In return, this would require evaluation of the CRLB and CCRLB for all possible combinations of placing the given number of receivers in the receiver grid. Therefore, suppose the objective is to place a set of n_c receivers, given that n_r possible receiver positions are available in the grid, then $\mathbf{c}(n_r, n_c)$ combinations exist for placing the n_c receivers, in which $\mathbf{c}(n_r, n_c)$ is given as

$$\mathbf{c}(n_r, n_c) = \frac{(n_r)!}{(n_c)!(n_r - n_c)!} = \frac{n_r(n_r - 1)\cdots(n_r - n_c + 1)}{(n_c)!} \tag{6.1}$$

As the objective of this chapter is to determine alternative, or possibly better receiver positions for the field trials, only a set of 4 receivers are considered here for a receiver grid size of 36. Hence, setting $n_c = 4$ and $n_r = 36$ in Equation 6.1 and accordingly, the number of receiver combinations required to evaluate for the CRLB and CCRLB are $\mathbf{c}(36, 4) = 58905$.

The selection of the best performing receiver combination is then obtained as follows: First, making use of the PDOP equation, the positional errors for respectively the CRLB and CCRLB are summed at discrete time intervals, t_n over the entire flight path of length L_f and over all $\mathbf{c}(36, 4)$ as

$$\Omega_{p,j} = \sum_{n=1}^{L_f} \sigma_{p,n} \qquad j = 1, 2, \cdots, \mathbf{c}(n_r, n_c) \tag{6.2}$$

where $\sigma_{p,n}$ was defined in Equation (4.35). The summed values for all the receiver combinations $\mathbf{c}(n_r, n_c)$ is then logged as a vector

$$\mathbf{\Omega} = \left[\Omega_{p,1}, \Omega_{p,2}, \cdots, \Omega_{p,C_c^r}\right]^T \tag{6.3}$$

where $\mathbf{c}_c^r$ is used as short notation for $\mathbf{c}(n_r, n_c)$. Lastly, the set of n_c receivers that resulted in the smallest sum of errors from Equation (6.3), is selected as

$$\min\{|\mathbf{\Omega}|\} = [X_{R1}, X_{R2}, \cdots, X_{Rn_c}] \tag{6.4}$$

that represents the best performing receivers. On the other hand, the set of receivers that resulted in the largest sum of errors are also logged and accordingly represents the worst performing receiver set. The positions of the best and worst performing receiver sets are shown in Figure 6.3.

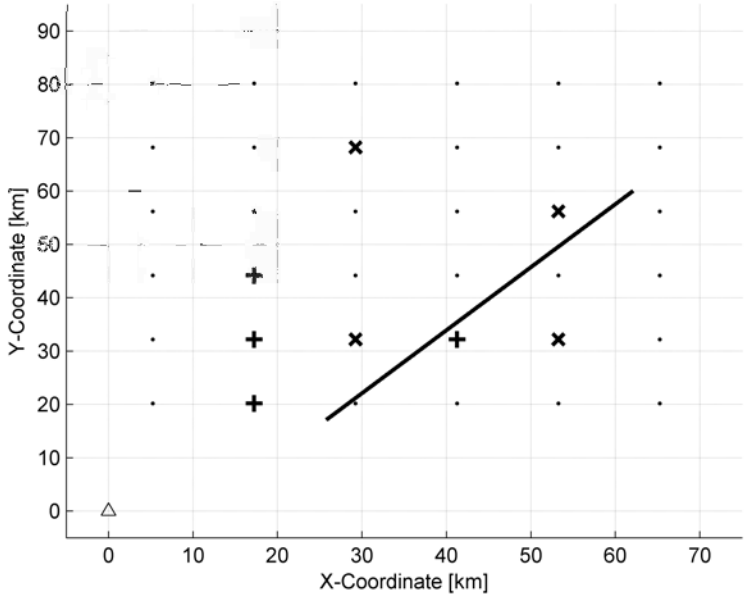

Figure 6.3: The best and worst receiver positions using 4 receivers. Possible receiver sites are identified with an "·", the set of best performing receivers with a "×" and the set of the worst performing receivers with a "+".

In addition to only displaying the best and worst receiver positions as in the case of Figure 6.3, the CRLB and CCRLB for all possible receiver combinations are also presented in respectively Figures 6.4 and 6.5 (grey colour) in which a logarithmic scaled is once again used on the y-axis with a unit of metres.

The CRLB results presented in Figure 6.4 suggests that target position errors as small as 100 m could be expected, but also in excess of 100 km if a poor choice of receiver positions are made.[2] In the case of the CCRLB results presented in Figure 6.5, the maximum target position errors are seen to be below 10 km, with the exception of some outliers and the minimum errors slightly below 10 m.

[2] Notice that these results are consistent with the findings from Chapter 5.

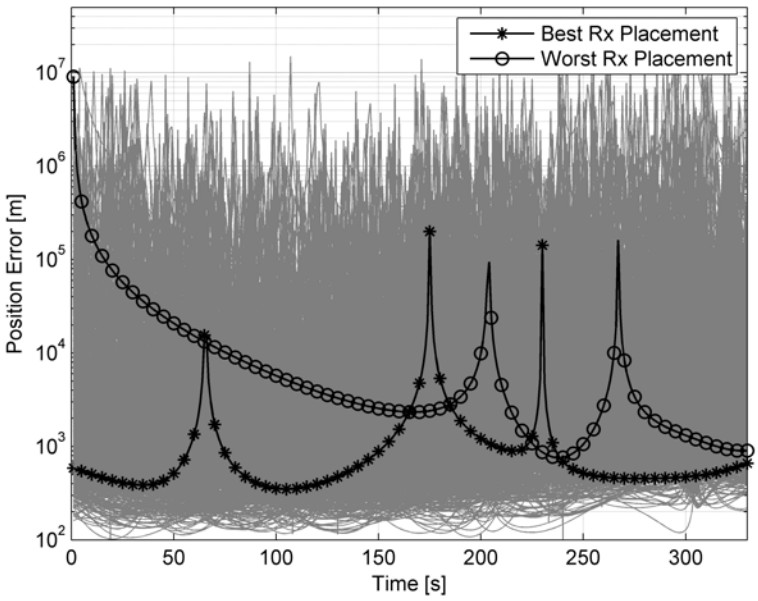

Figure 6.4: The CRLB performance prediction for a Doppler only tracking CR using all possible combinations of 4 receivers. The position errors for the best and worst receiver combinations are also presented.

Further, the best and worst performing receiver combinations are also displayed in Figures 6.4 and 6.5. In the case of the best performing receiver combination, the CRLB based target position errors are seen to lie within an error bound of 300 m and 100 km and in the case of the worst combination, between 800 m and in excess of 100 km. For the CCRLB based target positional errors, these error bounds are reduced to lie between 35 m and 200 m for the best combination, giving an average error of approximately 100 m over the flight path. In the case of the worst performing receiver combination, the expected target position errors is between 20 m and in excess of 100 km.

In summary of this section, the receiver placements used in Chapter 5 was based on a SNR and SINR criteria, that resulted in a best target position estimate of approximately 150 m and on average, around 400 m over the flight path (see Figure 5.4). Results presented in this section demonstrated that this error could be improved to an average of approximately 100 m for a similar CPI and

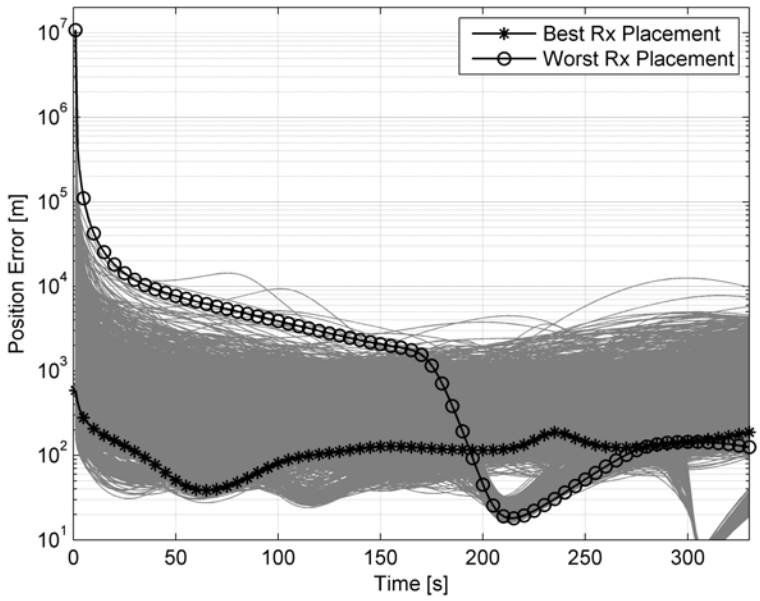

Figure 6.5: The CCRLB performance prediction for a Doppler only tracking CR using all possible combinations of 4 receivers. The position errors for the best and worst receiver combinations are also presented.

forgetting factor by placing the receivers optimally for the given flight path.

6.5 Conclusions

The performance of a Doppler only tracking systems is highly dependant on the receiver configuration in a single transmit, multiple receiver configuration system when a low number of receivers are used. Using the Cramèr-Rao analysis, target position errors are shown to be in excess of 100 km for some cases when 4 receiver placements are chosen non-optimally.

In this chapter a three step process is followed to place a low number of receivers optimally within a particular ROI. In the first step a virtual receiver grid, consisting of 36 possible receiver positions, is placed over the ROI. In the second step the CRLB and CCRLB are evaluated over all possible receiver combinations

within the grid and in the third step, the receiver set that optimises, providing the lowest error for the CCRLB are selected as the optimal receiver positions.

Seen from the results presented in this section, a large number of receivers, results in a very good Doppler only tracking performance. In the case of using 36 receivers, the average error over the flight path was calculated to be 20 m. However, in the case of reducing the number of receivers to 4 receivers and selecting the positions optimally, it is seen that the average tracking error increases to 100 m. This is exactly the same set-up considered for the field trials where the average error is seen to be 400 m.

Therefore, it is concluded that the results obtained from the field trails could probably be further improved,[3] by using the receiver selection process described in this chapter to choose the receiver sites. However, note that the SNR and SINR criteria [25] for site selection should not be omitted as this forms a critical part of the receiver site selection process.

[3] This is besides the fact that fairly encouraging results were obtained from the field trails.

Chapter 7

Conclusions and Future work

7.1 Conclusions

Commensal Radar is a class of radar system that make use of illuminators of opportunity for target illumination and accordingly processes the reflection of the target to establish target detection, followed by target geo-location and tracking. Despite the fact that CR has been known from as early as the 1930's, it only recently became popular as a possible cost effective solution for persistent surveillance due to today's powerful computers and fast, high-dynamic range digitizers that are available on the market for relatively low prices. Seen from the hardware description, as well as accompanying photos presented in Chapter 3, it is evident that a low cost radar solution is viable with such equipment. Further, fuelled by the digital advances being made at present, as well as the trend of ever increasing computational processing power becoming more affordable, it is foreseen that the current low cost CR will become even more affordable in future. As a result, many universities, research institutes and industry are actively researching this technology for various applications, for example military use and ATC, amongst other applications. The current, most widely used illuminator considered for accurate target tracking is DVB-T, due to the associated favourable high bandwidth properties of such signals. Further, FM illuminators

are typically considered for long range detections with reduced target position accuracy. In the case of developing nations, this approach cannot be followed due to the lack of DVB-T infrastructure. However, developing nations is currently well equipped with high powered FM transmitters and considered the primary illuminator of choice until DVB-T is rolled out.

Therefore, the objective of this research was to evaluate the feasibility of using an FM-based CR system as a cost effective solution for ATC in developing countries. Due to typical long integration times associated with CR, the frequency domain resolution of CR systems is typically very good. As a result, measurements of the target's Doppler shift are accurate which potentially makes FM illuminators, although currently seen as an illuminator for when the application allows for coarse target accuracy, a potential source for ATC purposes. Accordingly, this thesis aimed to obtain a comprehensive understanding of using only high resolution Doppler measurements to accurately track the position of a target.

This objective has been addressed by performing a comprehensive mathematical analysis for a Doppler only tracking CR system as described in Chapter 4. This analysis was verified by simulation as outlined in Chapter 5 and further also compared to real measured data in Chapter 5, that was obtained from the field experiment described in Chapter 3. Lastly, the geographical placement of the receivers was also proven to have a significant influence on the tracking performance of a Doppler only tracking system. Accordingly, methods to achieve an optimal receiver placement for a given flight trajectory was investigated in Chapter 6.

From these chapters, the main results are summarised below. In addition, notice that the research hypothesis questions presented in Chapter 1, Section 1.3.1 are directly answered with this summary.

Doppler only Tracking: One of the most significant achievements of this thesis was the Doppler only target tracking results based on real measurements. In this case, the RGNF was initialised from real measurement data and subsequently also successful in tracking the target based on Doppler only measurements.

Observability Criteria: The observability criteria determines if an unique solution exists for a given set of measurement data, for example Doppler measurements. As seen from Chapter 4, the linearised observation matrix needs to be of full rank to be observable, that in return determines the minimum number of receivers that could be used. In the context of estimating a target's 2-D state, consisting of position and velocity (4 parameters), requires 4 measurements to satisfy the full rank criteria. Therefore, using a single transmitter, multiple receiver configuration, where each receiver makes a single Doppler measurement of the target, a minimum of 4 receivers are required to satisfy the full rank criteria. Accordingly, this was the number of receivers considered for this thesis.

CRLB vs CCRLB: Using Cramèr-Rao theory, a theoretical equation was derived to determine the best possible target state estimate from noise corrupted measurements. This is known as the CRLB. However, as tracking filters, for example the RGNF, typically employ time history information, a direct comparison to the CRLB is unrealistic and therefore the CCRLB was derived that does account for time history measurements.

As seen from the simulations provided in Chapter 5, the RGNF is able to track a linear motion target using only the measurements of the target's Doppler shift from geographically separated receivers. Under such conditions, the target position accuracy is given by the CCRLB. Further, the simulation results were also compared to real data measurements. For these measurements, the target position accuracy lies between the CRLB and CCRLB error predictions as a result of the non-linear motion exercised by the target.

Conditioning of the Observation Matrix: Of utmost importance in Doppler only tracking applications, is to ensure that the observation matrix is properly conditioned, as failure to do so, results in the so called bad geometry regions. The factors identified to influence the conditioning of the observation matrix included; the number of receivers used (assuming the basic observation criteria is met), the placement of the receivers, also keeping in mind the possibility of Doppler correlation in the measurements and

lastly, using additional information to condition the observation matrix. In this thesis bistatic range measurements were used, but intuitively one would suspect that more optimal ways exist to accomplish this (see future research in Section 7.2).

Filter Selection and Initialisation: The filter initialisation method considered for this thesis is based on a closed form solution that makes use of noise corrupted bistatic range and Doppler measurements to estimate the initial target state vector. From classical estimation theory, the concern associated with this approach is that filter convergence might not occur due to the initial position estimate being too coarse. As the GN filter family are known to be fairly tolerant of large initialisation errors, the RGNF was selected as the filter of choice and also proved to be successful in tracking the target using real measurement data. As such, a closed form solution is proposed to initialise the RGNF from a single measurement of bistatic range and Doppler, collected from a minimum of 3 receiver sites.

Placement of receivers: The performance of a Doppler only tracking system is highly dependant on the receiver configuration in a single transmit, multiple receiver configuration system, where the number of receivers are close to the minimum number of receivers as required by the observability criteria. Besides the consideration of placing the receivers based on the SNR and SINR, as discussed by Inggs et al. [25], the geometry of the transmitter, target and receivers also plays an important role in Doppler only tracking as this directly effects the conditioning of the observation matrix. As demonstrated in Chapter 6 with a 4 receiver CR system, target position errors in excess of 100 km are possible when the receiver placements are chosen non-optimally.

It was further demonstrated that an increase in the number of receivers tends to improve the conditioning of the observation matrix and accordingly, improves the tracking results. For example, if the number of receivers placed over the ROI for the field trails were 36, tracking errors as small as 20 m could have been expected. In the case of reducing the number of receivers to 4 and placing them optimally as described in Chapter 6,

the average error increased to 100 m, but was still smaller than the average tracking error obtained for the receiver placement used during the field trails, which was 400 m. It is therefore concluded that the results in Chapter 5 could further be improved with an optimal receiver placement in addition to only using the SNR and SINR criteria [25].

Multiple Transmitters, Multiple Receivers Configuration: In addition to the single transmitter case, that was the primary focus of this thesis, MIMO for Doppler only tracking was also considered, hence using multiple transmitters together with multiple receivers. In the MIMO case, it was shown that Doppler correlation amongst the receivers is experienced. However, as the Doppler measurements that would cause the correlation are known a-priori, it is only required to pick the Doppler measurements that does not cause correlation. A rule of thumb equation was also provided to calculate the number of Doppler measurements that do not cause correlation, given the number of transmitters and receivers.

CPI consideration: Two different CPI lengths were considered for this thesis, namely a 1 s CPI and 4 s CPI, in which case the 4 s CPI proved to deliver the best results due to the extremely high Doppler resolution obtained.

Processing Considerations: The proposed signal processing scheme for tracking a target with Doppler only measurements, collected from geographically separated receivers, was also described in Chapter 3.

The first stage involves the detection of a target's Doppler shift at the respective receivers sites, in which the first step is to perform DPI cancellation and clutter suppression in the surveillance channel by means of the CGLS method. This is then followed by the cross-correlation between the reference and surveillance channels and lastly, the GOCA-CFAR was used to declare target detections that operated only in Doppler dimension. In the second stage, these Doppler shift detections would then be used to initialise the RGNF, together with the bistatic range measurements and once initialised, maintain the track using only the Doppler measurements.

In conclusion, the principle of a Doppler only tracking CR, using FM band illuminators of opportunity has been proven with this thesis. Although promising results were obtained, the performance is not yet at a stage where it can be proposed as a solution for ATC purposes. Therefore, future research aspects should be focussed to improve the results obtained in this thesis, in which the most important aspects are proposed in the following section.

7.2 Future Work

From the outset of this work, the scope of this thesis was limited (see Section 1.4.1) to demonstrate that Doppler only tracking is feasible for CR. Therefore, future work should concentrate on expanding some of the concepts in Section 7.1, increase the reliability of the algorithms and consider optimisation trade-off's in the aim to make it a feasible for ATC purposes. These are outlined below.

Extend Integration Time: Although this thesis proved that Doppler only target tracking could be achieved for long CPIs (4 s) while the target is manoeuvring, the effect of Doppler walk was not considered or investigated. However, Doppler walk is a known phenomenon within the SAR community and a paper by Malanowski et al. [62] showed that long CPIs (up to 10 s) could also be used for FM band CR with suitable processing. Hence, Doppler walk is an area of focus that requires further investigation and would probably further improve on the results obtained in this thesis.

It was also concluded in Chapter 5 that the Doppler standard deviation results under performed compared to the theoretical standard deviation given by Howland [91], due to Doppler walk. To justify this statement, the standard deviation results should be re-evaluated once Doppler walk compensation is taken into account.

Target Motion Model: A higher order motion model is currently required for the CCRLB, as this bound is only valid for linear target motion and could therefore, strictly speaking not be used for the real data measurements.

Further, as mentioned in Weinstein [112], bias errors are introduced when the motion model differs from the true motion of the target. However, these bias errors are considerably reduced when the target model closely resembles the true target motion. Therefore, an important consideration for future research is to expand the linear target motion model to a higher order motion model.

CCRLB vs. Posterior CRLB: The motion model assumed for the CCRLB is based on a deterministic dynamic system, whereas the Posterior CRLB is based on a stochastic dynamic system, in which case the CCRLB would then be lower than the Posterior CRLB. The comparison between the two bounds is set as future research.

Filter Investigation: The performance of the RGNF should also be compared to other tracking filters using the real measured data. A particular filter that is fairly tolerant to initialisation errors is the particle filter. On the one hand the particle filter would be more processing intensive than the RGNF, but the particle filter is able to directly utilise the non-linear measurement data. Therefore, use of the particle filter does not require the local linearisation step and accordingly, could potentially bypass the ill-conditioning matter of the observation matrix.

One powerful aspect of the RGNF that was not explored in this thesis, was the adaptive filter memory capability. Therefore, exploiting this capability should also be evaluated in future for target manoeuvring. What is important under this consideration is to known whether the target is in a bad geometry region. If this is the case, the filter memory length should not be to short as it might result in a scenario where the observation matrix becomes ill-conditioned.

Conditioning of Observation Matrix: In this thesis, additional bistatic range measurements were used to condition the observation matrix. However, as these are typically of bad range resolution, on would intuitively believe additional and more optimal ways exist to condition the observation matrix and accordingly set for further investigation.

Extended Trial Period: As mentioned in Chapter 1, CR is currently still in a development phase, but rapidly maturing. Therefore, in order for CR to get an uptake in industry, sufficient statistical data needs to be produced over long periods of time. Therefore, future trails (not only for Doppler only tracking) are envisioned in which sufficient data will be gathered to derive the PoD, PFA and accuracy for a given target of interest.

In order to achieve this, the work in this thesis needs to be expanded to automatic target association, automatic ARD line tracking and 3-D Cartesian tracking. Lastly, the effect of missed detections (non-ideal PoD) also needs to be evaluated. All these factors should then be taken into account to determine how they affect the lower bound of the tracking accuracy.

Receiver Placement: From the field experiment, encouraging results were obtained in which the target was tracked by using only the Doppler shift measurements of the target. However, as seen from Chapter 6, these results could probably be further improved if the receiver positions were chosen optimally. Therefore, combining the findings of Chapter 6 with the SNR and SINR criteria is set as future work, as well as validating the results thereof with real measurement data in a future experiment.

Further, using the method described in Chapter 6 to evaluate the optimal receiver placements, is a time consuming exercise and a more effective way to accomplish this is required. This in return would also allow for very fine grids to be evaluated over large areas and ultimately get to the conclusion of what the optimum receiver grid resolution is, given that Doppler correlation becomes a problem when the receivers are to closely spaced.

Doppler Correlation: In Chapter 5, a conclusion was made that the Doppler correlation becomes significant amongst the receiver measurements when the target is sufficiently far from the cluster of receivers. Future work in this regard should include an investigation on how the receiver placements, integration times, etc. influences this range, in which the aim would be to derive a rule of thumb equation to determine what the maximum range would be before Doppler correlation becomes significant.

Trade-off Comparisons: As a final thought, trade-off studies should also be performed comparing the categories listed above, for example the last two categories; receiver placement and Doppler correlation. A particular approach envisioned would be as follows; determine the optimal receiver placement for a given flight path based on the CCRLB, SNR and SINR criteria for the minimum number of receivers required. If the maximum filter memory length cannot suppress the bad geometry regions, add 1 more receiver (one method to improve the conditioning of the observation matrix) to the ROI and re-evaluate the receiver positions to see if the bad geometry region is eliminated. If not, repeat until the bad geometry region is eliminated.

Including the Ambiguity Function: In this thesis, only the geometry was considered in the performance analysis of the multistatic Doppler-only tracking CR. In future research, this analysis should include the ambiguity function [51, 69, 136] to enhance the understanding of the bad geometry regions.

Bibliography

[1] N. J. Willis and H. D. Griffiths, *Advances in Bistatic Radar*. Scitech Publishing, 2007. 2, 4

[2] H. Kuschel, "Approaching 80 years of passive radar," in *Radar, 2013 International Conference on*, 2013. 3, 4

[3] H. Griffiths, "New directions in bistatic radar," in *Radar Conference, 2008. RADAR '08. IEEE*, pp. 1–6, May 2008. 4

[4] G. E. Galati, *Advanced Radar Techniques and Systems*. IEE Radar, Sonar, Navigation, and Avionics, Series 4, 1993. 4

[5] H. Griffiths and N. Long, "Television-based bistatic radar," *Communications, Radar and Signal Processing, IEE Proceedings F*, vol. 133, pp. 649 –657, Dec 1986. 4, 5, 23, 64

[6] P. E. Howland, "Passive tracking of airborne targets using only Dppler and DOA information," *IEE Colloquium on Algorithms for Target Tracking*, 1995. 4, 5, 20

[7] P. Howland, D. Maksimiuk, and G. Reitsma, "FM radio based bistatic radar," *Radar, Sonar and Navigation, IEE Proceedings* -, vol. 152, pp. 107 – 115, Jun 2005. 5, 8, 24, 36, 48, 119

[8] M. Malanowski, K. Kulpa, P. Samczynski, J. Misiurewicz, and J. Kulpa, "Long range FM-based passive radar," in *Radar Systems (Radar 2012), IET International Conference on*, pp. 1–4, 2012. 5, 25

[9] C. Bongioanni, F. Colone, D. Langellotti, P. Lombardo, and T. Bucciarelli, "A new approach for DVB-T cross-ambiguity function evaluation," in *Radar Conference, 2009. EuRAD 2009. European*, pp. 37–40, 2009. 5, 25

[10] M. Conti, F. Berizzi, D. Petri, A. Capria, and M. Martorella, "High range resolution DVB-T passive radar," in *Radar Conference (EuRAD), 2010 European*, pp. 109 –112, Oct 2010. 5, 32

[11] P. Falcone, F. Colone, P. Lombardo, and T. Bucciarelli, "Range sidelobes reduction filters for WiFi-based passive bistatic radar," in *Radar Conference, 2009. EuRAD 2009. European*, pp. 133–136, 2009. 5, 26

[12] D. K. P. Tan, H. Sun, and Y. Lu, "Sea and air moving target measurements using a GSM based passive radar," in *Radar Conference, 2005 IEEE International*, pp. 783–786, 2005. 5, 26, 31

[13] K. Chetty, K. Woodbridge, H. Guo, and G. Smith, "Passive bistatic WiMAX radar for marine surveillance," in *Radar Conference, 2010 IEEE*, pp. 188–193, 2010. 5, 27

[14] D. Petri, A. Capria, M. Martorella, and F. Berizzi, "Ambiguity function study for UMTS passive radar," in *Radar Conference, 2009. EuRAD 2009. European*, pp. 41–44, Sept 2009. 5, 26

[15] M. Edrich and A. Shroeder, "Design, implementation and test of a multiband multistatic passive radar system for operational use in airspace surveillance," in *Radar Conference (RADAR), 2014 IEEE*, May 2014. 5, 44

[16] J. Scavullo and F. Paul, *Aerospace Ranges: Instrumentation.* Van Nost. Reinhold, 1965. 6

[17] C. Gauss, *Theory of the combination of observations least subject to errors.* SIAM, Philadelphia, 1995. Translation by G.W. Steward. 7

[18] A. Aitken, "On least-squares and linear combinations of observations," in *Proceedings of the Royal Scociety Edinburgh*, vol. A, pp. 42–48, 1935. 7

[19] P. Swerling, *Proposed stagewise differential correction procedure for satellite tracking and prediction*. P (Rand Corporation), Rand Corporation, 1958. 7

[20] R. Kalman, "A new approach to linear filtering and prediction problems," *Journal of Basic Engineering, Transactions of the AMSE*, vol. 82D, pp. 33–45, 1960. 7

[21] N. Morrison, *Tracking Filter Engineering: The Gauss-Newton and Polynomial Filters*. Tracking Filter Engineering, Institution of Engineering and Technology, 2012. 7, 79, 112, 114

[22] R. Nadjiasngar and M. Inggs, "The recursive Gauss-Newton filter," *arXiv preprint arXiv:1110.5212*, 2011. 7

[23] H. Griffiths and C. Baker, "Passive coherent location radar systems. part 1: performance prediction," *Radar, Sonar and Navigation, IEE Proceedings -*, vol. 152, no. 3, pp. 153–159, 2005. 8, 24

[24] D. W. O'Hagan, *Passive Bistatic Radar Performance Characterisation Using FM Radio Illuminators of Opportunity*. PhD thesis, University College London, 2009. 8, 24

[25] M. Inggs, C. Tong, R. Nadjiasngar, G. Lange, A. Mishra, and F. Maasdorp, "Planning and design phases of a commensal radar system in the FM broadcast band," *Aerospace and Electronic Systems Magazine, IEEE*, vol. 29, pp. 50–63, July 2014. 8, 54, 56, 153, 154, 162, 166, 167

[26] D. Waltenegus and C. Poellabauer, *Fundamentals of Wireless Sensor Networks: Theory and Practice*. Wiley Publishing, 2010. 9

[27] M. Inggs, G. Inggs, S. Sandenbergh, W. Al-Ashwal, K. Woodbridge, and H. Griffiths, "Multistatic networked radar for sea clutter measurements," in *Geoscience and Remote Sensing Symposium (IGARSS), 2011 IEEE International*, pp. 4449–4452, IEEE, 2011. 9

[28] M. Inggs, A. Balleri, W. Al-Ashwal, K. D. Ward, K. Woodbridge, M. Ritchie, W. Miceli, R. J. Tough, C. J. Baker, S. Watts, *et al.*, "NetRAD multistatic sea clutter database," in *Geoscience and Remote Sensing Symposium (IGARSS), 2012 IEEE International*, pp. 2937–2940, IEEE, 2012. 9

[29] C. A. Tong, *A Scalable Real-time Processing Chain for Radar Exploiting Illuminators of Opportunity*. Doctoral thesis, University of Cape Town - RRSG, Oct 2014. 11, 61, 65, 138

[30] M. Inggs, C. Tong, A. Mishra, and F. Maasdorp, "Modelling and simulation in commensal radar system design," in *Radar Systems (Radar 2012), IET International Conference on*, pp. 1–5, 2012. 15

[31] C. Tong, F. Maasdorp, and M. R. Inggs, "Performance improvements using the separated reference configuration in a multi-site commensal radar system," in *International Conference on Radar*, pp. 1 – 6, Sep 2013. 15, 60

[32] F. Maasdorp, J. Cilliers, M. Inggs, and C. Tong, "Simulation and measurement of propeller modulation using FM broadcast band commensal radar," *Electronics Letters*, vol. 49, pp. 1481–1482, Nov 2013. 15

[33] M. Inggs, C. Tong, R. Nadjiasngar, G. Lange, A. Mishra, and F. Maasdorp, "Planning and design phases of a commensal radar system in the FM broadcast band," *Aerospace and Electronic Systems Magazine, IEEE*, vol. 29, pp. 50–63, July 2014. 15

[34] F. Maasdorp, R. Nadjiasngar, and M. Inggs, "A Cramer Rao analysis on receiver placement in a FM band Commensal Radar system based on Doppler only measurements," in *Radar Conference (Radar), 2014 International*, pp. 1–6, Oct 2014. 15, 17

[35] F. Maasdorp, R. Nadjiasngar, and M. Inggs, "Target tracking using Doppler only measurements in an FM broadcast band commensal radar," *Electronics Letters*, p. ??, July 2015. 15, 17

[36] F. Maasdorp, J. Cilliers, M. Inggs, and C. Tong, "FM Band commensal radar technology used for the detection of small aircraft and the measurement of propeller modulation," in *Radar Conference (Radar), 2015 International*, pp. 1–5, May 2015. 15

[37] M. J. Shensa, "On the uniqueness of Doppler tracking," *The Journal of the Acoustical Society of America*, vol. 70, no. 4, pp. 1062–1064, 1981. 20

[38] S. M. Kay, *Fundamentals of Statistical Signal Processing: Estimation Theory*. Prentice Hall, New Jersey, 1993. 21, 81

[39] A. Schroeder, M. Edrich, and V. Winkler, "Multi-illuminator passive radar performance evaluation," in *Radar Symposium (IRS), 2012 13th International*, pp. 61–64, 2012. 22

[40] R. Saini and M. Cherniakov, "DTV signal ambiguity function analysis for radar application," *Radar, Sonar and Navigation, IEE Proceedings* -, vol. 152, no. 3, pp. 133–142, 2005. 24

[41] A. Lauri, F. Colone, R. Cardinali, C. Bongioanni, and P. Lombardo, "Analysis and emulation of FM radio signals for passive radar," in *Aerospace Conference, 2007 IEEE*, pp. 1–10, 2007. 24

[42] M. Malanowski, K. Kulpa, P. Samczynski, J. Misiurewicz, J. Kulpa, P. Roszkowski, P. Dzwonkowski, D. Gromek, L. Maslikowski, M. Misiurewicz, and L. Podkalicki, "Experimental results of the PaRaDe passive radar field trials," in *Radar Symposium (IRS), 2012 13th International*, pp. 65–68, May 2012. 25

[43] D. Tan, H. Sun, Y. Lu, and W. Liu, "Feasibility analysis of GSM signal for passive radar," in *Radar Conference, 2003. Proceedings of the 2003 IEEE*, pp. 425 – 430, May 2003. 25

[44] H. Guo, S. Coetzee, D. Mason, K. Woodbridge, and C. Baker, "Passive radar detection using wireless networks," in *Radar Systems, 2007 IET International Conference on*, pp. 1–4, 2007. 26

[45] H. Guo, K. Woodbridge, and C. Baker, "Evaluation of WiFi beacon transmissions for wireless based passive radar," in *Radar Conference, 2008. RADAR '08. IEEE*, pp. 1–6, 2008. 26

[46] P. Falcone, F. Colone, C. Bongioanni, and P. Lombardo, "Experimental results for OFDM WiFi-based passive bistatic radar," in *Radar Conference, 2010 IEEE*, pp. 516–521, 2010. 26

[47] P. Falcone, F. Colone, and P. Lombardo, "Doppler frequency sidelobes level control for WiFi-based passive bistatic radar," in *Radar Conference (RADAR), 2011 IEEE*, pp. 435–440, 2011. 26

[48] F. Colone, P. Falcone, and P. Lombardo, "Ambiguity function analysis of WiMAX transmissions for passive radar," in *Radar Conference, 2010 IEEE*, pp. 689–694, 2010. 27

[49] P. Krysik, K. Kulpa, M. Baczyk, L. Maslikowski, and P. Samczynski, "Ground moving vehicles velocity monitoring using a GSM based passive bistatic radar," in *Radar (Radar), 2011 IEEE CIE International Conference on*, vol. 1, pp. 781–784, 2011. 27

[50] P. Krysik, P. Samczynski, M. Malanowski, L. Maslikowski, and K. Kulpa, "Detection of fast maneuvering air targets using GSM based passive radar," in *Radar Symposium (IRS), 2012 13th International*, pp. 69–72, 2012. 27

[51] P. Stinco, M. Greco, F. Gini, and M. Rangaswamy, "Ambiguity function and Cramer-Rao bounds for universal mobile telecommunications system-based passive coherent location systems," *Radar, Sonar Navigation, IET*, vol. 6, pp. 668–678, August 2012. 27, 171

[52] E. Glennon, A. Dempster, and C. Rizos, "Feasibility of air target detection using GPS as a bistatic radar," *Journal of Global Positioning Systems*, vol. 1, pp. 119–126, Dec 2006. 28

[53] J. Palmer, S. Palumbo, A. Summers, D. Merrett, and S. Howard, "DSTO's experimental geosynchronous satellite based PBR," in *Radar Conference*

- *Surveillance for a Safer World, 2009. RADAR. International*, pp. 1–6, 2009. 28

[54] S. Haykin, *Adaptive Filter Theory, Third Edition.* Prentice Hall, New Jersey, 1995. 28

[55] R. Saini, M. Cherniakov, and V. Lenive, "Direct path interference suppression in bistatic system: DTV based radar," in *Radar Conference, 2003. Proceedings of the International*, pp. 309–314, 2003. 28

[56] F. Colone, R. Cardinali, and P. Lombardo, "Cancellation of clutter and multipath in passive radar using a sequential approach," in *Radar, 2006 IEEE Conference on*, pp. 7 pp.–, April. 29

[57] F. Colone, D. O'Hagan, P. Lombardo, and C. Baker, "A multistage processing algorithm for disturbance removal and target detection in passive bistatic radar," *Aerospace and Electronic Systems, IEEE Transactions on*, vol. 45, pp. 698 –722, Apr 2009. 29

[58] M. Malanowski, "Comparison of adaptive methods for clutter removal in PCL radar," in *Radar Symposium, 2006. IRS 2006. International*, pp. 1–4, 2006. 29

[59] R. Cardinali, F. Colone, C. Ferretti, and P. Lombardo, "Comparison of clutter and multipath cancellation techniques for passive radar," in *Radar Conference, 2007 IEEE*, pp. 469–474, 2007. 29

[60] J. Palmer and S. Searle, "Evaluation of adaptive filter algorithms for clutter cancellation in passive bistatic radar," in *Radar Conference (RADAR), 2012 IEEE*, pp. 0493–0498, May. 30, 65

[61] K. Kulpa and J. Misiurewicz, "Stretch processing for long integration time passive covert radar," in *Radar, 2006. CIE '06. International Conference on*, pp. 1–4, Oct 2006. 30

[62] M. Malanowski and K. Kulpa, "Analysis of integration gain in passive radar," in *Radar, 2008 International Conference on*, pp. 323–328, Sept 2008. 30, 67, 152, 168

[63] M. Malanowski, K. Kulpa, and K. Olsen, "Extending the integration time in DVB-T-based passive radar," in *Radar Conference (EuRAD), 2011 European*, pp. 190–193, 2011. 31

[64] Y. Lu, D. K. P. Tan, and H. Sun, "Air target detection and tracking using a multi-channel GSM based passive radar," in *Waveform Diversity and Design Conference, 2007. International*, pp. 122–126, 2007. 31

[65] C. Bongioanni, F. Colone, and P. Lombardo, "Performance analysis of a multi-frequency FM based passive bistatic radar," in *Radar Conference, 2008. RADAR '08. IEEE*, pp. 1–6, 2008. 31, 43

[66] D. Petri, A. Capria, M. Conti, F. Berizzi, M. Martorella, and E. Dalle Mese, "High range resolution multichannel DVB-T passive radar: Aerial target detection," in *Digital Communications - Enhanced Surveillance of Aircraft and Vehicles (TIWDC/ESAV), 2011 Tyrrhenian International Workshop on*, pp. 129–132, 2011. 32

[67] K. Olsen and K. Woodbridge, "FM based passive bistatic radar range resolution improvement," in *Radar Symposium (IRS), 2011 Proceedings International*, pp. 327–332, 2011. 32

[68] K. E. Olsen, *Investigation of Bandwidth Utilisation Methods to Optimise Performance in Passive Bistatic Radar*. PhD thesis, University College London, Dec 2011. 32

[69] M. Greco, P. Stinco, F. Gini, and A. Farina, "Cramer-Rao bounds and selection of bistatic channels for multistatic radar systems," *Aerospace and Electronic Systems, IEEE Transactions on*, vol. 47, pp. 2934–2948, Oct 2011. 33, 171

[70] F. Colone, C. Bongioanni, and P. Lombardo, "Multifrequency integration in FM radio-based passive bistatic radar. part I: Target detection," *Aerospace and Electronic Systems Magazine, IEEE*, vol. 28, no. 4, pp. 28–39, 2013. 33

[71] F. Colone, C. Bongioanni, and P. Lombardo, "Multifrequency integration in FM radio-based passive bistatic radar. part II: Direction of arrival estimation," *Aerospace and Electronic Systems Magazine, IEEE*, vol. 28, no. 4, pp. 40–47, 2013. 33

[72] R. Kolb and F. Hollister, "Bearings-only target estimation," in *Proceedings of the 1st Asilomar Conference Circuits and Systems*, 1967. 33

[73] S. Nardone and V. Aidala, "Observability Criteria for Bearings-Only Target Motion Analysis," *Aerospace and Electronic Systems, IEEE Transactions on*, vol. AES-17, pp. 162–166, March 1981. 34

[74] S. Nardone, A. G. Lindgren, and K. F.Gong, "Fundamental properties and performance of conventional bearings-only target motion analysis," *Automatic Control, IEEE Transactions on*, vol. 29, pp. 775–787, Sep 1984. 34

[75] S. Hammel and V. Aidala, "Observability requirements for three-dimensional tracking via angle measurements," *Aerospace and Electronic Systems, IEEE Transactions on*, vol. AES-21, pp. 200–207, March 1985. 34

[76] H. Lee, "A novel procedure for assessing the accuracy of hyperbolic multilateration systems," *Aerospace and Electronic Systems, IEEE Transactions on*, vol. AES-11, pp. 2–15, Jan 1975. 34

[77] Y. Chan and K. Ho, "A simple and efficient estimator for hyperbolic location," *Signal Processing, IEEE Transactions on*, vol. 42, pp. 1905–1915, Aug 1994. 34

[78] I. Mellen, G., M. Pachter, and J. Raquet, "Closed-form solution for determining emitter location using time difference of arrival measurements," *Aerospace and Electronic Systems, IEEE Transactions on*, vol. 39, pp. 1056–1058, July 2003. 34

[79] D. Torrieri, "Statistical theory of passive location systems," *Aerospace and Electronic Systems, IEEE Transactions on*, vol. AES-20, pp. 183–198, March 1984. 34

[80] V. Anastasio, F. Colone, and P. Lombardo, "A procedure for effective receiver positioning in multistatic passive radar," in *Radar Conference, 2009. EuRAD 2009. European*, pp. 493–496, 2009. 34, 48

[81] V. Anastasio, F. Colone, A. Di Lallo, A. Farina, F. Gumiero, and P. Lombardo, "Optimization of multistatic passive radar geometry based on CRLB with uncertain observations," in *Radar Conference (EuRAD), 2010 European*, pp. 340–343, 2010. 34

[82] F. Gumiero, C. Nucciarone, V. Anastasio, P. Lombardo, and F. Colone, "Multistatic passive radar geometry optimization for target 3D positioning accuracy," in *Radar Conference (EuRAD), 2010 European*, pp. 467–470, 2010. 34, 35, 48

[83] F. Gumiero, S. Santarelli, C. Bongioanni, F. Colone, and P. Lombardo, "Using real data for the implementation of multistatic passive radar geometry optimization procedure," in *Radar Conference (EuRAD), 2011 European*, pp. 93–96, 2011. 34

[84] J. Caspers, "Bistatic and Multistatic Radar," in *Radar Handbook* (M. Skolnik, ed.), ch. 36, McGraw-Hill, New York, 1970. 35

[85] A. Mrstik, "Multistatic-radar binomial detection," *Aerospace and Electronic Systems, IEEE Transactions on*, vol. AES-14, pp. 103–108, Jan 1978. 35

[86] C. Jauffret and Y. Bar-Shalom, "Track formation with bearing and frequency measurements in clutter," *Aerospace and Electronic Systems, IEEE Transactions on*, vol. 26, pp. 999–1010, Nov 1990. 35

[87] Y. Chan and S. Rudnicki, "Bearings-only and Doppler-bearing tracking using instrumental variables," *Aerospace and Electronic Systems, IEEE Transactions on*, vol. 28, pp. 1076–1083, Oct 1992. 35

[88] P. Blanc-Benon and G. Bienvenu, "Passive target motion analysis using multipath differential time-delay and differential Doppler shifts," in *Acoustics, Speech, and Signal Processing, 1995. ICASSP-95., 1995 International Conference on*, vol. 5, pp. 3139–3142 vol.5, May 1995. 35

[89] K. Becker, "Passive localization of frequency-agile radars from angle and frequency measurements," *Aerospace and Electronic Systems, IEEE Transactions on*, vol. 35, pp. 1129–1144, Oct 1999. 35

[90] K. Becker, "Three-dimensional target motion analysis using angle and frequency measurements," *Aerospace and Electronic Systems, IEEE Transactions on*, vol. 41, pp. 284–301, Jan 2005. 35

[91] P. E. Howland, *Television Based Bistatic Radar*. PhD thesis, University of Birmingham, 1997. 36, 83, 151, 168

[92] P. E. Howland, "Target tracking using television-based bistatic radar," in *IEE Proceedings on Radar, Sonar and Navigation*, vol. 146, pp. 166–174, Institute of Electrical Engineers (United Kingdom), Jun 1999. 36

[93] M. Tobias and A. Lanterman, "Probability hypothesis density-based multitarget tracking with bistatic range and doppler observations," *Radar, Sonar and Navigation, IEE Proceedings* -, vol. 152, pp. 195–205, June 2005. 36

[94] N. Morrison, R. Lord, and M. Inggs, "The Gauss-Newton algorithm in passive aircraft tracking using Doppler and bearings," in *Radar Systems, 2007 IET International Conference on*, pp. 1–5, Oct 2007. 36, 51, 155, 157

[95] M. Malanowski, "An algorithm for 3D target localization from passive radar measurements," in *Proceedings of SPIE*, vol. 7502, pp. 75021B–1 – 75021B–6, May 2009. 37, 49, 114, 115

[96] M. Malanowski and K. Kulpa, "Two methods for target localization in multistatic passive radar," *Aerospace and Electronic Systems, IEEE Transactions on*, vol. 48, pp. 572–580, Jan 2012. 37

[97] P. Falcone, F. Colone, and P. Lombardo, "Localization of moving targets with a passive radar system based on WiFi transmissions," in *Radar Systems (Radar 2012), IET International Conference on*, pp. 1–6, Oct 2012. 37

[98] R. Patton, "Orbit Determination from Single Pass Doppler Observations," *Military Electronics, IRE Transactions on*, vol. MIL-4, pp. 336–344, April 1960. 38

[99] M. I. Skolnik, "An Analysis of Bistatic Radar," *Aerospace and Navigational Electronics, IRE Transactions on*, vol. ANE-8, pp. 19 –27, Mar. 1961. 38, 50, 72

[100] S. Salinger and J. Brandstatter, "Application of recursive estimation and Kalman filtering to Doppler tracking," *Aerospace and Electronic Systems, IEEE Transactions on*, vol. AES-6, pp. 585–592, July 1970. 38

[101] Y.-C. Xiao, P. Wei, and T. Yuan, "Observability and Performance Analysis of Bi/Multi-Static Doppler-Only Radar," *Aerospace and Electronic Systems, IEEE Transactions on*, vol. 46, no. 4, pp. 1654–1667, 2010. 39, 80, 86, 94, 96, 192

[102] A. Bishop and M. Smith, "Remarks on the Cramer-Rao inequality for Doppler-based target parameter estimation," in *Intelligent Sensors, Sensor Networks and Information Processing (ISSNIP), 2010 Sixth International Conference on*, pp. 199–204, Dec 2010. 39

[103] R. Nadjiasngar and M. Inggs, "Gauss–Newton filtering incorporating Levenberg–Marquardt methods for tracking," *Digital Signal Processing*, vol. 23, no. 5, pp. 1662–1667, 2013. 39, 91, 107, 108, 114

[104] R. Nadjiasngar, S. Middleton, and M. Inggs, "Doppler-only tracking with the recursive Gauss-Newton filter," in *Radar Systems (Radar 2012), IET International Conference on*, pp. 1–5, Oct 2012. 39

[105] B. Ristic and A. Farina, "Target tracking via multi-static Doppler shifts," *Radar, Sonar Navigation, IET*, vol. 7, pp. 508–516, June 2013. 39

[106] N. Levanon, "Some results from utilizing Doppler derivatives," *Aerospace and Electronic Systems, IEEE Transactions on*, vol. AES-16, pp. 727–729, Sept 1980. 39, 40

[107] R. Webster, "An exact trajectory solution from Doppler shift measurements," *Aerospace and Electronic Systems, IEEE Transactions on*, vol. AES-18, pp. 249–252, March 1982. 40

[108] D. Torney, "Localization and Observability of Aircraft via Doppler Shifts," *Aerospace and Electronic Systems, IEEE Transactions on*, vol. 43, pp. 1163–1168, July 2007. 40

[109] I. Shames, A. Bishop, M. Smith, and B. Anderson, "Analysis of target velocity and position estimation via Doppler-shift measurements," in *Australian Control Conference (AUCC), 2011*, pp. 507–512, Nov 2011. 40

[110] G. Battistelli, L. Chisci, C. Fantacci, A. Farina, and A. Graziano, "A new approach for Doppler-only target tracking," in *Information Fusion (FUSION), 2013 16th International Conference on*, pp. 1616–1623, July 2013. 40

[111] P. M. Schultheiss and E. Weinstein, "Estimation of differential Doppler shifts," *The Journal of the Acoustical Society of America*, vol. 66, no. 5, 1979. 41

[112] E. Weinstein and N. Levanon, "Passive array tracking of a continuous wave transmitting projectile," *Aerospace and Electronic Systems, IEEE Transactions on*, vol. AES-16, pp. 721–726, Sept 1980. 41, 169

[113] E. Weinstein, "Measurement of the differential Doppler shift," *Acoustics, Speech and Signal Processing, IEEE Transactions on*, vol. 30, pp. 112–117, Feb 1982. 42

[114] J. Statman and E. R. Rodemich, "Parameter estimation based on Doppler frequency shifts," *Aerospace and Electronic Systems, IEEE Transactions on*, vol. AES-23, pp. 31–39, Jan 1987. 42

[115] Y.-T. Chan and F. Jardine, "Target localization and tracking from Doppler-shift measurements," *Oceanic Engineering, IEEE Journal of*, vol. 15, pp. 251–257, Jul 1990. 42

[116] A. Macera, M. Caruso, C. Bongioanni, F. Colone, P. Lombardo, E. Anniballi, and R. Cardinali, "Civil Air Traffic Surveillance with Passive Radar for Anti-Terrorism," in *Advances in Radar and Remote Sensing (TyWRRS), 2012 Tyrrhenian Workshop on*, pp. 296–303, 2012. 42

[117] F. Berizzi, M. Martorella, D. Petri, M. Conti, and A. Capria, "USRP technology for multiband passive radar," in *Radar Conference, 2010 IEEE*, pp. 225–229, 2010. 43

[118] A. Schroeder, M. Edrich, and F. Wolschendorf, "Multiband experimental PCL system: Concept and measurement results," in *Radar Symposium (IRS), 2010 11th International*, pp. 1–4, 2010. 43

[119] A. Schroeder and M. Edrich, "Cassidian multiband mobile passive radar system," in *Radar Symposium (IRS), 2011 Proceedings International*, pp. 286–291, 2011. 43

[120] M. Edrich and A. Schroeder, "Multiband multistatic passive radar system for airspace surveillance: A step towards mature PCL implementations," in *Radar, 2013 International Conference on*, 2013. 43

[121] H. Kuschel, J. Heckenbach, D. O'Hagan, and M. Ummenhofer, "A hybrid multi-frequency passive radar concept for medium range air surveillance," in *Microwaves, Radar and Remote Sensing Symposium (MRRS), 2011*, pp. 275–279, 2011. 44

[122] K. Olsen and K. Woodbridge, "Performance of a multiband passive bistatic radar processing scheme; part I," *Aerospace and Electronic Systems Magazine, IEEE*, vol. 27, no. 10, pp. 16–25, 2012. 44

[123] K. Olsen and K. Woodbridge, "Performance of a multiband passive bistatic radar processing scheme-part II," *Aerospace and Electronic Systems Magazine, IEEE*, vol. 27, no. 11, pp. 4–14, 2012. 44

[124] A. Macera, C. Bongioanni, F. Colone, and P. Lombardo, "Receiver architecture for multi-standard based Passive Bistatic Radar," in *Radar Conference (RADAR), 2013 IEEE*, pp. 1–5, 2013. 44

[125] C. Baker, H. Griffiths, and I. Papoutsis, "Passive coherent location radar systems. part 2: waveform properties," *Radar, Sonar and Navigation, IEE Proceedings* -, vol. 152, no. 3, pp. 160–168, 2005. 56

[126] C. Tong, M. Inggs, and C. Van Dyk, "ComRad3, a multichannel direct conversion receiver for FM broadcast band radar," in *Radar Conference (RADAR), 2014 IEEE (Accepted)*, May 2014. 59

[127] M. Inggs and C. Tong, "Commensal radar using separated reference and surveillance channel configuration," *Electronics Letters*, vol. 48, no. 18, pp. 1158–1160, 30. 60

[128] N. Willis, *Bistatic Radar, Second Edition.* Institution of Engineering and Technology, 2005. 71

[129] H. Van Trees, *Detection, Estimation and Modulation Theory, PartI.* Wiley, New York, 1968. 81, 82

[130] N. Levanon, "Lowest GDOP in 2-D scenarios," *Radar, Sonar and Navigation, IEE Proceedings* -, vol. 147, pp. 149–155, June 2000. 88

[131] P. Tichavsky, C. Muravchik, and A. Nehorai, "Posterior Cramer-Rao bounds for discrete-time nonlinear filtering," *Signal Processing, IEEE Transactions on*, vol. 46, pp. 1386–1396, May 1998. 89

[132] P. Stinco, M. S. Greco, F. Gini, and A. Farina, "Posterior Cramer-Rao lower bounds for passive bistatic radar tracking with uncertain target measurements," *Signal Processing*, vol. 93, no. 12, pp. 3528 – 3540, 2013. Special Issue on Advances in Sensor Array Processing in Memory of Alex B. Gershman. 89

[133] R. Nadjiasngar, *On Improving the Performance of the Gauss-Newton Filter.* Doctoral thesis, University of Cape Town - RRSG, Nov 2013. 111

[134] B. Bell and F. Cathey, "The iterated Kalman filter update as a Gauss-Newton method," *Automatic Control, IEEE Transactions on*, vol. 38, pp. 294–297, Feb 1993. 114

[135] R. Tharmarasa, T. Kirubarajan, and M. McDonald, "Passive multitarget tracking using transmitters of opportunity," in *Computational Intelligence for Security and Defense Applications, 2009. CISDA 2009. IEEE Symposium on*, pp. 1–8, July 2009. 141

[136] T. Tsao, M. Slamani, P. Varshney, D. Weiner, and H. Schwarzlander, "Ambiguity function for a bistatic radar," *Aerospace and Electronic Systems, IEEE Transactions on*, vol. 33, pp. 1041–1051, July 1997. 171

Appendix A

Local Linearisation

Mentioned throughout this thesis, the bistatic range and Doppler equations defined in Chapter 3, are non-linear functions of the parameter space $\mathbf{x}$. In order to cope with these non-linear functions, a method called local linearisation was presented in Chapter 4, where the non-linear function, $\mathbf{y} = \mathbf{g}(\mathbf{x})$ (Equation (4.5)) is linearised by taking the partial derivative of the function with respect to the parameter space $\mathbf{x}$, hence

$$\frac{\partial \mathbf{y}}{\partial \mathbf{x}} = \frac{\partial \mathbf{g}(\mathbf{x})}{\partial \mathbf{x}} \tag{A.1}$$

where $\mathbf{g}(\mathbf{x})$ is given by Equation (5.3) for Doppler measurements and by Equation (5.4) for range-Doppler measurements. Therefore, taking the the partial derivative with respect to the 3-D parameter space[1] for Doppler measurements, the following functions are obtained;

$$\begin{aligned}\frac{\partial f_{di}[n]}{\partial x_n} = &\frac{-\dot{x}_n\left[(\Delta^E_{y,n})^2 + (\Delta^E_{z,n})^2\right] + \Delta^E_{x,n}\left[\Delta^E_{y,n}\dot{y}_n + \Delta^E_{z,n}\dot{z}_n\right]}{\lambda(R_{E,n})^3} \\ &+ \frac{-\dot{x}_n\left[(\Delta^{Ri}_{y,n})^2 + (\Delta^{Ri}_{z,n})^2\right] + \Delta^{Ri}_{x,n}\left[\Delta^{Ri}_{y,n}\dot{y}_n + \Delta^{Ri}_{z,n}\dot{z}_n\right]}{\lambda(R_{Ri,n})^3}\end{aligned} \tag{A.2}$$

[1] In the case of a 2-D parameter space, all z entries are set to zero. These include the target height and speed, z_n and $\dot{z}_n$, the transmitter height z_E and lastly, all k receiver heights, z_{R1} to z_{Rk}.

$$\frac{\partial f_{di}[n]}{\partial y_n} = \frac{-\dot{y}_n\left[(\Delta^E_{x,n})^2 + (\Delta^E_{z,n})^2\right] + \Delta^E_{y,n}\left[\Delta^E_{x,n}\dot{x}_n + \Delta^E_{z,n}\dot{z}_n\right]}{\lambda(R_{E,n})^3} + \frac{-\dot{y}_n\left[(\Delta^{Ri}_{x,n})^2 + (\Delta^{Ri}_{z,n})^2\right] + \Delta^{Ri}_{y,n}\left[\Delta^{Ri}_{x,n}\dot{x}_n + \Delta^{Ri}_{z,n}\dot{z}_n\right]}{\lambda(R_{Ri,n})^3} \tag{A.3}$$

$$\frac{\partial f_{di}[n]}{\partial z_n} = \frac{-\dot{z}_n\left[(\Delta^E_{x,n})^2 + (\Delta^E_{y,n})^2\right] + \Delta^E_{z,n}\left[\Delta^E_{x,n}\dot{x}_n + \Delta^E_{y,n}\dot{y}_n\right]}{\lambda(R_{E,n})^3} + \frac{-\dot{z}_n\left[(\Delta^{Ri}_{x,n})^2 + (\Delta^{Ri}_{y,n})^2\right] + \Delta^{Ri}_{z,n}\left[\Delta^{Ri}_{x,n}\dot{x}_n + \Delta^{Ri}_{y,n}\dot{y}_n\right]}{\lambda(R_{Ri,n})^3} \tag{A.4}$$

$$\frac{\partial f_{di}[n]}{\partial \dot{x}_n} = \frac{-\dot{x}_n}{\lambda\sqrt{R_E}} - \frac{\dot{x}_n}{\lambda\sqrt{R_{Ri}}} \tag{A.5}$$

$$\frac{\partial f_{di}[n]}{\partial \dot{y}_n} = \frac{-\dot{y}_n}{\lambda\sqrt{R_E}} - \frac{\dot{y}_n}{\lambda\sqrt{R_{Ri}}} \tag{A.6}$$

$$\frac{\partial f_{di}[n]}{\partial \dot{z}_n} = \frac{-\dot{z}_n}{\lambda\sqrt{R_E}} - \frac{\dot{z}_n}{\lambda\sqrt{R_{Ri}}} \tag{A.7}$$

where $f_{di}[n]$ is the bistatic Doppler measurement at the i^{th}-receiver as defined in Chapter 3. All additional notation used in Equations (A.2) to (A.7) were also defined in Chapter 3. In the case of using bistatic range equations, the partial derivatives with respected to the 3-D parameters space results in;

$$\frac{\partial R_{bi}[n]}{\partial x_n} = \frac{\Delta^E_x}{\sqrt{R_E}} + \frac{\Delta^{Ri}_x}{\sqrt{R_{Ri}}} \tag{A.8}$$

$$\frac{\partial R_{bi}[n]}{\partial y_n} = \frac{\Delta^E_y}{\sqrt{R_E}} + \frac{\Delta^{Ri}_y}{\sqrt{R_{Ri}}} \tag{A.9}$$

$$\frac{\partial R_{bi}[n]}{\partial z_n} = \frac{\Delta^E_z}{\sqrt{R_E}} + \frac{\Delta^{Ri}_z}{\sqrt{R_{Ri}}} \tag{A.10}$$

$$\frac{\partial R_{bi}[n]}{\partial \dot{x}_n} = 0 \tag{A.11}$$

$$\frac{\partial R_{bi}[n]}{\partial \dot{y}_n} = 0 \tag{A.12}$$

$$\frac{\partial R_{bi}[n]}{\partial \dot{z}_n} = 0 \tag{A.13}$$

where $R_{bi}[n]$ is the bistatic range measurement at the i^{th} receiver and also previously defined in Chapter 3. Recalling from Chapter 4, local linearisation is also used to linearise the non-linear observation matrix. Therefore, reprinting the equations defined in Chapter 4 here for ease of read, the linearisation of the observation matrix is given by;

$$\overline{\mathbf{M}} = \frac{\partial \mathbf{y}}{\partial \mathbf{x}} = \frac{\partial \mathbf{g}(\mathbf{x})}{\partial \mathbf{x}} \tag{A.14}$$

where the matrix entries, $m_{i,j}$ are given by;

$$m_{i,j} = \left.\frac{\partial g_i\left(x_1, \cdots, x_c\right)}{\partial x_j}\right|_{\overline{\mathbf{x}}} \qquad \begin{matrix} 1 \leq i \leq k \\ 1 \leq j \leq c \end{matrix} \tag{A.15}$$

around the nominal point $\overline{\mathbf{x}}$. Noticing that this is identical to what is described above, the matrix entries $m_{i,j}$ are therefore given by Equations (A.2) to (A.13), depending on the scenario.

In summary of Appendix A, the linearisation of the observation matrix is explained by means of an example. Assume the objective is to track a target's position and velocity in 2-D space that is represented by the target state vector $\mathbf{x}$ as defined in Chapter 3. Hence $c = 4$ in Equation (A.15) and at least 4 receivers are required in the multi-static CR system ($k = 4$) to fulfil the observability criteria for a Doppler only tracking system, as described in Chapter 4. Therefore, $\overline{\mathbf{M}}$ would be of the form:

$$\overline{\mathbf{M}} = \begin{bmatrix} m_{1,1} & m_{1,2} & m_{1,3} & m_{1,4} \\ m_{2,1} & m_{2,2} & m_{2,3} & m_{2,4} \\ m_{3,1} & m_{3,2} & m_{3,3} & m_{3,4} \\ m_{4,1} & m_{4,2} & m_{4,3} & m_{4,4} \end{bmatrix} \tag{A.16}$$

with the matrix entries given as follows; $m_{1,1}$ would be given by Equation (A.2) for receiver $i = 1$, $m_{1,2}$ would be given by Equation (A.5) for receiver $i = 1$, $m_{1,3}$ would be given by Equation (A.3) for receiver $i = 1$ and $m_{1,4}$ would be given by Equation (A.6), also for receiver $i = 1$. $m_{2,1}$ would then again be given by Equation (A.2), but for receiver $i = 2$ and so forth, till all 16 matrix entries are obtained.

Lastly, notice that when bistatic range and Doppler measurements are used, the number of matrix entries in the row dimension would be double that of Doppler only measurements.

Appendix B

Proof of Ill-condition State

Recalling, Section 4.4.1, a target tracking scenario was presented where a single T-R pair is used to make 4 consecutive Doppler measurements of the target. For this scenario, it is stated that the observation matrix will be singular when the target moves along $x_0 = \frac{x_R}{2}$ in the y-direction, hence the target motion is 90° perpendicular to the centre point of the transmitter and receiver baseline. Following, analytical proof is provided that this condition indeed results in the observation matrix being ill-conditioned. Therefore, considering the equations derived in [101], but rewritten to the notation used in this thesis, the linearisation equations are given as:

$$\frac{\partial f_{d1}[n]}{\partial x_0} = \frac{\Delta^E_{y,n}\left[\dot{x}_n\,\Delta^E_{y,n} - \dot{y}_n\,\Delta^E_{x,n}\right]}{\lambda(R_E)^3} + \frac{\Delta^{R1}_{y,n}\left[\dot{x}_n\,\Delta^{R1}_{y,n} - \dot{y}_n\,\Delta^{R1}_{x,n}\right]}{\lambda(R_{R1})^3} \tag{B.1}$$

$$\frac{\partial f_{d1}[n]}{\partial y_0} = \frac{\Delta^E_{x,n}\left[\dot{y}_n\,\Delta^E_{x,n} - \dot{x}_n\,\Delta^E_{y,n}\right]}{\lambda(R_E)^3} + \frac{\Delta^{R1}_{x,n}\left[\dot{y}_n\,\Delta^{R1}_{x,n} - \dot{x}_n\,\Delta^{R1}_{y,n}\right]}{\lambda(R_{R1})^3} \tag{B.2}$$

$$\begin{aligned}\frac{\partial f_{d1}[n]}{\partial \dot{x}_n} = &\frac{\Delta^E_{x,n}(R_E)^2 + \dot{x}_n t_n(\Delta^E_{y,n})^2 - \dot{y}_n t_n \Delta^E_{y,n}\Delta^E_{x,n}}{\lambda(R_E)^3} \\ &+ \frac{\Delta^{R1}_{x,n}(R_{R1})^2 + \dot{x}_n t_n(\Delta^{R1}_{y,n})^2 - \dot{y}_n t_n \Delta^{R1}_{y,n}\Delta^{R1}_{x,n}}{\lambda(R_{R1})^3}\end{aligned} \tag{B.3}$$

$$\frac{\partial f_{d1}[n]}{\partial \dot{y}_n} = \frac{\Delta^E_{y,n}(R_E)^2 + \dot{y}_n t_n(\Delta^E_{x,n})^2 - \dot{x}_n t_n \Delta^E_{y,n}\Delta^E_x}{\lambda(R_E)^3} + \frac{\Delta^{R1}_{y,n}(R_{R1})^2 + \dot{y}_n t_n(\Delta^{R1}_{x,n})^2 - \dot{x}_n t_n \Delta^{R1}_{y,n}\Delta^{R1}_{x,n}}{\lambda(R_{R1})^3} \tag{B.4}$$

where $k = 1$ (one receiver) and all other variables are defined in Chapter 3. However, the following variables are reprinted here for ease of read;

$$\begin{aligned} \Delta^E_{x,n} &= x_n - x_E\,,\ \Delta^E_{y,n} = y_n - y_E \\ \Delta^{Ri}_{x,n} &= x_n - x_E\ ,\ \Delta^{Ri}_{y,n} = y_n - y_E \end{aligned} \tag{B.5}$$

First, the following are assumed; 1.) the transmitter and receiver coordinates are respectively given as $\mathbf{x}_E = [x_E, 0]$ and $\mathbf{x}_{R1} = [0, 0]$ m, 2.) the target is moving in the y-direction with $\mathbf{v}_{\mathrm{x}} = [0, 1]$ m/s and 3.) the target starting position is given as $[x_0, y_0] = [\frac{x_E}{2}, 0]$. Substitution of the target starting position, transmitter position and receiver positions into Equation (B.5) results in the following two simplified equations, namely; $\Delta^E_{y,n} = \Delta^{R1}_{y,n}$ and $\Delta^E_{x,n}$ = -$\Delta^{Ri}_{x,n}$. Next, the substitution of all $\Delta^E_{x,n}$ values with $-\Delta^{R1}_{x,n}$ and $\Delta^E_{y,n}$ with $\Delta^{R1}_{y,n}$ into Equations (B.1) to (B.4), together with velocities defined by $\mathbf{v}_{\mathrm{x}}$ above, results in;

$$\frac{\partial f_{d1}[n]}{\partial x_0} = \frac{\dot{y}_n\,\Delta^{R1}_{x,n}\,\Delta^{R1}_{y,n}}{\lambda(R_{R1})^3} - \frac{\dot{y}_n\,\Delta^{R1}_{x,n}\,\Delta^{R1}_{y}}{\lambda(R_{R1})^3} = 0 \tag{B.6}$$

$$\frac{\partial f_{d1}[n]}{\partial y_0} = \frac{(\Delta^{R1}_{x,n})^2\dot{y}_n}{\lambda(R_{R1})^3} + \frac{(\Delta^{R1}_{x,n})^2\dot{y}_n}{\lambda(R_{R1})^3} \neq 0 \tag{B.7}$$

$$\frac{\partial f_{d1}[n]}{\partial \dot{x}_n} = \frac{-\Delta^{R1}_{x,n}(R_{R1})^2 + \dot{y}_n t_n \Delta^{R1}_{y,n}\Delta^{R1}_{x,n}}{\lambda(R_{R1})^3} + \frac{\Delta^{R1}_{x,n}(R_{R1})^2 - \dot{y}_n t_n \Delta^{R1}_{y,n}\Delta^{R1}_{x,n}}{\lambda(R_{R1,n})^3} = 0 \tag{B.8}$$

$$\frac{\partial f_{d1}[n]}{\partial \dot{y}_n} = \frac{\Delta^{R1}_{y,n}(R_{R1})^2 + \dot{y}_n t_n(\Delta^{R1}_{x,n})^2}{\lambda(R_{R1})^3} + \frac{\Delta^{R1}_{y,n}(R_{R1})^2 + \dot{y}_n t_n(\Delta^{R1}_{x,n})^2}{\lambda(R_{R1})^3} \neq 0 \tag{B.9}$$

and accordingly, with $n = [1,2,3,4]$, the observation matrix is written as

$$\left.\frac{\partial \mathbf{y}_D}{\partial \mathbf{x}_0}\right|_{n=1,2,3,4} = \begin{pmatrix} 0 & 0 & \frac{\partial f_{d1}[1]}{\partial y_0} & \frac{\partial f_{d1}[1]}{\partial \dot{y}} \\ 0 & 0 & \frac{\partial f_{d1}[2]}{\partial y_0} & \frac{\partial f_{d1}[2]}{\partial \dot{y}} \\ 0 & 0 & \frac{\partial f_{d1}[3]}{\partial y_0} & \frac{\partial f_{d1}[3]}{\partial \dot{y}} \\ 0 & 0 & \frac{\partial f_{d1}[4]}{\partial y_0} & \frac{\partial f_{d1}[4]}{\partial \dot{y}} \end{pmatrix} \tag{B.10}$$

where all non-zero entries in Equation (B.10) are given by the function description as used in Equation (B.7) and (B.9). Lastly, having two zero columns in Equation (B.10), will result in $\det(\frac{\partial \mathbf{y}_D}{\partial \mathbf{x}_0}) = 0$ and proves that the observation matrix will be singular when the target moves along the track $\mathbf{x}_p = (\frac{x_E}{2}, y \in \mathbb{R})$.